62-4-6

U. S. ARMY
TRANSPORTATION RESEARCH COMMAND
FORT EUSTIS, VIRGINIA

TCREC TECHNICAL REPORT 62-74

RECIRCULATION PRINCIPLE FOR GROUND EFFECT MACHINES, THREE-DIMENSIONAL WIND TUNNEL TESTS

Task 9R99-01-005-04

Contract DA 44-177-TC-710

July 1962

prepared by:

MARTIN COMPANY
Orlando, Florida

4217-62

DISCLAIMER NOTICE

When Government drawings, specifications, or other data are used for any purpose other than in connection with a definitely related Government procurement operation, the United States Government thereby incurs no responsibility nor any obligation whatsoever; and the fact that the Government may have formulated, furnished, or in any way supplied the said drawings, specifications, or other data is not to be regarded by implication or otherwise as in any manner licensing the holder or any other person or corporation, or conveying any rights or permission, to manufacture, use, or sell any patented invention that may in any way be related thereto.

ASTIA AVAILABILITY NOTICE

Qualified requesters may obtain copies of this report from

Armed Services Technical Information Agency
Arlington Hall Station
Arlington 12, Virginia

This report has been released to the Office of Technical Services, U. S. Department of Commerce, Washington 25, D. C., for sale to the general public.

The information contained herein will not be used for advertising purposes.

The findings and recommendations contained in this report are those of the contractor and do not necessarily reflect the views of the Chief of Transportation or the Department of the Army.

HEADQUARTERS
U. S. ARMY TRANSPORTATION RESEARCH COMMAND
Fort Eustis, Virginia

The recirculation principle is of interest to the U. S. Army in its program of research on Ground Effect Machines (GEM) since, theoretically, the power required for lift can be substantially reduced. In addition, there are other important benefits which result from this principle, such as reduced drag in forward flight, reduced dust and spray, reduced structural weight, and increased stability.

This report presents the results of an experimental wind-tunnel test of a three-dimensional model of a recirculation GEM. One of the weaknesses of the state of the art in GEM is the lack of an adequate understanding of behavior in forward flight. Therefore, this program was undertaken to demonstrate that the apparent advantages in power continue in forward flight.

The results indicate that the recirculation configuration exhibits no unusual characteristics in forward flight and that the advantages of this concept are not limited to hover.

FOR THE COMMANDER:

John H. Parry Jr.

JOHN H. PARRY, JR.
1st Lt, TC
Adjutant

W. D. Hinshaw

WILLIAM D. HINSHAW
Project Engineer

CONTRACT DA 44-177-TC-710

MAY 1962

RECIRCULATION PRINCIPLE FOR GROUND EFFECT MACHINES

THREE-DIMENSIONAL WIND TUNNEL TESTS

OR 2497

Prepared by

MARTIN COMPANY

ORLANDO AEROSPACE DIVISION

for

U. S. ARMY TRANSPORTATION RESEARCH COMMAND

FORT EUSTIS, VIRGINIA

FOREWORD

This report is submitted as an interim report in full compliance with the requirements of Clause 3, Paragraph e of Contract DA 44-177-TC-710 as amended by modifications Nos. 1 and 5 thereof. It contains experimental data on a model recirculation GEM in forward flight and is a logical extension of two-dimensional ejector data reported in OR 2073. The tests were conducted in the David Taylor Model Basin subsonic wind tunnel during December 1961 and January 1962.

Mr. P. Vinson planned and supervised the tests under the direction of Mr. K. Cossairt, GEM Project Engineer. Mr. E. Linthicum was in charge of the design and construction of the test model. Messrs. G. Martin, C. Casteleiro, and P. Vinson contributed to the analysis of test results reported herein. This report has been reviewed and approved by Mr. K. Cossairt, GEM Project Engineer.

Acknowledgement is made of the able assistance of Mr. Norman K. Walker in analysis and correlation of drag data.

CONTENTS

LIST OF ILLUSTRATIONS

LIST OF SYMBOLS

A	Lift Augmentation	-
a	Model Characteristic Width	ft.
b	Model Characteristic Length	ft.
c	Circumference	ft.
C_D	Total Drag Coefficient	-
$C_{D_{mom}}$	Momentum Drag Coefficient	-
C_{D_f}	Profile Drag Coefficient	-
C_m	Pitching Moment Coefficient	-
C_n	Yawing Moment Coefficient	-
C_ℓ	Rolling Moment Coefficient	-
C_L	Total Lift Coefficient	-
C_{L_o}	Lift Coefficient Due to External Flow Field	-
C_Y	Side Force Coefficient	-
D	Total Drag	lbs.
D	Characteristic Dimension	ft.
D_f	Profile Drag	lbs.
D_{mom}	Momentum Drag	lbs.
g	Acceleration Due to Gravity	32.17 ft/sec^2.
h	Height of Base Above the Ground	in.
J	Total Momentum Flux of Ejector Exit Flow	lbs.
J'	Total Momentum Flux of Primary Flow	lbs.

K	Constant in Cushion Drag Analysis	-
L	Lift	ft-lbs.
$\mathscr{L}$	Rolling Moment	ft-lbs.
M	Pitching Moment	ft-lbs.
m	Total Mass Flow at Ejector Exit	lb/sec.
m'	Total Primary Mass Flow	lb/sec.
N	Yawing Moment	ft-lbs.
p_a	Ambient Static Pressure (Gage)	psfg
p_o'	Total Pressure in Primary Nozzles (Gage)	psig
p_{tj}	Average Total Pressure of Recirculating Flow	psig
p_{f_j}	Average Total Pressure of Recirculating Flow (Front Ejector) (Gage)	psfg
p_{s_j}	Average Total Pressure of Recirculating Flow (Side Ejector) (Gage)	psfg
p_b	Average Base Pressure (Gage)	psfg
p_c	Average Cavity Pressure (Gage)	psfg
q_c	Critical Free Stream Dynamic Pressure	psf
q_j	Recirculating Flow Dynamic Pressure	psf
q_∞	Free Stream Dynamic Pressure	psf
S	Platform Area	$ft.^2$
S_b	Base Area	$ft.^2$
S_c	Cavity Area	$ft.^2$
S_j	Total Ejector Exit Flow Area	$ft.^2$

S_r	Reference Area	$ft.^2$
t	Ejector Mixing Section Thickness	in.
t_e	Ejector Exit Thickness	in.
V_j	Average Recirculating Flow Velocity	ft/sec.
V_∞	Free Stream (Forward Flight) Velocity	ft/sec.
$\bar{x}$	Distance Between c.p. and c.g. (Longitudinal)	ft.
$\bar{y}$	Distance Between c.p. and c.g. (Lateral)	ft.
Y	Side Force	lbs.
α	Pitch Angle from Horizontal	Degrees
β	Ejector Tilt Angle from Horizontal	Degrees
θ_1	Ejector Inlet Angle from Horizontal	Degrees
θ_2	Ejector Exit Angle from Horizontal	Degrees
ϕ	Roll Angle	Degrees
ψ	Yaw Angle	Degrees
ϵ	Ejector Efficiency	-
ρ	Density of Air	$slugs/ft^3$

SUMMARY

Results of forward flight tests of a model, recirculating ejector, ground effect machine are presented in this report. The tests were conducted at the David Taylor Model Basin, 8 foot by 12 foot subsonic wind tunnel, Washington, D. C., during December 1961 and January 1962. Principal variables investigated were height, speed, ejector primary air pressure, angle of pitch, angle of roll and angle of yaw. Force and base pressure data were recorded for a range of each one of the above variables while holding all others constant. Test results confirm that the model tested has an inherent hovering stability over an h/D range of 0.05 to 0.1. The effects of forward flight are generally destabilizing with the speed at which instability occurs being influenced strongly by height. A cushion drag of the order 2 to 3 times the model profile drag was observed. This cushion drag was found to be strongly influenced by height and speed.

CONCLUSIONS

Results of the tests of the small scale three dimensional model using recirculating ejectors for the lift generating system showed the following.

1. The tests, especially at heights of 3 inches or over in the low portion of the velocity range, were influenced strongly by flow attachment and the resulting degradation in the base pressure and total lift. Additional runs were made to investigate the cause of the high slopes in the curves of lift vs. height. It was found that a spoiler attached to the exit of the recirculating ejector could be used to cause the flow to detach and thus increase the lift at heights of 3 inches and over. The influence of this attached flow is evidenced in the effects of forward flight on lift, drag, and stability but since the main purpose of these tests was to obtain the trends of these effects in forward flight, and since the effect of the attached flow could be evaluated, the tests results obtained were still valuable.

2. The attached flow was found to be a three dimensionsl effect since in the two dimensional testing of the ejectors this effect was not present. The importance of proper corner design for 3 dimensional models or full scale machines was therefore emphasised. This corner design would also circumvent the corner leakage that was present at the higher heights.

3. The model profile drag coefficient is only slightly influenced by ground effect. The aerodynamic lift coefficient, due to upper surface lift, is 0.45 which is in essential agreement with Chaplin's findings for annular GEMs.

4. A cushion drag of from 2 to 3 times the magnitude of the model profile drag was encountered at certain combinations of speed and height. The magnitude of the cushion drag correlates well with a cushion momentum drag parameter and generally follows trends observed by N. K. Walker for several annular GEMs.

5. The model exhibited hovering static stability in the h/D range of 0.05 to 0.1. Although the ejector geometry was not varied during these tests, two-dimensional data have shown that the ejector exit angle, θ_2, has a strong influence on the stability limits. It must be concluded that variable geometry would have been effective in expanding the observed stability range. The effects of forward flight were found to be generally destabilizing although the speed at which instability was encountered varied strongly with height.

RECOMMENDATIONS

1. Since the main contribution to pitching moments in forward flight is aerodynamic lift acting at approximately 1/4 chord, it appears desirable to investigate the feasibility of controlling pitching moment through proper contouring of the upper surface. The effectiveness of various upper surfaces in extending the range of roll stability should also be investigated.

2. Although the cushion drag observed in these tests correlates well with the curtain momentum drag parameter, an adequate understanding of the origin and mechanism of the cushion drag is not available. Further, experimental studies are required to investigate the effects of planform streamlining, etc. on cushion drag.

3. The effect of varying mass augmentation on the stability derivatives should be investigated in future testing. The mass augmentation can be varied by changing the size or spacing of the primary nozzles.

I. DESCRIPTION OF MODEL, TEST FACILITY AND INSTRUMENTATION

A. Description of Model

The model tested was derived from early concepts of a man carrying test vehicle. A rectangular planform was selected as a reasonable compromise between a circular planform which affords maximum base area for a given circumference and an elliptical planform which provides a measure of streamlining. In addition the rectangular planform simplified construction of the ejectors and the basic model structure. The basic structure was formed of balsa wood and silk, utilizing model airplane construction techniques.

Basic model dimensions are shown in Figure 1. The base is a rectangle two feet wide by three feet long providing a base area of six ft.^{2}. A 9 inch overhang from the base perimeter provides compartmented cavities for the recirculating ejectors which generate and contain the pressurized air in the base region. Since the model was powered with shop air, no air intakes were provided on the model. This was considered to be desirable from a performance standpoint since only the effect of the air cushion would be present during testing and it would not be necessary to determine the effect of intakes.

During the course of the wind tunnel test it became desirable to provide additional streamlining to the model to reduce the value of profile drag coefficient (C_{D_f}) and to observe the effects on cushion performance. To this end, nose and tail fairings as shown in Figure 2 were constructed. These fairings were attached to the basic model with tape and wire.

The ejectors were constructed of vacuum formed plastic sheets reinforced with plastic ribs and spacers; the various pieces being bonded together with ethyline chloride. A typical ejector is shown in Figure 3. A balsa wood block was bonded at the ejector inlet providing a hinge line for attaching the ejectors to the base perimeter. The primary nozzles were attached to a cylindrical feed pipe which was recessed in the balsa wood block. The feed pipe was in turn connected through a flexible hose to a plenum which followed the base perimeter and distributed primary air equally to each of the separate ejectors. The plenum was finally connected to the wind tunnel shop air line which was routed through the hollow support strut as shown in Figure 4. The ejectors were retained by bolts through the bulkheads forming the ejector compartments. Three bulkhead bolt hole positions were provided to give ejector tilt angles (β) of -10°, 0° and +10°. Corner ejectors were provided which could be rotated 90° providing either continuous front and rear or continuous side curtains.

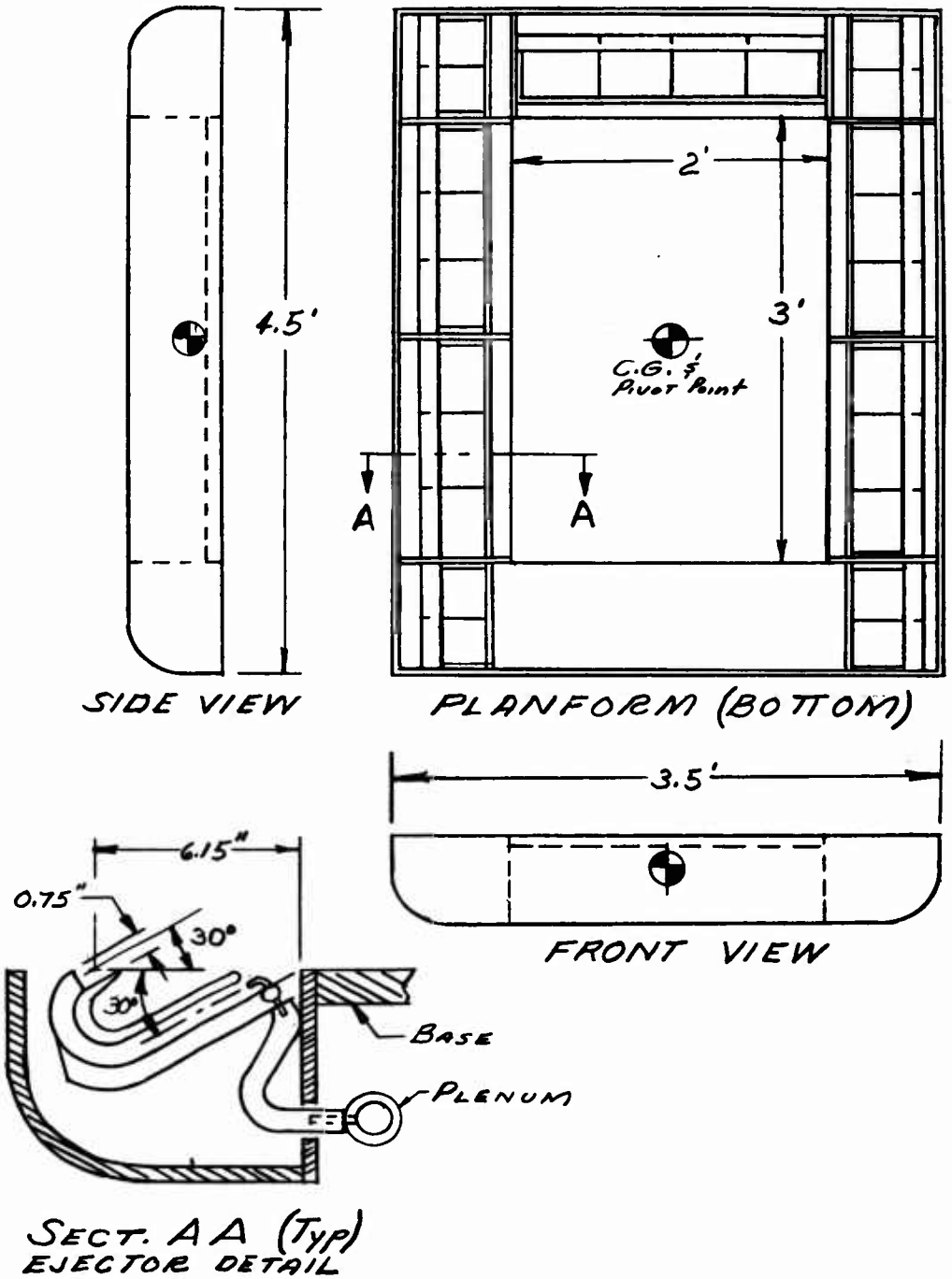

Figure 1. Basic Model Configuration.

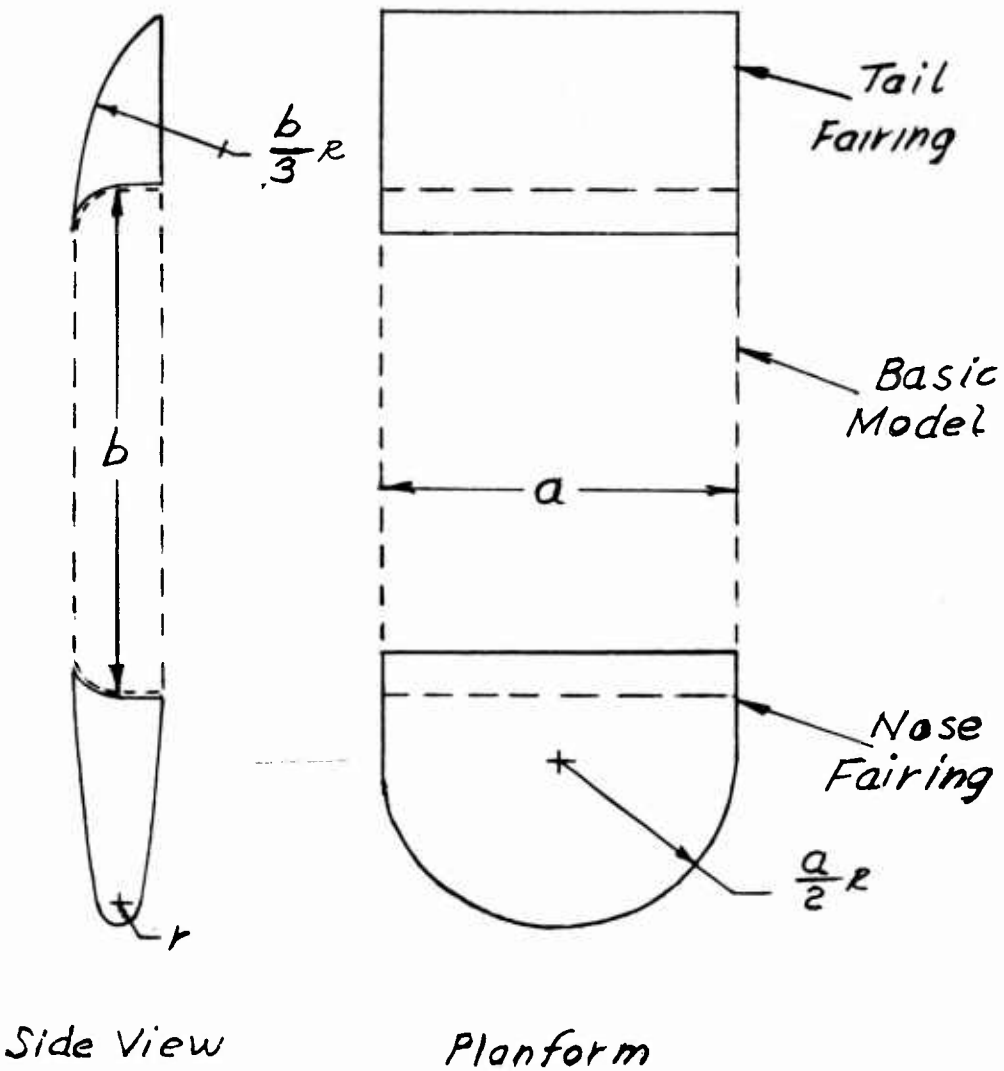

Figure 2. Streamlined Configuration.

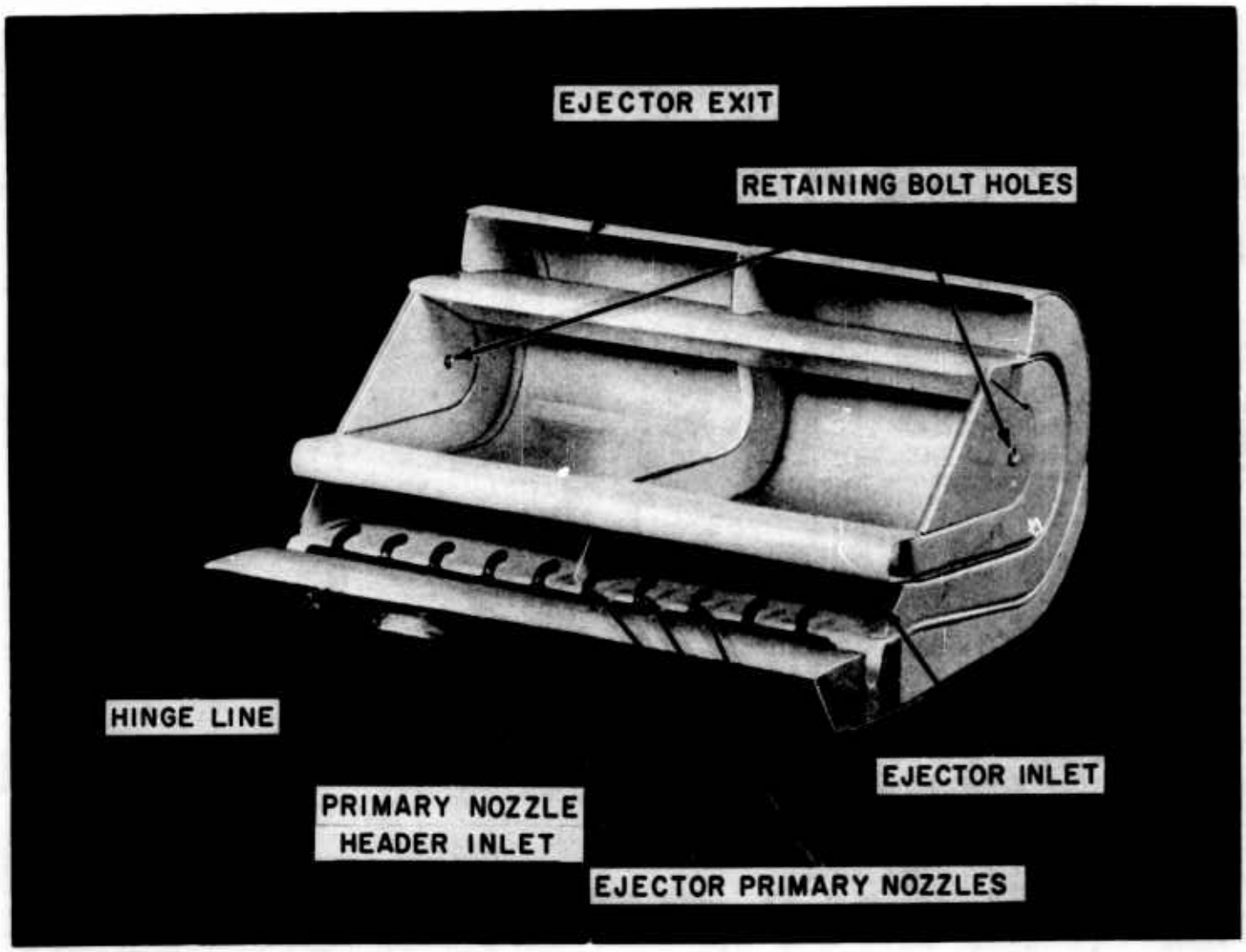

Figure 3. Ejector Details.

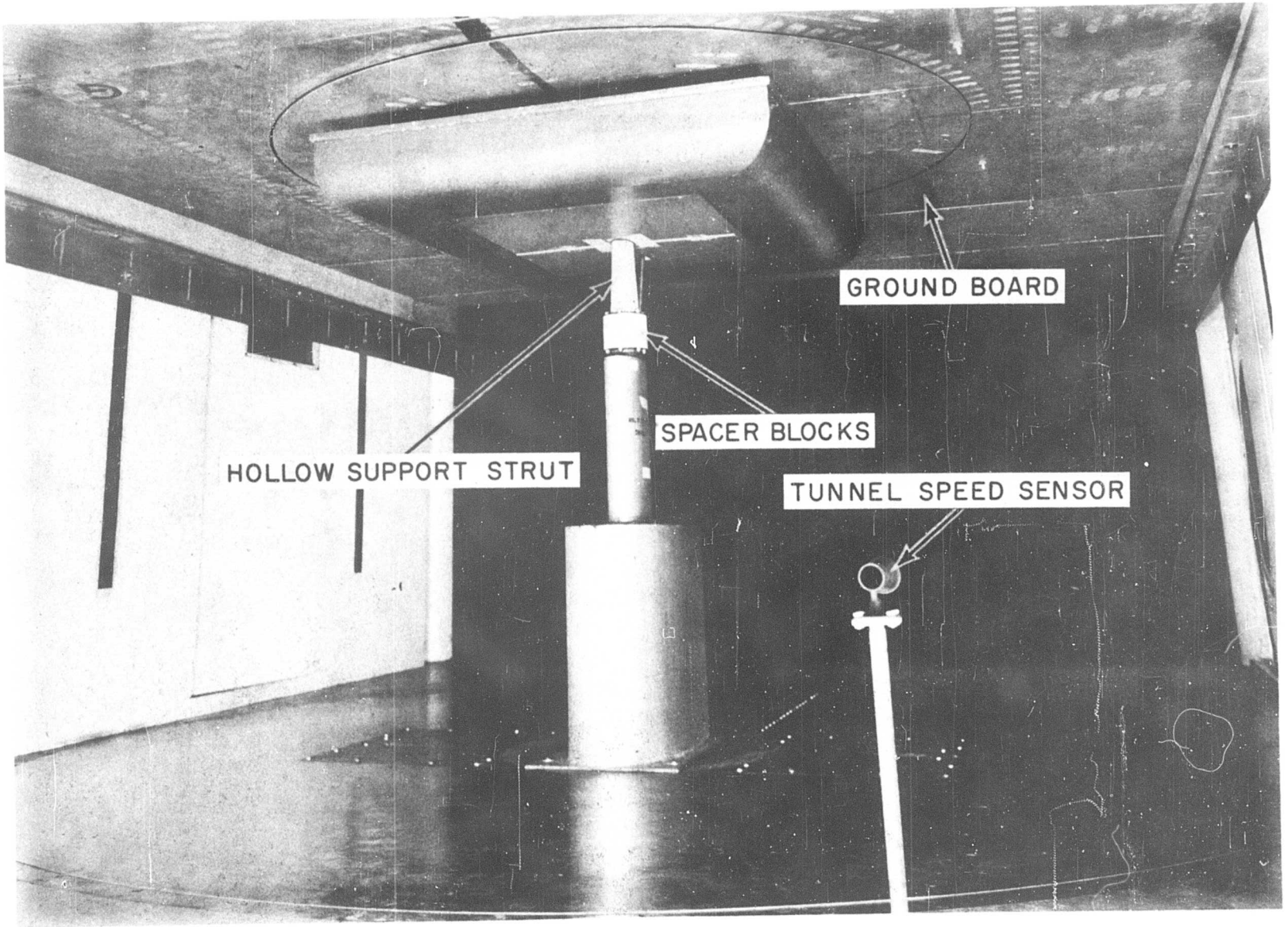

Figure 4. Tunnel Installation (Looking Downstream).

B. Description of Tunnel and Model Installation

A schematic of the wind tunnel installation is shown in Figure 5. The north, 8' x 12', subsonic tunnel at the David Taylor model basin was utilized for the tests. A fabricated metal ground board and hollow mounting strut were available from previous tests and were utilized for this program. For simplicity the model was mounted and tested in an inverted position. Split one inch spacer rings near the tip of the mounting strut provided height adjustment from 1 inch to 5 inches. The primary air hose and the 1/16 inch tygon tubing instrumentation lines were fed through the hollow mounting strut. Flexible couplings were provided on all lines at the point where they left the force balance system to eliminate their effect on force measurements. An orifice in the primary air supply line was used to monitor and set primary mass flow.

Pressure instrumentation terminated at a vertical alcohol photo-manometer. Force data were acquired on printed tapes produced semi-automatically by the tunnel balance system.

C. Instrumentation

The tunnel balance system gave a record of 6 force components, lift, drag, yaw force, pitching moment, yawing moment and rolling moment for each test point. In addition pressure taps were located on the model base in sufficient quantity to indicate the effect of forward flight on curtain and cushion pressures. Figure 8 summarizes model pressure instrumentation. In reducing the test data all base pressure taps were averaged together while the 4 cavity pressure taps were averaged separately. The 5 total head taps on the front ejector were averaged as p_{f_j} while the 5 total head taps on the side ejector were averaged as p_{s_j}. Tunnel velocity, V_∞, was monitored and controlled by observing free stream dynamic pressure, q_∞.

D. Summary of Configurations Tested

The basic model configuration tested is shown in Figures 1, 6 and 7. For this configuration air cushion data were obtained over a range of 0 to 80 fps forward velocity, -4 to +8 degrees angle of attack, -2 to +6 degrees roll angle, -5 to +10 degrees yaw angle, 1 to 5 inch height and ejector primary pressure of 0 to 92.5 psig. In addition, data were obtained on the model alone (without a cushion) and on a dummy (solid) cushion attached to the model and again attached to the ground board. Dummy curtain geometry is defined in Figure 9.

The model alone data simulates the limiting case where the curtain is blown away and through flow passes under the model while the dummy cushion data represents the opposite extreme where an extremely strong curtain completely blocks flow under the model. These data then provide the basis for computing the effects chargeable to the air cushion.

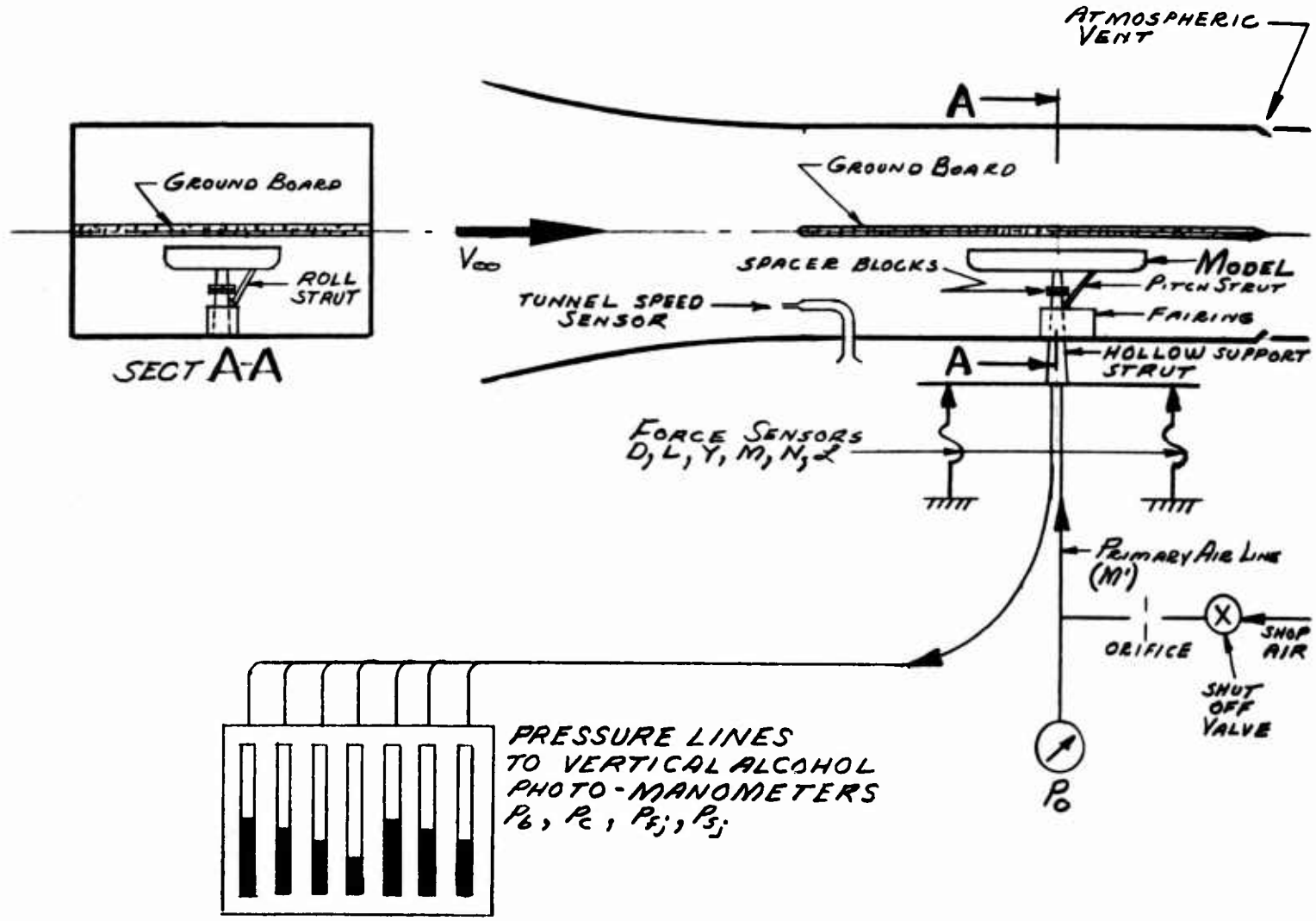

Figure 5. Schematic of Wind Tunnel Installation.

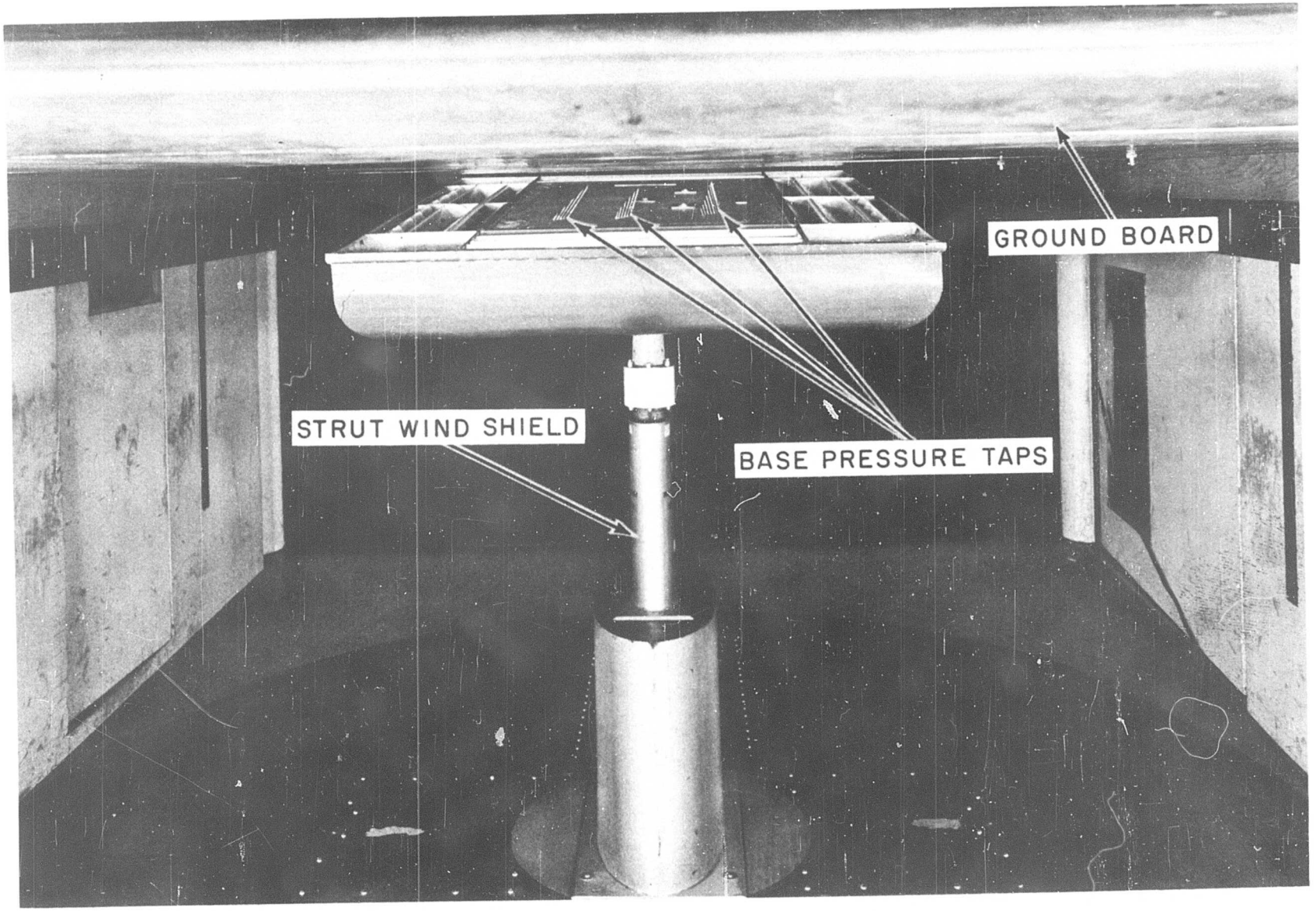

Figure 6. Tunnel Installation (Looking Downstream Showing Base Pressure Instrumentation).

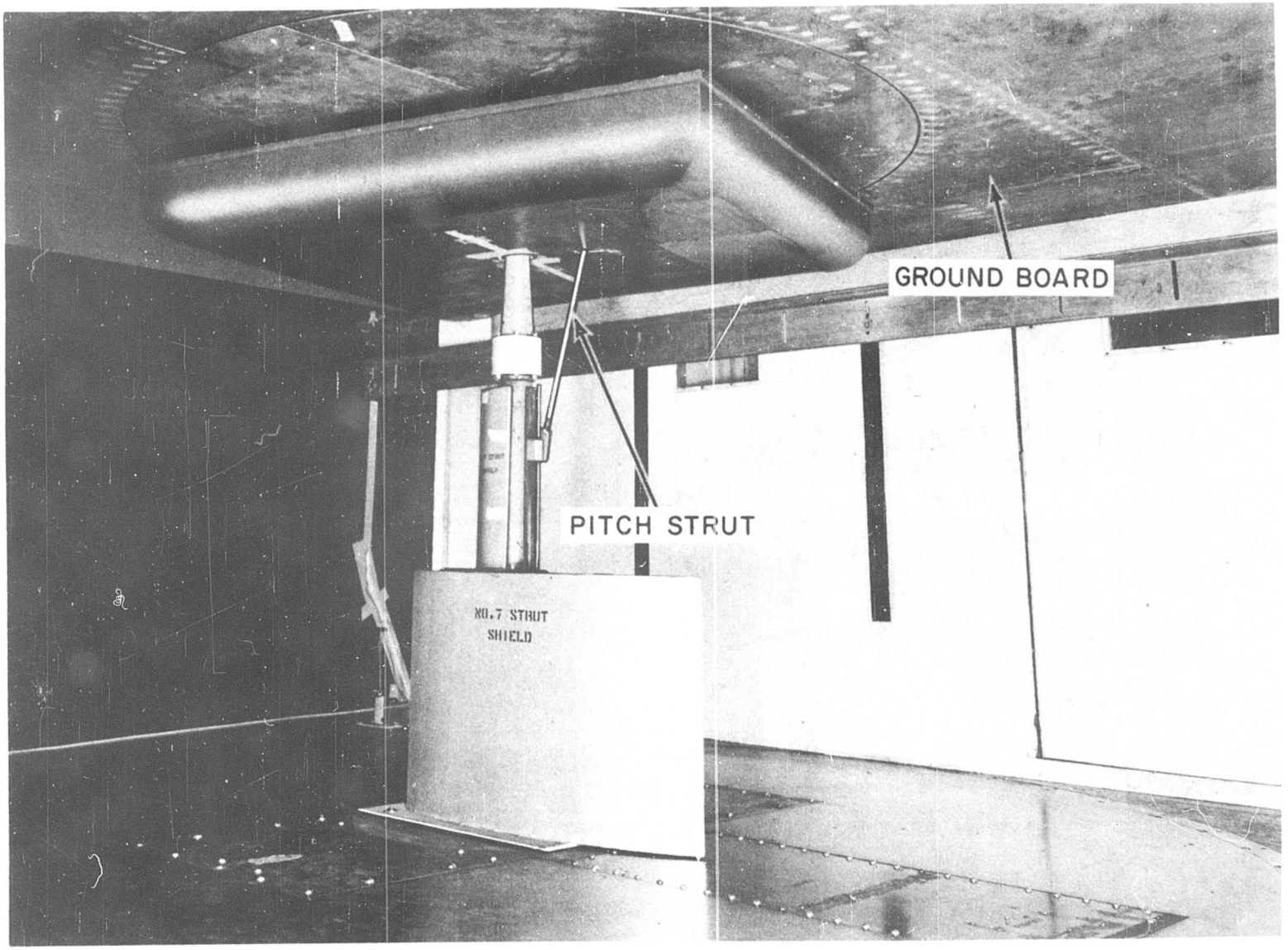

Figure 7. Tunnel Installation (Looking Upstream).

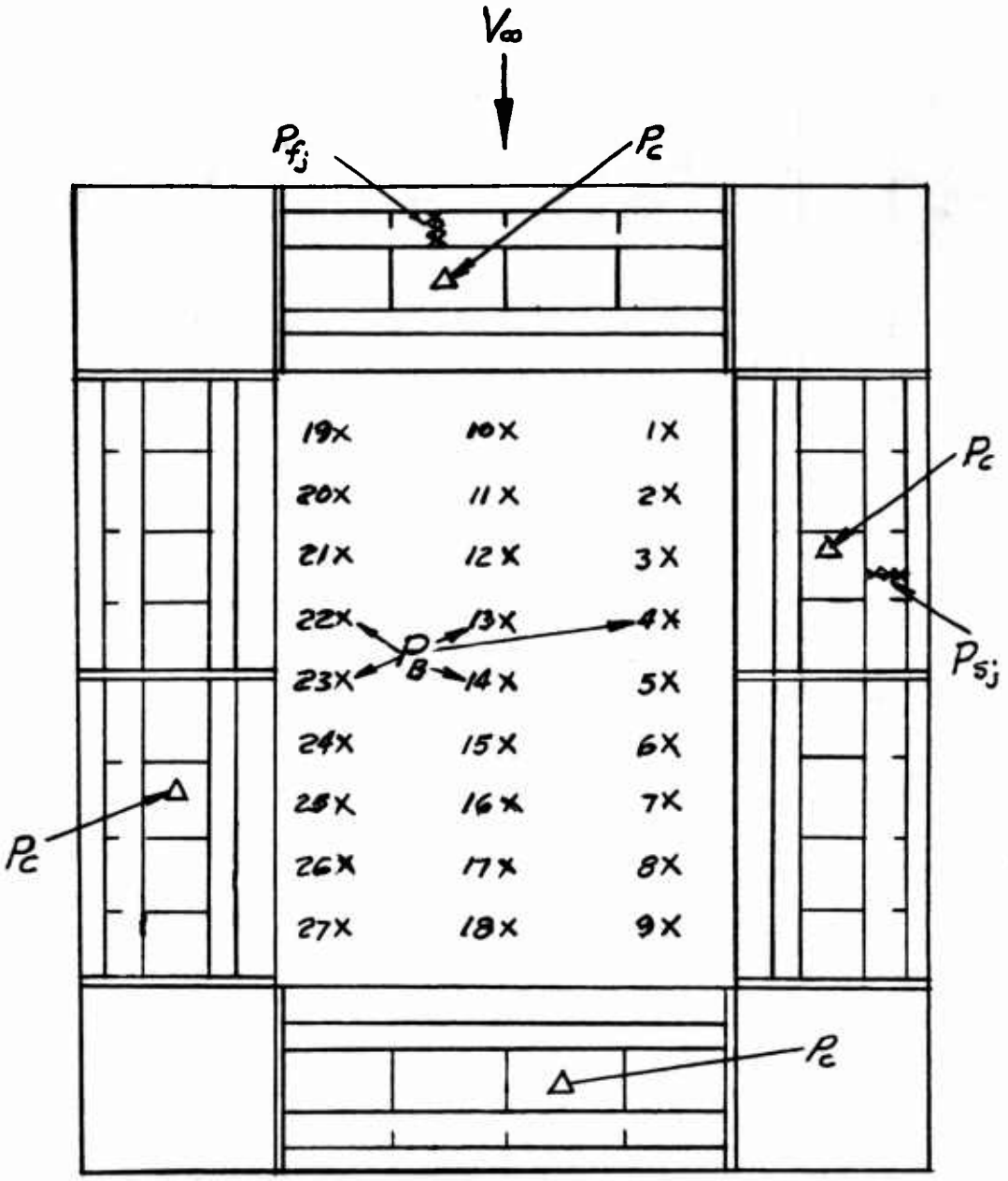

Figure 8. Base and Curtain Instrumentation.

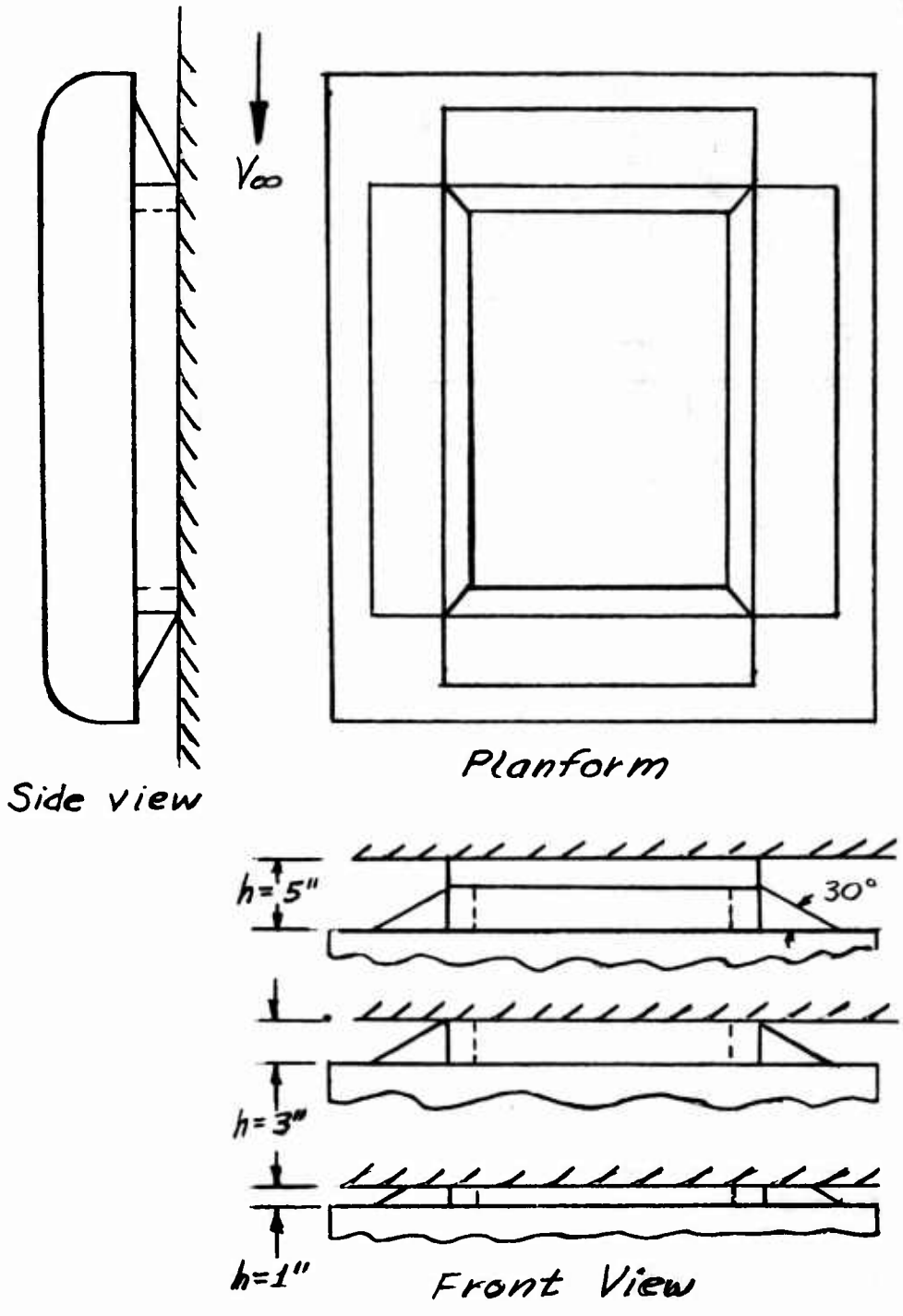

Figure 9. Dummy Cushion Configuration.

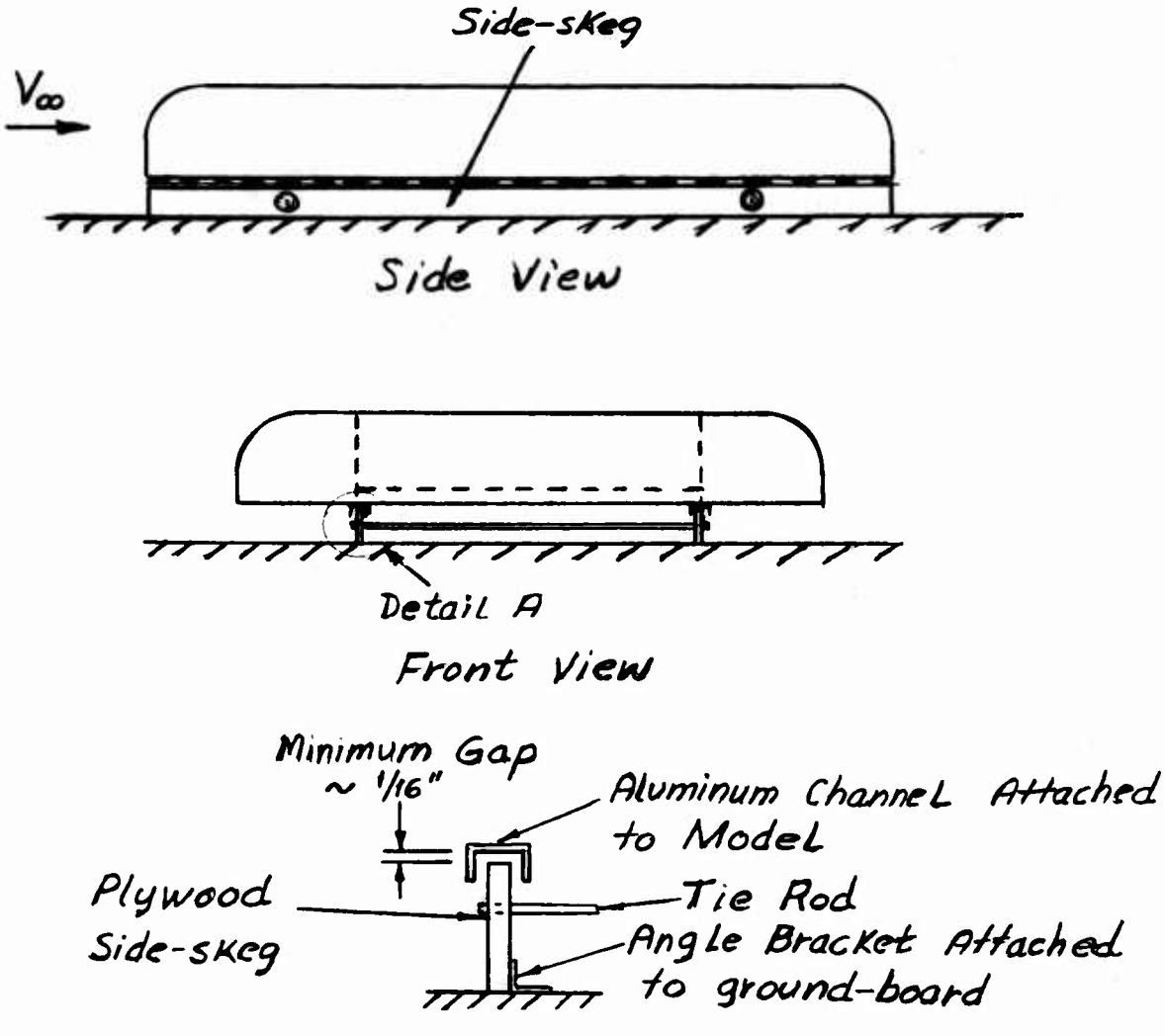

Figure 10. Side Skeg Configuration.

The streamlined configuration shown in Figure 2 was tested at the design height of 3 inches and over a range of 0 to 80 fps forward velocity and through a range of 0 to 92.5 psig primary nozzle pressure. Data were obtained with the nose and the tail fairings separately and in combination.

The side skeg configuration shown in Figure 10 was tested at the design height of 3 inches and over the velocity and primary nozzle pressure range.

In conjunction with the side-skeg tests it was found that a spoiler attached to the ejector exit lip markedly improved the hovering performance by causing the recirculating flow to detach from the ejector cavity. The spoiler consisted of masking tape as shown in Figure 11.

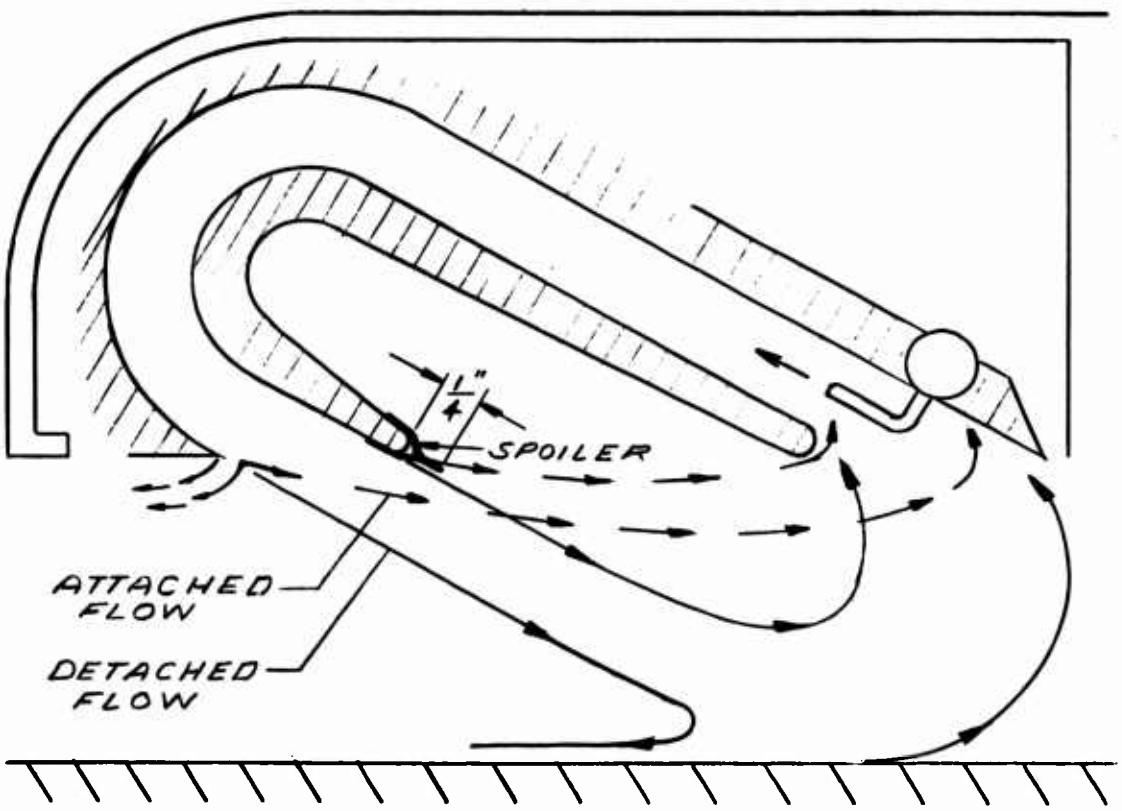

Figure 11. Ejector Spoiler Details.

Subsequent runs were made with the spoiler in position at the design height of 3 inches and with the streamlined nose fairing to observe the effect of detached flow on the hovering and low speed performance of the basic three dimensional configuration.

A complete summary of the test data, in tabular and graphical form is contained in Reference 1.

A. General Theory of Generation of Base Pressure by Ejector Action

In the recirculating ejector system® used on the model tested, the total lift is composed of five parts. These are:

1. Base pressure lift
2. Cavity pressure lift
3. Upper surface lift
4. Jet momentum lift
5. Primary momentum lift

These are shown schematically in the following figures.

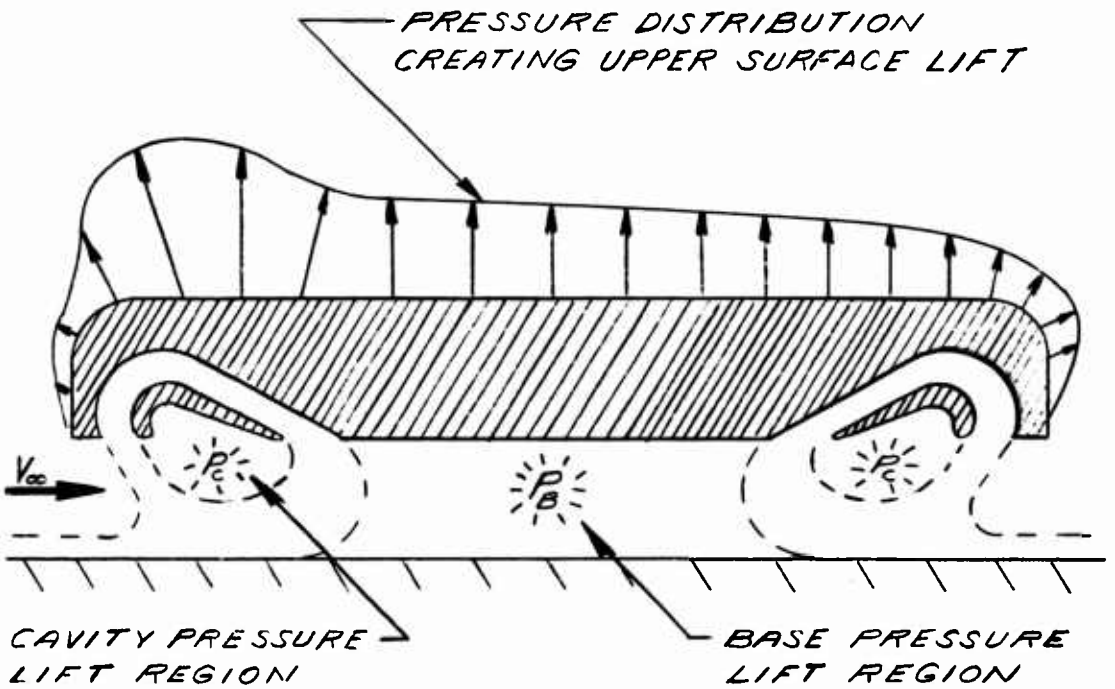

Figure 12. Cross Sectional View of the Model Showing the Regions of Base Pressure, Cavity Pressure, and Upper Surface Lifts.

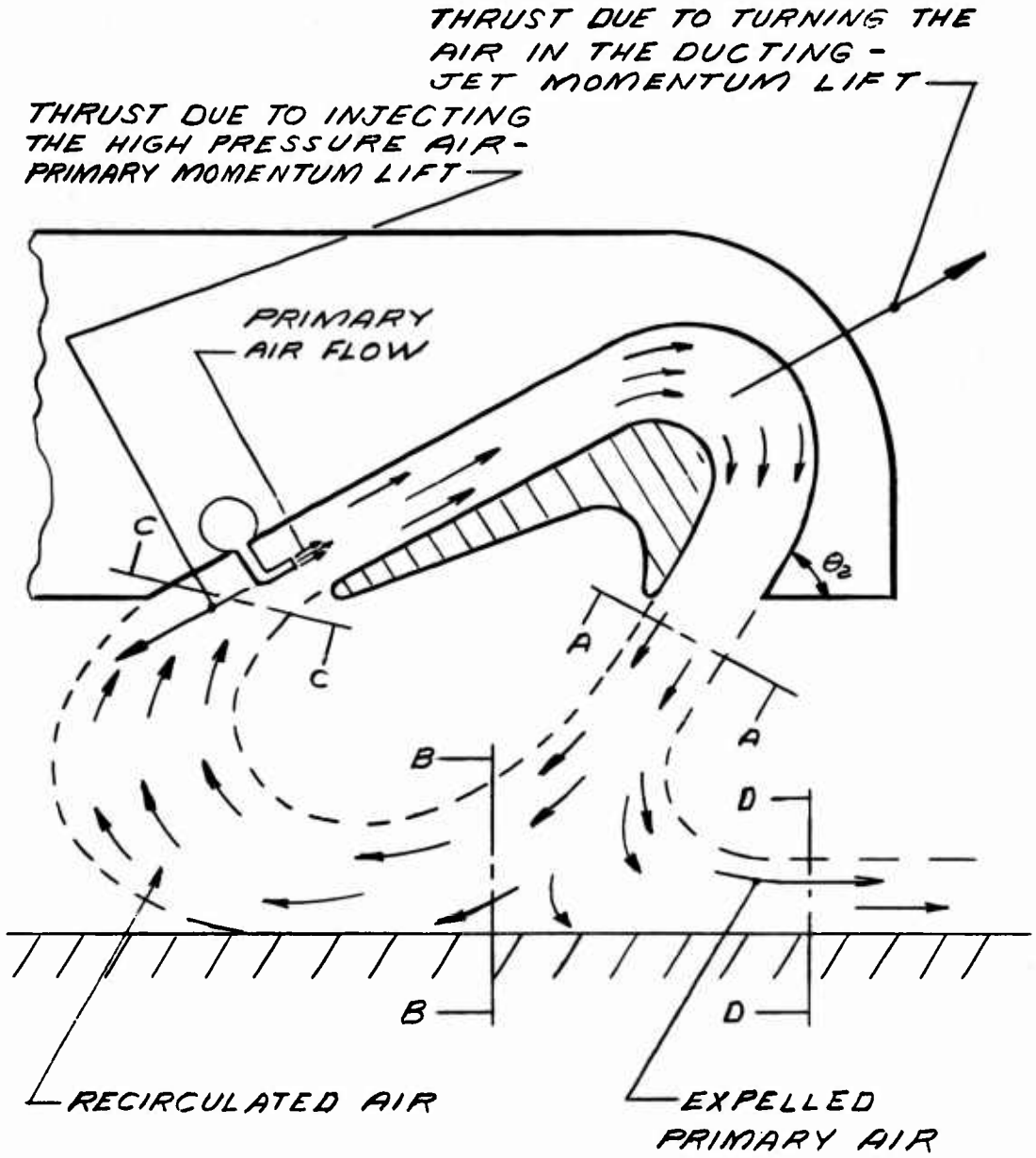

Figure 13. Regions of Primary Momentum Lift and Jet Momentum Lift.

In the recirculating ejector system a small amount of high pressure air, anywhere from 3 percent to 10 percent of the total amount of air recirculated through the ejector, is used to entrain the secondary or recirculated air. This entrained air is pumped through the system from section C-C to section A-A of Fig. 13. The tertiary flow, at section A-A, is then pumped to section B-B where it splits according to the specific geometry and positioning of the vehicle such as in heave or roll. In a steady state, level condition, with $V_\infty = 0$, the amount of air expelled at section D-D equals the amount of injected primary air while the remaining air is recirculated. A pressure, p_c, is generated in the region under the center block of the ejector. This cavity pressure is generally dependent on such parameters as operating height, mass augmentation, tertiary momentum, and discharge angle, θ_2. Since the magnitude of the subsequent base pressure generated during the recirculation phase is dependent on the cavity pressure, it is usually best to design the ejector so that this cavity pressure is either the same as or slightly higher than atmospheric pressure. Most 2-D testing was done on ejectors in which the gauge cavity pressure was approximately zero since positive cavity pressures were fairly difficult to create.

Experimental performance of the scale model ejectors is shown below.

p_o', psig	67.5	92.5
m/m'	20	18
ϵ, %	9.2	11.5

While the efficiency (ϵ) is considerably lower than values obtained on full scale models, the mass augmentation ratios (m/m') are representative of full scale values.

The recirculated stream, passing from section B-B to C-C, is forced to travel a curved path to re-enter the ejector so that a pressure jump is generated in the process. This pressure jump is referenced to the cavity pressure, p_c, so that the base pressure will be the sum of this cavity pressure and the pressure jump. The importance of zeroing out the gauge cavity pressure then becomes very apparent.

Due to the presence of these two pressure regions, as opposed to only one in the annular jet, a peak can be exhibited in the curve of p_b, or lift, versus height. The height at which this peak is obtained depends again on the geometry of the ejector but generally it can be made to occur at fairly low heights in respect to the operating height if the exhaust angle is kept flat (i.e. $\theta_2 \leq 30°$) and the mass augmentation used is fairly low (i.e., m/m' ≤ 15). There are other problems

introduced if the exhaust angle is made too flat. One of these is excessive required horizontal length of the ejector while another is the possibility of obtaining attached flow.

In the latter case the bottom of the center block has a coanda effect on the flow and instead of allowing the tertiary air stream to flow to the ground it causes part of the flow to move parallel to the base from the tertiary exhaust to the secondary inlet. When this condition is encountered, the cavity pressure becomes more negative and the base pressure drops. This is usually more of a problem at or above design height than it is below design height.

When the air is ingested at the secondary and passes through the ducting it imparts a force on the ducting that is dependent on the momentum of the flow and the angle through which it is turned. This is referred to as the jet momentum lift.

The primary momentum lift is the thrust applied to the nozzles when the high pressure primary air is expelled through them. In the present configuration this constitutes a down load or a loss in lift.

The last contribution to lift is obtained from the pressure distribution generated when the free stream air passes over the upper surface of the model. This is somewhat comparable to the upper surface lift of a conventional airfoil.

Although fairly extensive testing had been completed on the two dimensional recirculating ejector facility described in Ref. 3, (2-D report), additional experimental data was required to evaluate the effects of forward flights on a full recirculating curtain. The effects on lift, drag, and the resulting moments were to be investigated. This first wind tunnel test was made primarily to evaluate trends rather than to obtain specific design information.

The wind tunnel tests were run at heights ranging from 1 to 5 inches while using a primary total pressure of 67.5 and 92.5 p.s.i.g. The effects of yaw, pitch, and roll were evaluated during these runs.

As can be seen in the planform view of the model used in this test, Fig. 1, the ejector assemblies used at the corners are separate units from the side or front ejectors and as such can be either used or left off. In order to evaluate the need for these corner ejectors, several initial tests were run at design height of 3 inches with the corners in various configurations. These configurations were:

1. Corners left off
2. All corners aligned front and rear
3. All corners aligned sideways
4. Rear corners aligned with rear
5. Front corners aligned with front

The results of these tests are shown in Figure 14 and indicate that the corner configuration used apparently had little effect on the lifting performance of the model. The effect on drag was approximately the same, as shown in Figure 15, and for this reason the configuration used in the testing, and referred to in the report as the basic configuration, was the one with corners left off.

Tests were run to evaluate the lift generated by the model in several configurations from which the effect of upper surface lift and body drag could be obtained. The results of these runs are shown in Figure 16. The points shown are average values from the test runs over the prescribed velocity range. The dummy cushion referred to is a wooden mockup of the external geometry of the recirculating air curtain around the machine (Figure 9). The runs were made with the dummy curtain mounted on the model or on the ground board in addition to ones made with the model alone. The dummy curtain would simulate a complete air curtain allowing no through flow under the machine. The model alone data would simulate the effect of a collapsed air curtain under the vehicle so that the free stream could flow under the vehicle.

The test runs were made to evaluate the following effects in forward flight.

1. Effect of height on lift, drag and stability
2. Effect of pitch on lift, drag and stability
3. Effect of roll on lift, drag and stability
4. Effect of yaw on lift, drag and stability

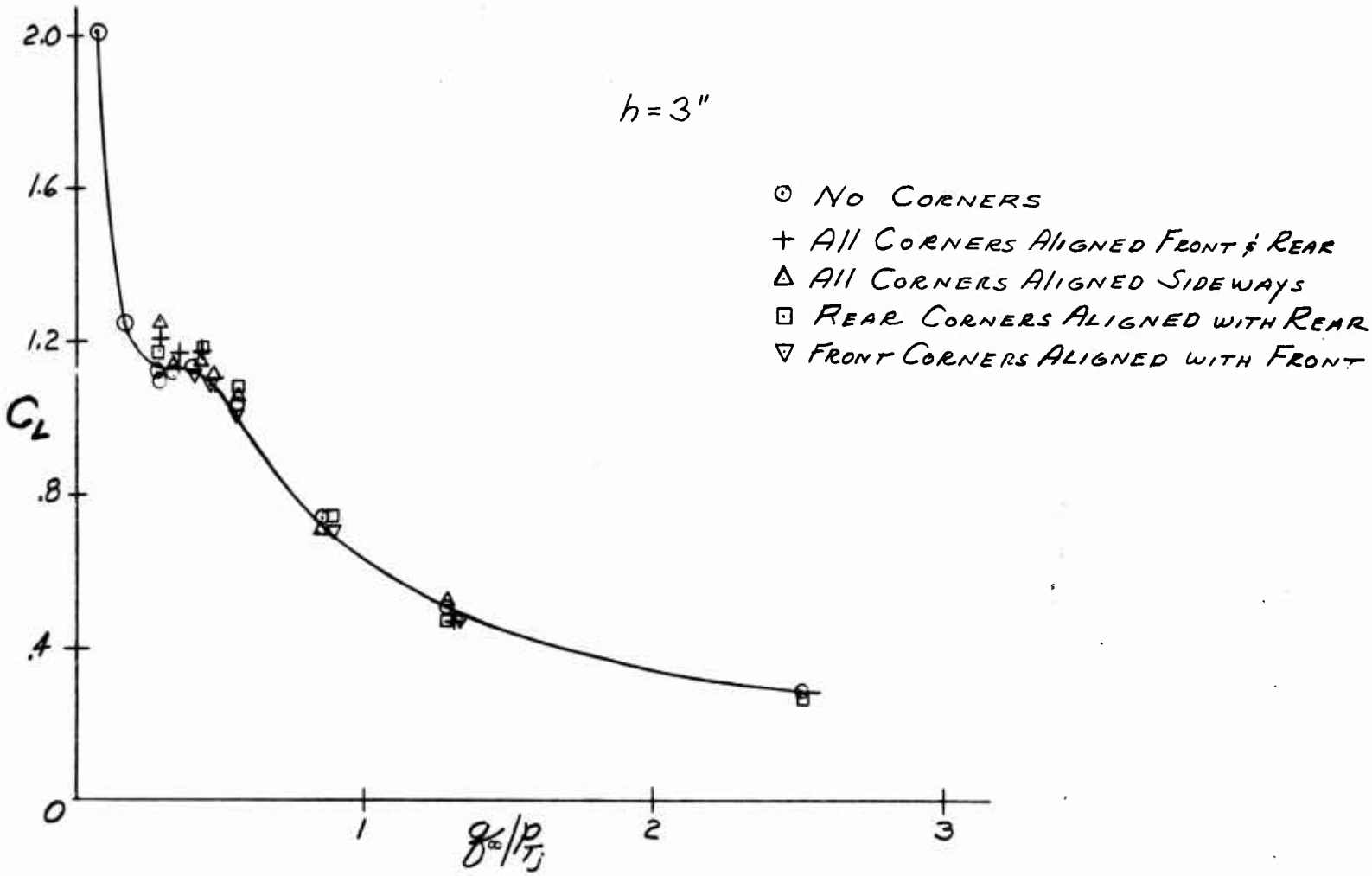

Figure 14. Effect of Corner Configuration on Lift.

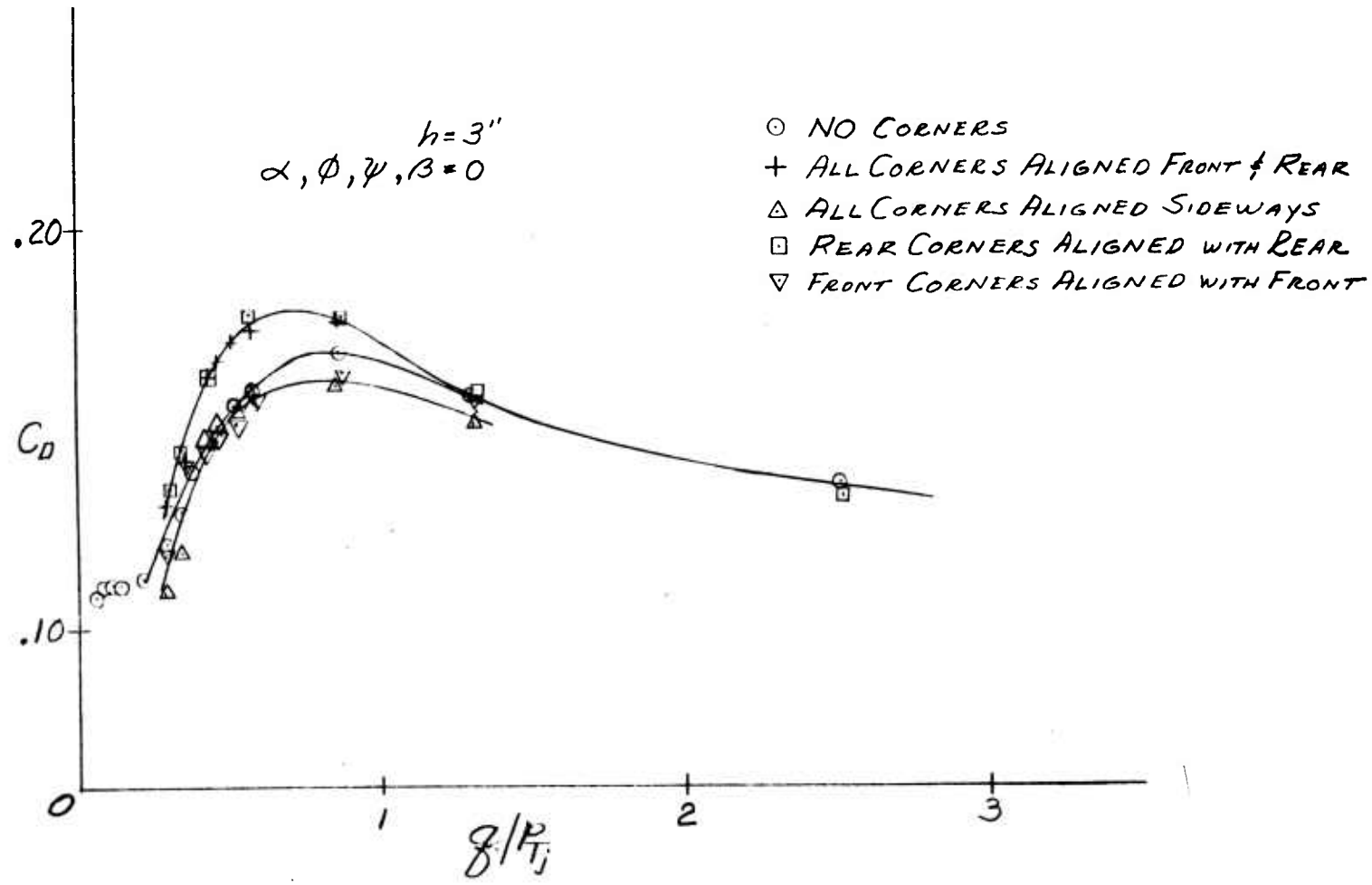

Figure 15. Effect of Corners on Cushion Drag.

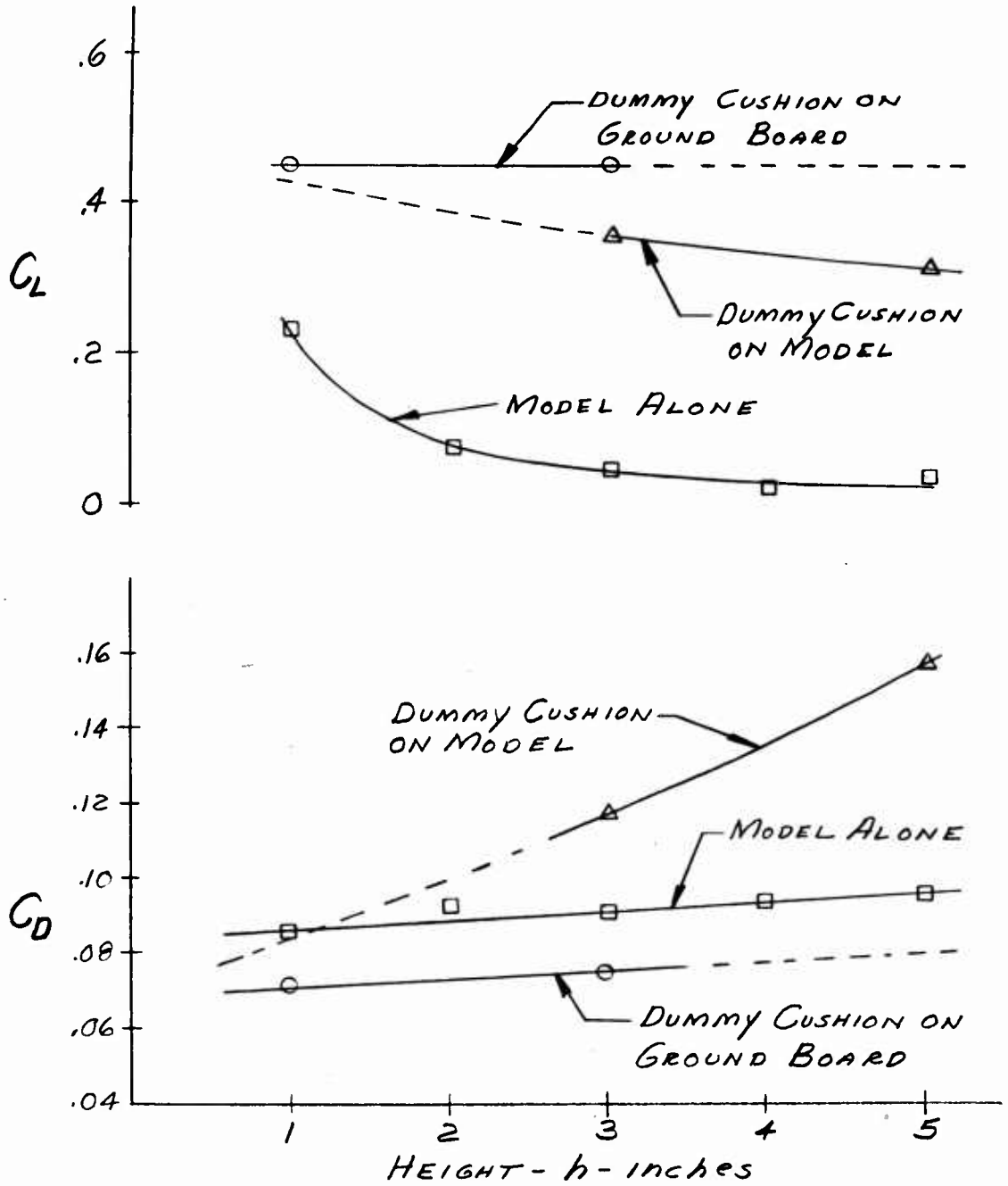

Figure 16. Profile Lift and Drag Coefficients.

B. Experimental Lift Data

1. Effect of Height on Lift

The results of the runs to obtain the lift variation with height are shown in Figures 17 and 18. The previously mentioned peak in the lift curve is exhibited in the runs for both primary pressures although the peaking effect does diminish for the higher velocities. The curves show a very pronounced increase in lift at the higher velocities for heights of 3" and above and additional runs were made to investigate the cause of this. The results of these tests, run at h = 3 inches and p_o' = 67.5 psig, are shown in Figures 19 and 20. It was apparent that the flow had attached at this height for the basic configuration thus yielding a decreased cavity pressure and base pressure. When a spoiler was attached at the tertiary exhaust the flow detached and the base pressure and cavity pressure became more positive. A comparison is also given in Figure 21 between the three dimensional test values, with and without the spoiler, and those obtained in the two dimensional tests of the original configuration. The two dimensional test was made using one of the ejectors of the test model in a test facility with solid side and back walls. This again demonstrates the loss in performance due to the attached flow.

In the plot of base pressure and cavity pressure of Figure 19, it can be seen that the curves for the basic configuration and the basic configuration with the front ejector turned off are approximately the same. This can be explained since in the former case the front jet is only partially effective due to attachment and as the dynamic head of the free stream increases it will have the tendency of breaking down the front jet even further. The ram pressure of the free stream, while breaking down the front jet, will tend to replace it since a base pressure can be created by the side and rear jets while being fed by this dynamic head.

At the heights above 3 inches the effect of corner leakage was an additional factor in the loss of lift. From these considerations it is apparent that a properly designed corner configuration is required on a GEM utilizing recirculation in order to bring the 3-D performance up to the 2-D potential.

Lift data are summarized in Figure 22 for pitch, roll, yaw and ejector tilt angles of zero degrees. The quantity $C_L\ (q_\infty/p_{T_j})$ represents the ratio of the lift developed to that which would be developed if the curtain pressure, p_{T_j} acted on the reference area, S_r; while the quantity q_∞/p_{T_j} is the ratio of free stream dynamic pressure to curtain total pressure.

Two regimes of operation are immediately apparent. True GEM operation is to the left of the dotted line through the breaks in the lift curves while to the right of the dotted line the curtain is at least partially blown away and through-flow passes under the vehicle.

It will be noted, particularly for the 3, 4, and 5 inch heights that the lift curve slopes are considerably greater than that observed with the dummy cushion in place. This phenomenon may be explained by both corner leakage which becomes pronounced at these heights and ejector flow attachment (in hover). At the 1 and 2 inch heights where the aforementioned effects are negligible, the lift curve slope closely approximates the dummy cushion lift coefficient.

Figure 23 presents hovering lift augmentation data and illustrates the performance penalty encountered at the 3, 4, and 5 inch heights. Lift augmentation is defined as the lift generated divided by the lift out of ground effect (momentum lift). Thus the observed augmentation was computed as:

$$A = \frac{L}{J - J' \sin\Theta}$$

while the theoretical augmentation was computed as:

$$A = 1 + \frac{(1-e^{-2\frac{t}{h}(1 + \cos\Theta_1)}) (\frac{S_B}{S}) (\frac{S}{hc})}{2(\frac{t}{h})}$$

where the cavity pressure p_c is assumed to be zero.

The good agreement between theory and the data at h = 1 inch and h = 2 inches indicate that the effects of corner leakage and flow attachment were minimal at these heights. The slope of the lift curve at the 1 inch and 2 inch heights in Figure 22 is in fair agreement with the dummy cushion lift coefficient as might then be expected.

The low hovering lift augmentation observed at the 3, 4, and 5 inch heights must be attributed to both corner leakage and flow attachment at these heights. In forward flight the ram effect of the free stream apparently offsets these effects somewhat, and causes the flow to detach, accounting for the high lift curve slope at the 3, 4, and 5 inch heights.

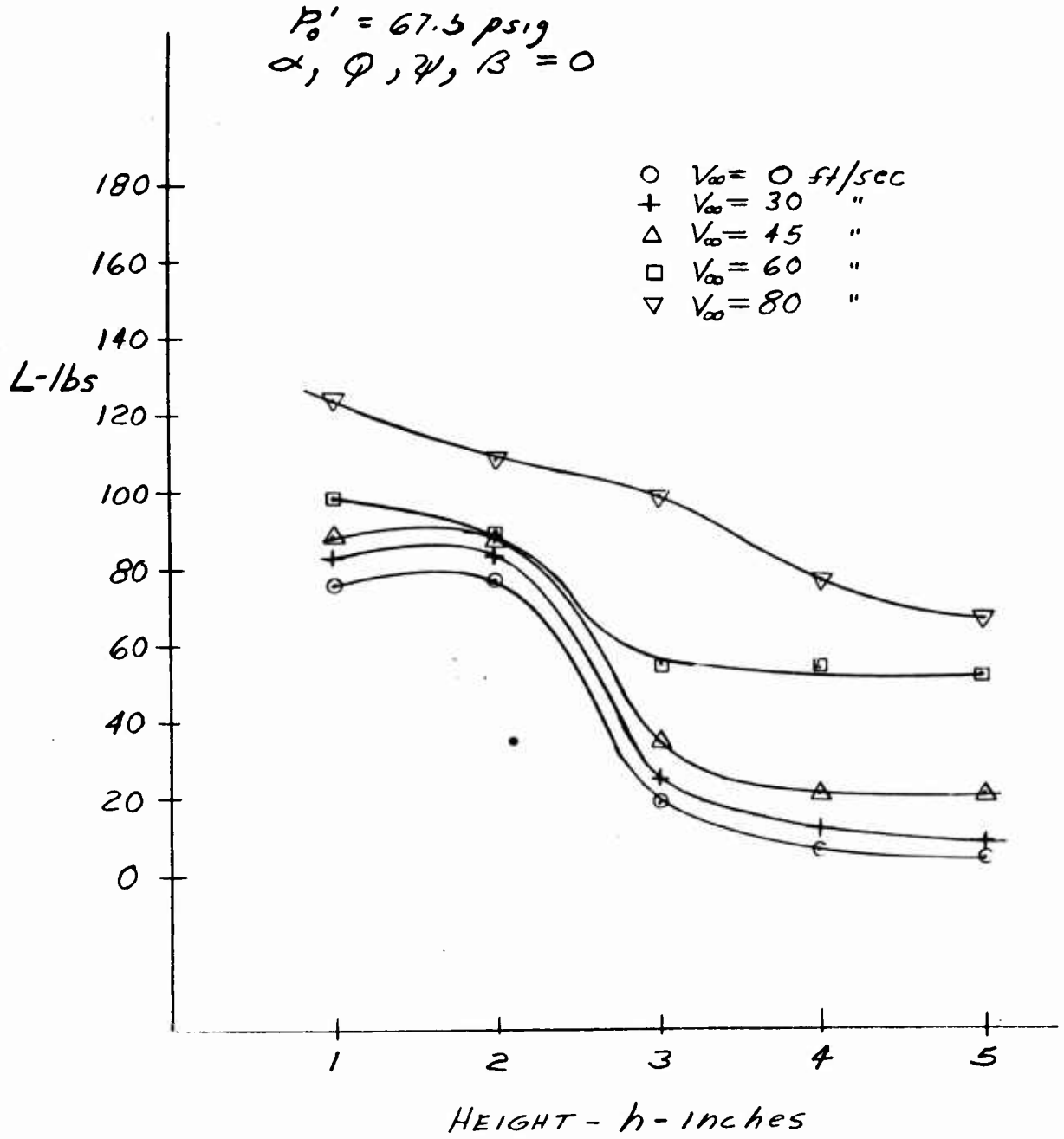

Figure 17. Effect of Height on Lift.

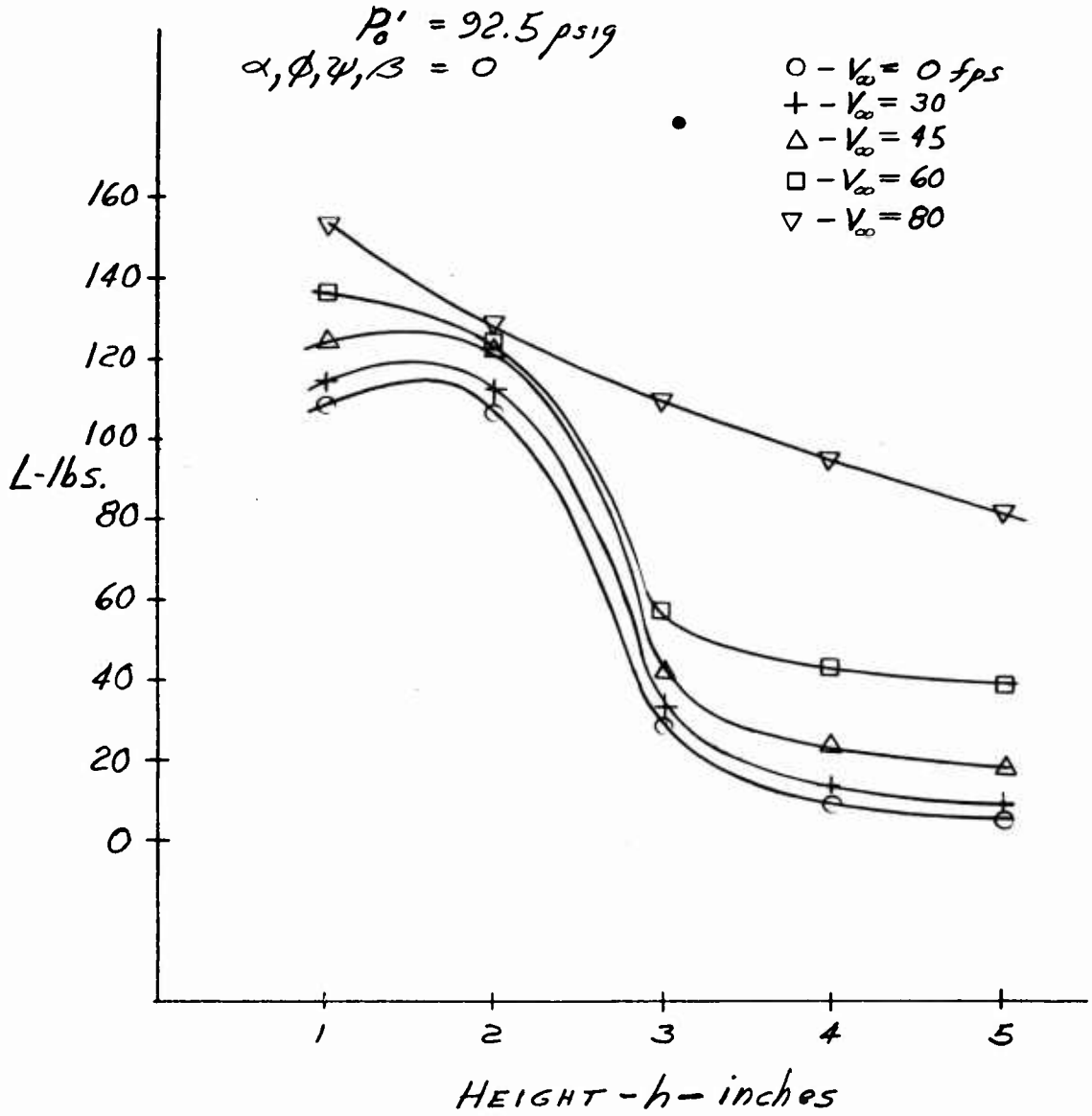

Figure 18. Effect of Height on Lift.

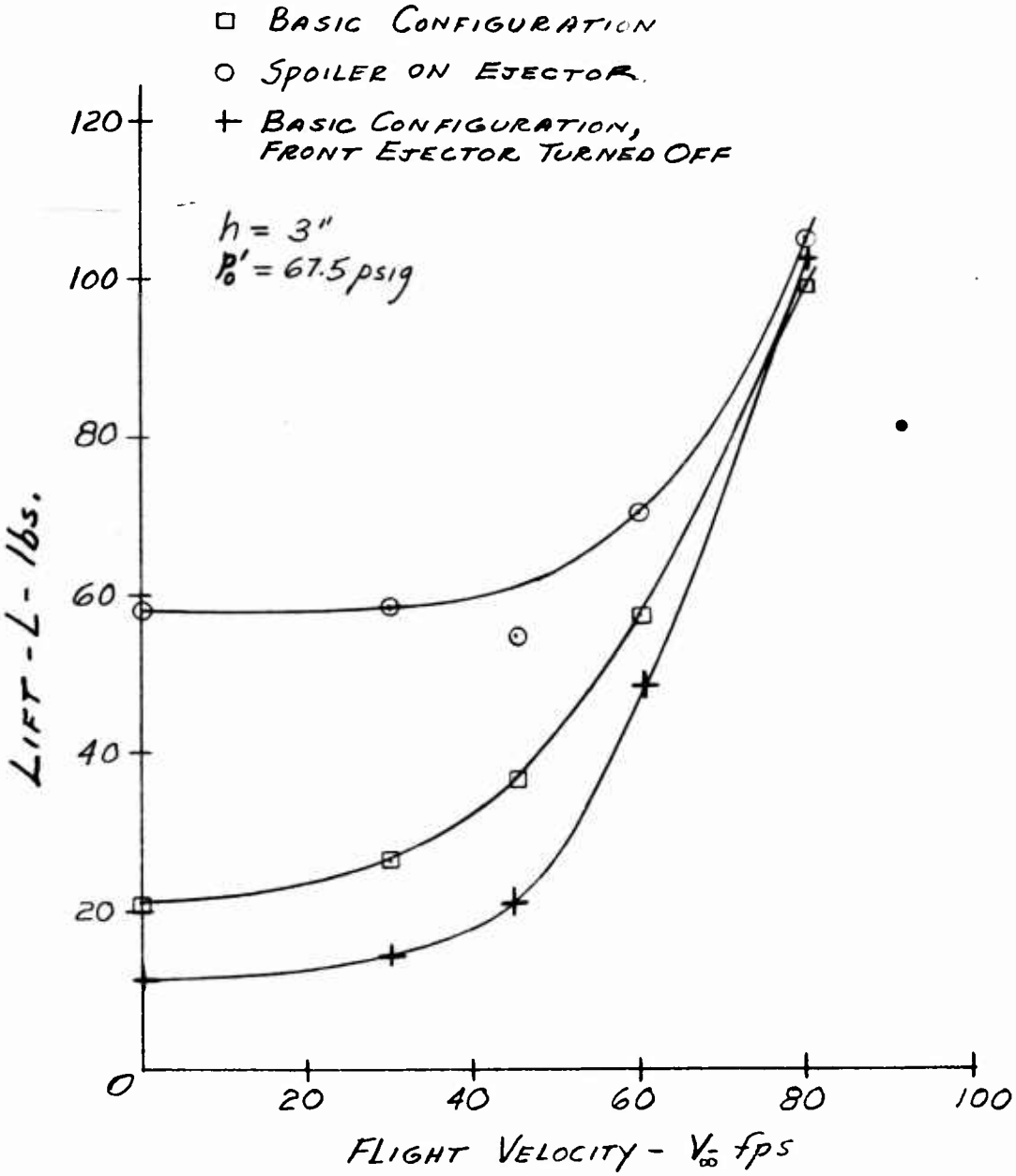

Figure 19. Effect of Speed on Lift.

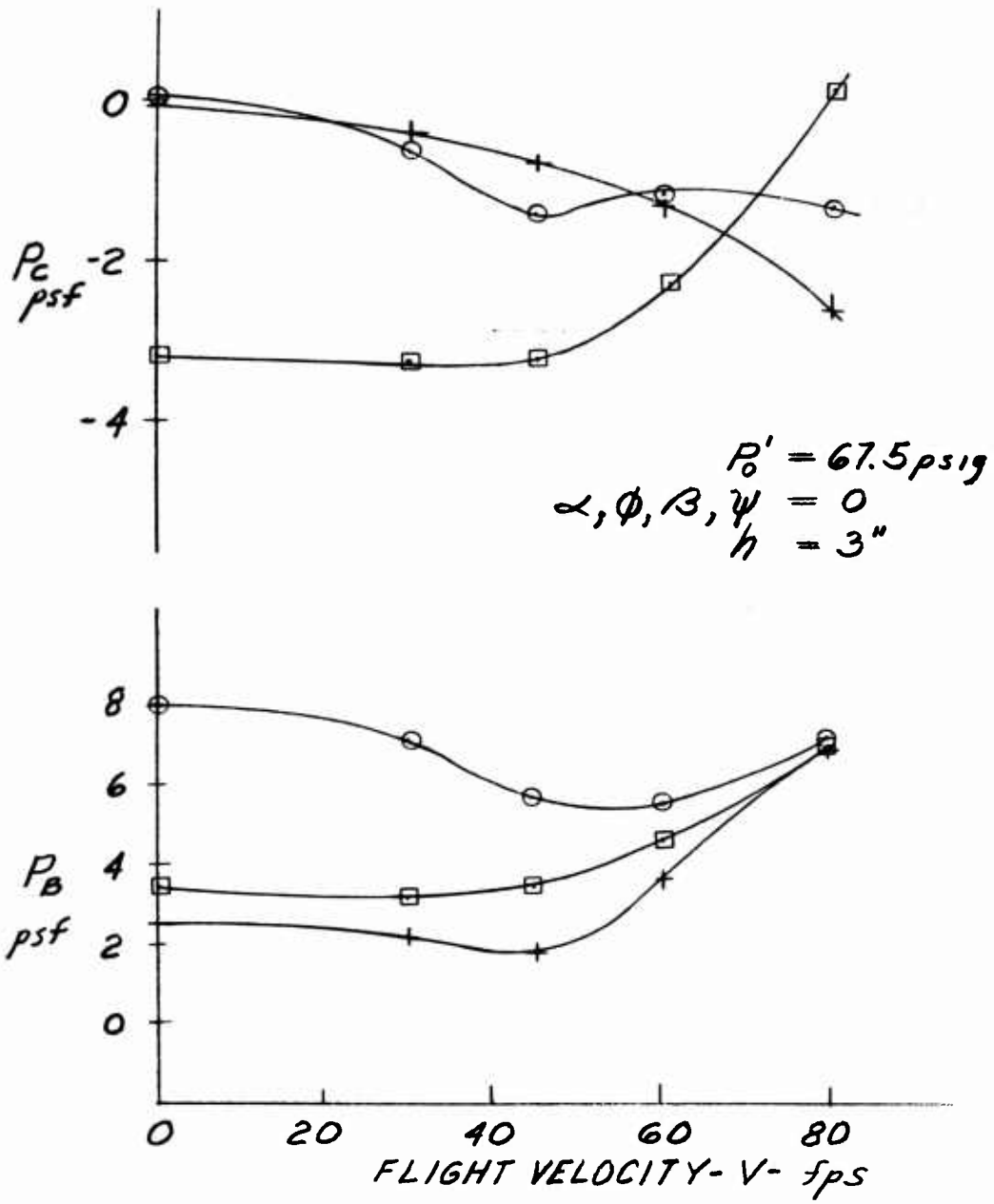

Figure 20. Effect of Speed on Base and Cavity Pressure.

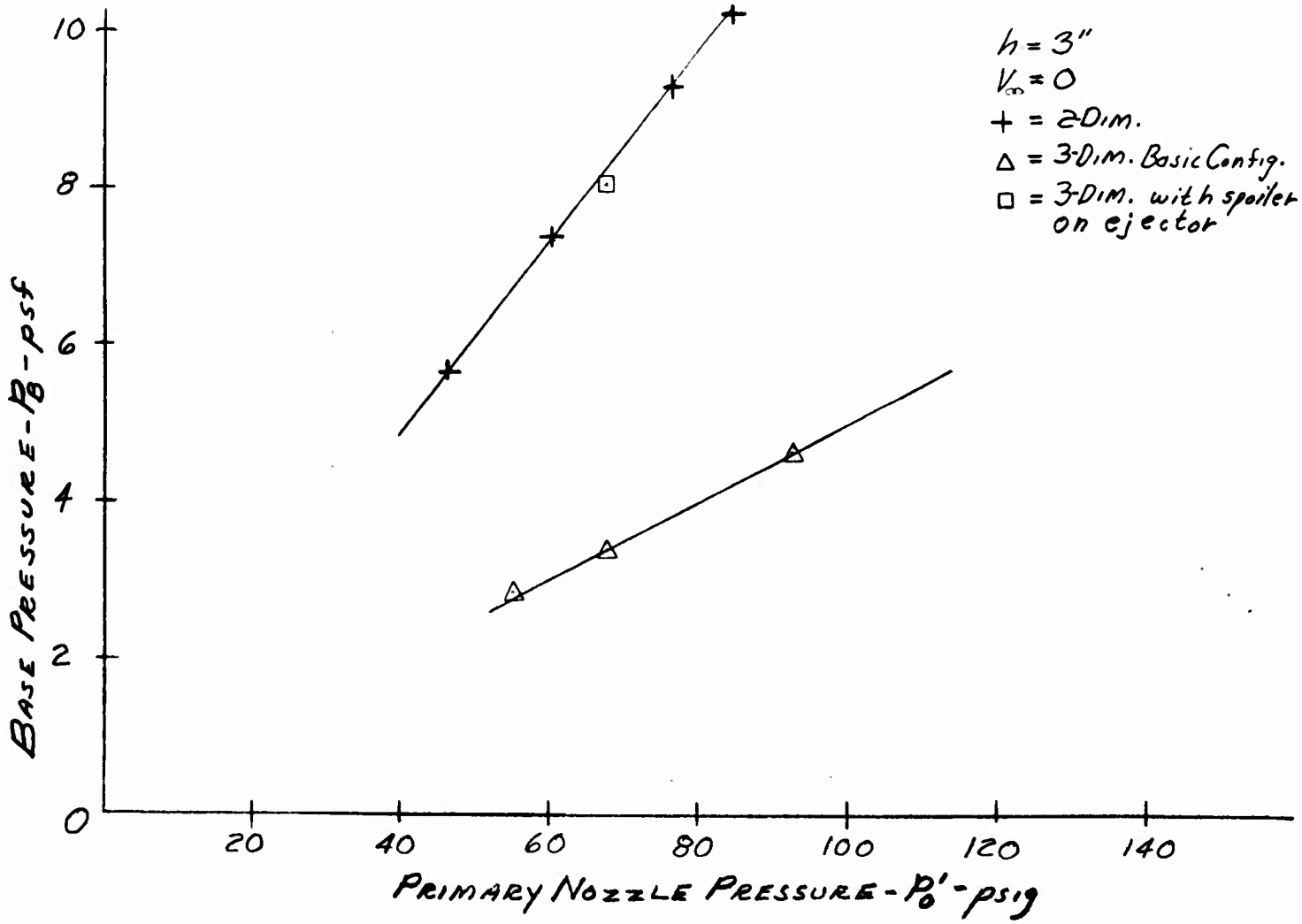

Figure 21. Comparison of 2-Dim. and 3-Dim. Base Pressure.

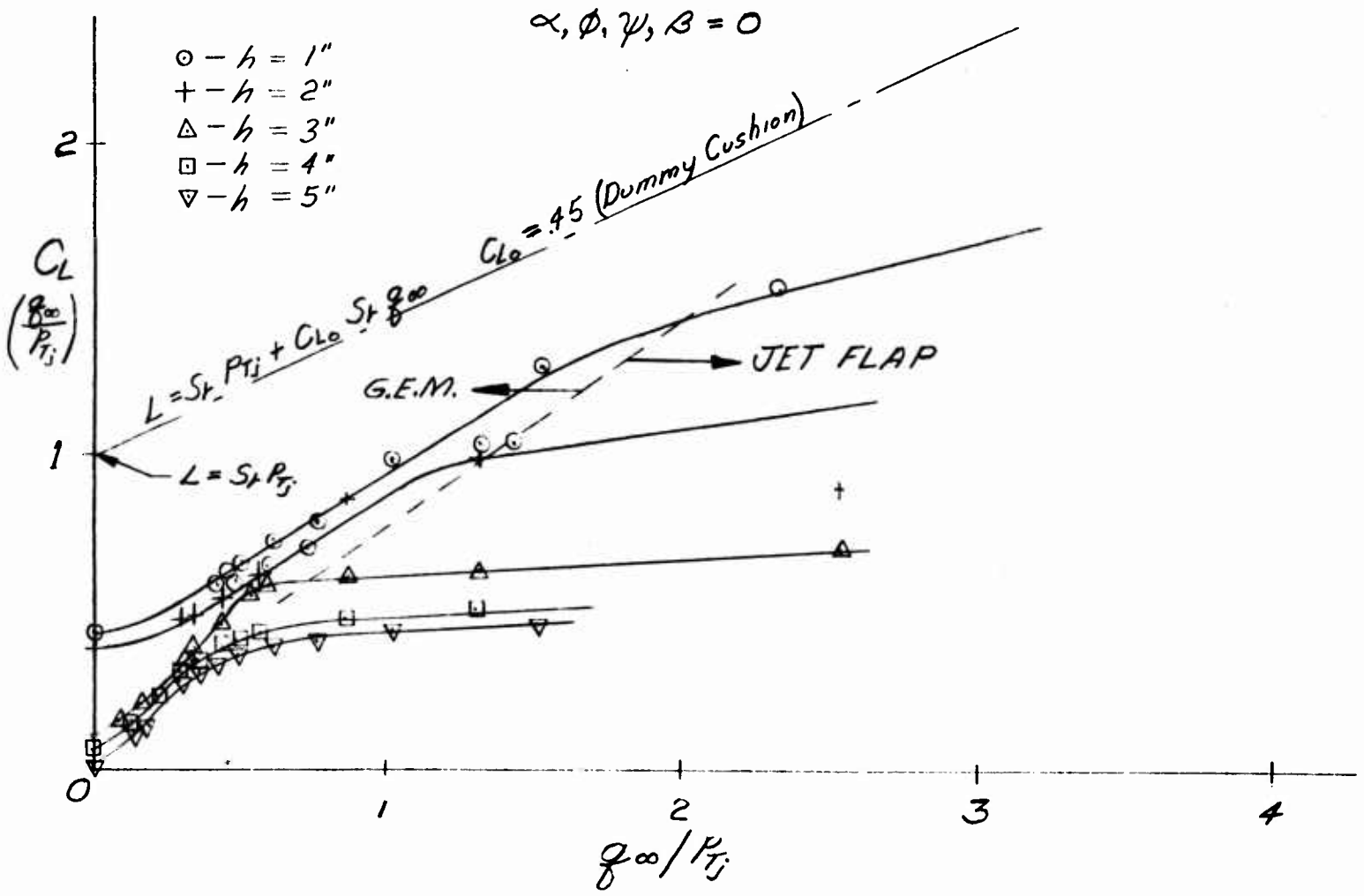

Figure 22. Effect of Speed on Lift.

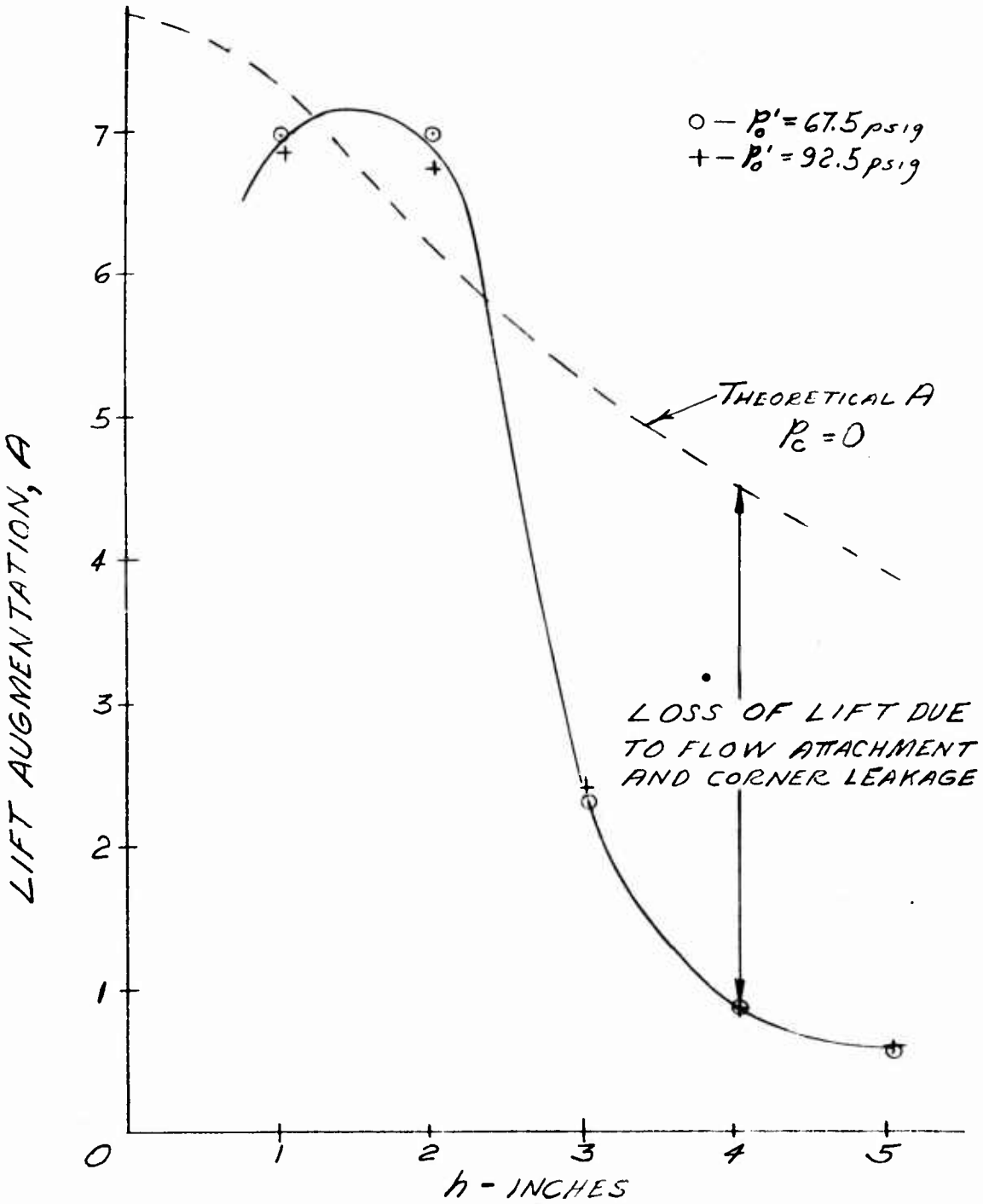

Figure 23. Hovering Lift Augmentation.

2. Effect of Pitch on Lift

In the runs evaluating the effect of pitch summarized in Figures 24 thru 28, two separate effects account for the change in lift. The first of these is the contribution of the upper surface lift. As the machine tilts nose up the upper surface lift increases as would the lift due to the upper surface of an airfoil. The opposite is true in the nose down case. The next effect that needs to be considered is the change in base pressure due to the variation in ejector height from the front to the rear of the machine as it pitches.

In the hovering mode the high jet, which generates the lowest base pressure, governs the base pressure so that the curves of lift versus pitch angle are symmetrical about the α = 0 line. This symmetry is present at all heights.

At the low heights, h = 1 and 2 inches, the allowable pitch variation was small. Since the total lift is such a strong function of base pressure, as is evidenced by the value at zero velocity, the base pressure would still dominate the variation in lift versus pitch angle and the curves are again symmetrical about α = 0.

At the higher heights and velocities the curves lose their symmetrical pattern. This can be explained by analyzing the effect of the free stream dynamic head on the tilted machine in addition to the upper surface lift. In the case of the nose down configuration the upper surface lift is decreased and the base pressure decreases also since it is dependent on the high rear jet. When the machine pitches up, the upper surface lift is increased. In addition the dynamic head of the free stream fortifies the front portion of the recirculation system and allows the lower rear portion to regulate the base pressure thus increasing it.

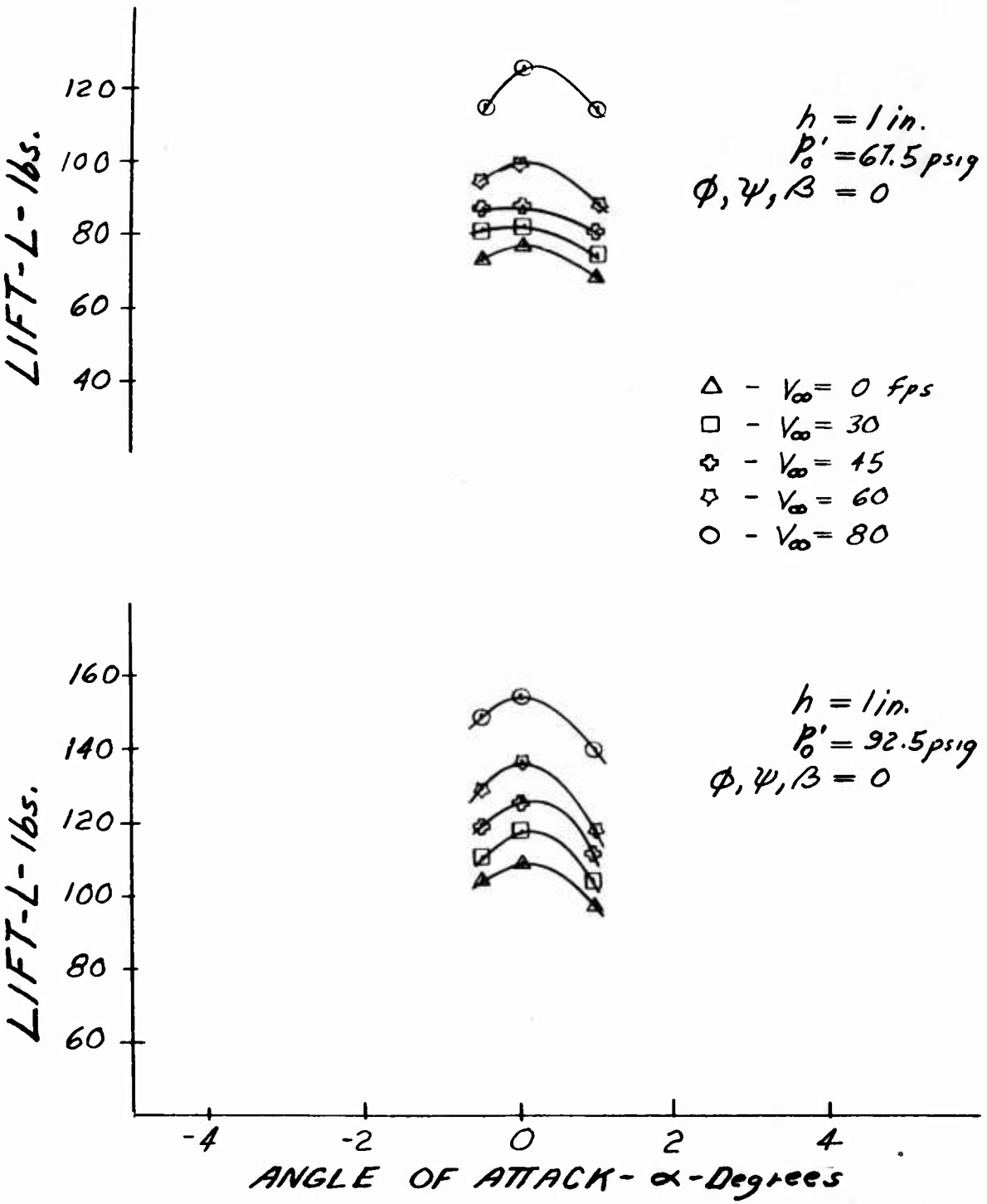

Figure 24. Effect of Pitch on Lift.

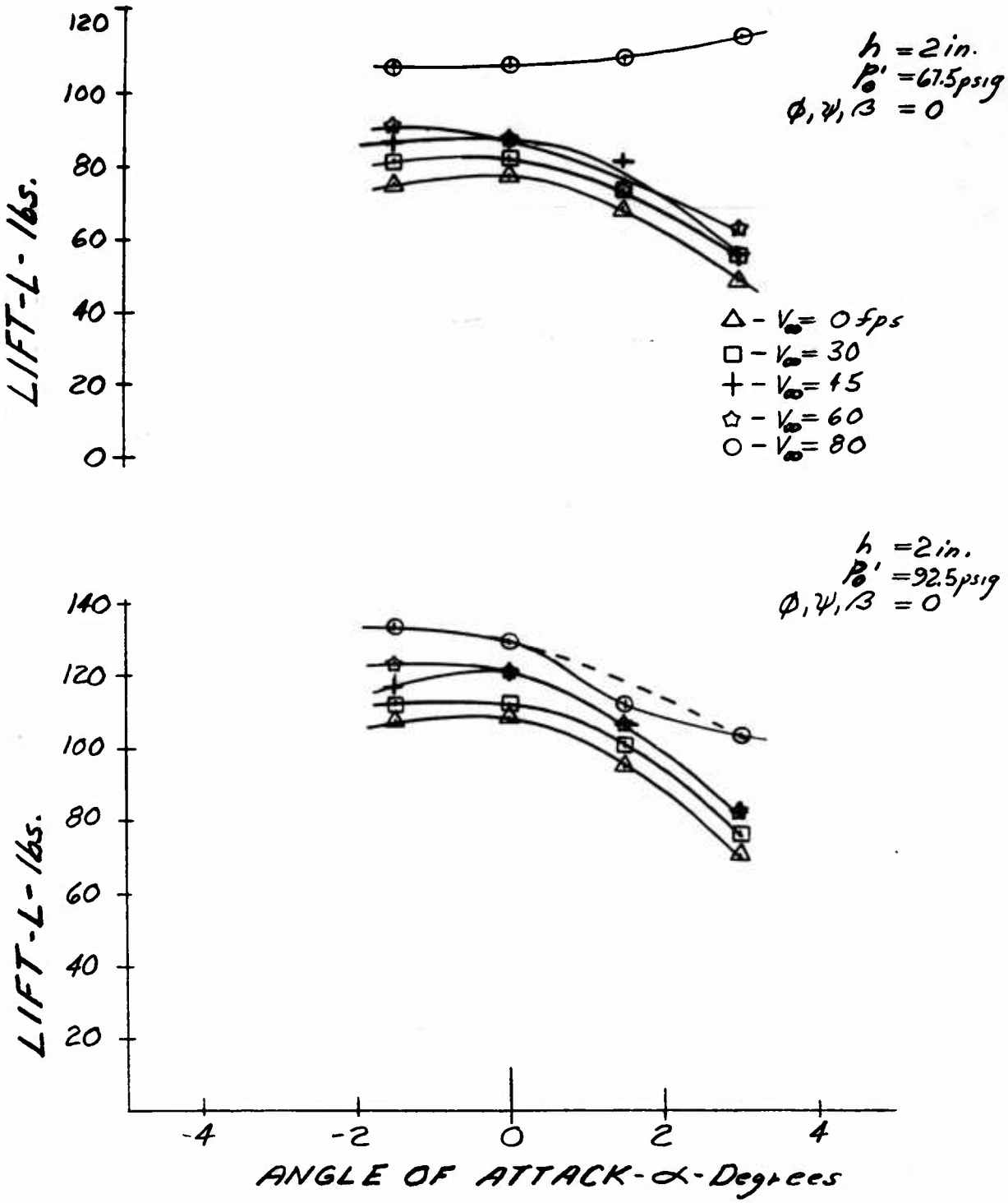

Figure 25. Effect of Pitch on Lift.

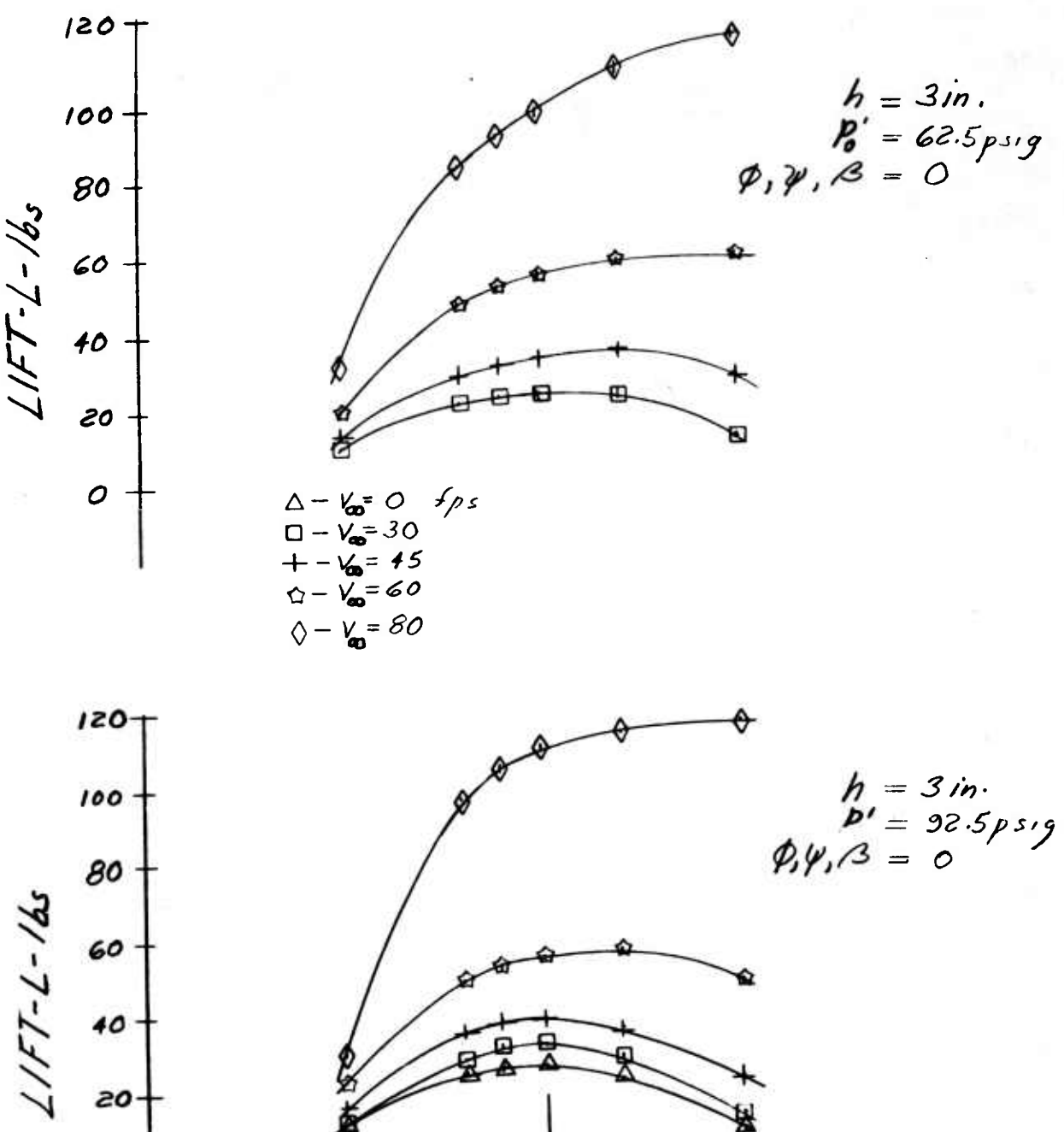

Figure 26. Effect of Pitch on Lift.

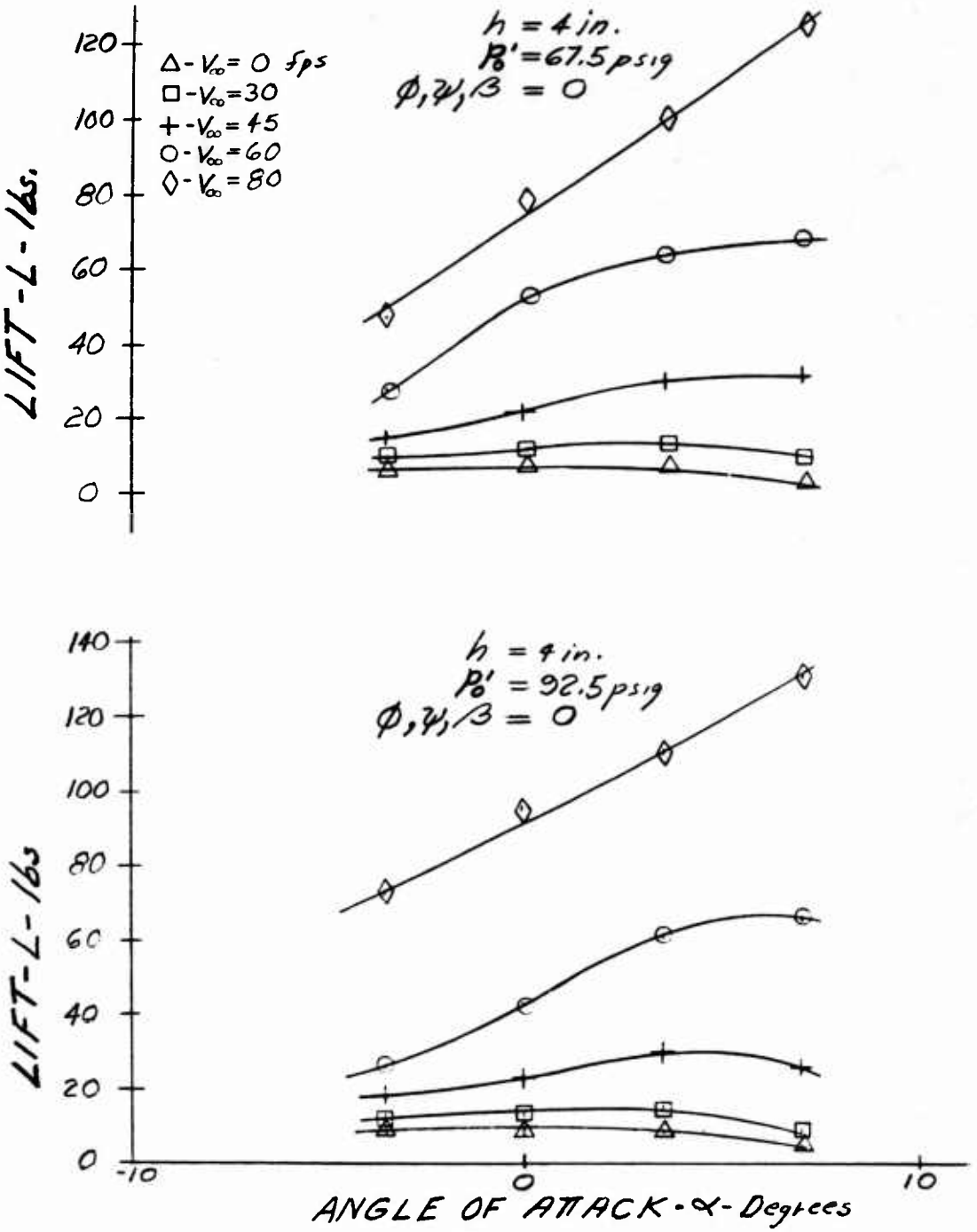

Figure 27. Effect of Pitch on Lift.

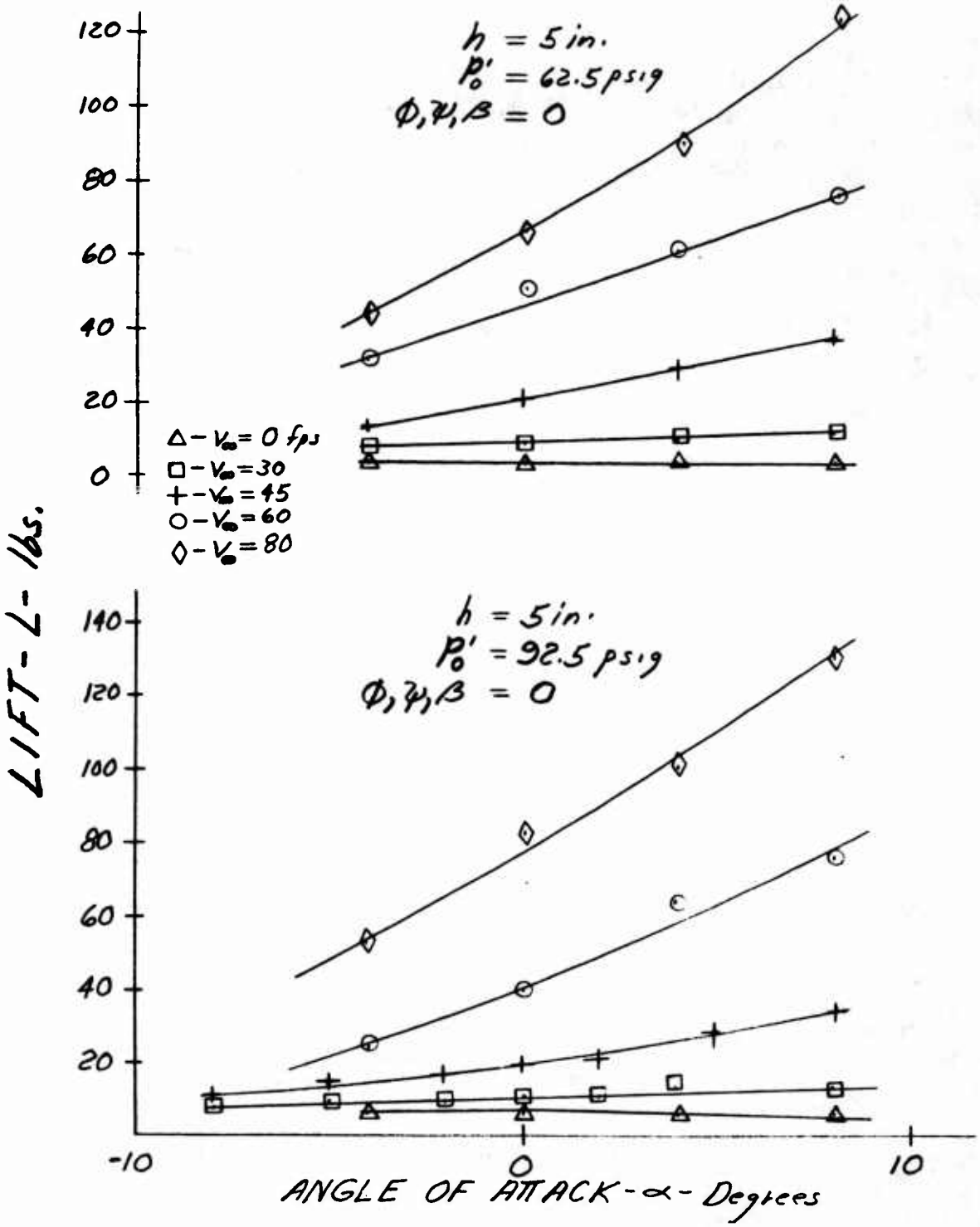

Figure 28. Effect of Pitch on Lift.

3. Effect of Roll on Lift

The variation in lift due to roll angle, being a symmetric function of $\emptyset$, was tested predominantly in the positive $\emptyset$ range. Since the upper surface lift does not change appreciably in the roll condition, due to a constant centerline α_c, the curve of lift versus roll angle is mainly dependent on base pressure changes.

The variation of lift versus roll angle at h = 3 inches is presented in Figure 29. The total lift decreases at all velocities as the roll angle is increased. In this case, where the jet height varies around the machine, the base pressure is determined by the weakest jet which occurs at the high side of the vehicle.

A comparison is given in Figure 29 between the lift measured in the roll runs and that predicted by referring to the plots of lift versus height. The increment in lift was predicted by evaluating the change in lift from a 3" height to that obtained at a 4.4" height which corresponds to the height of the high secondary inlet at a roll angle of 6°. The predicted values are shown as flagged symbols in Figure 29. The trends of reduced lift due to the high jet weakening the curtain are borne out by this comparison.

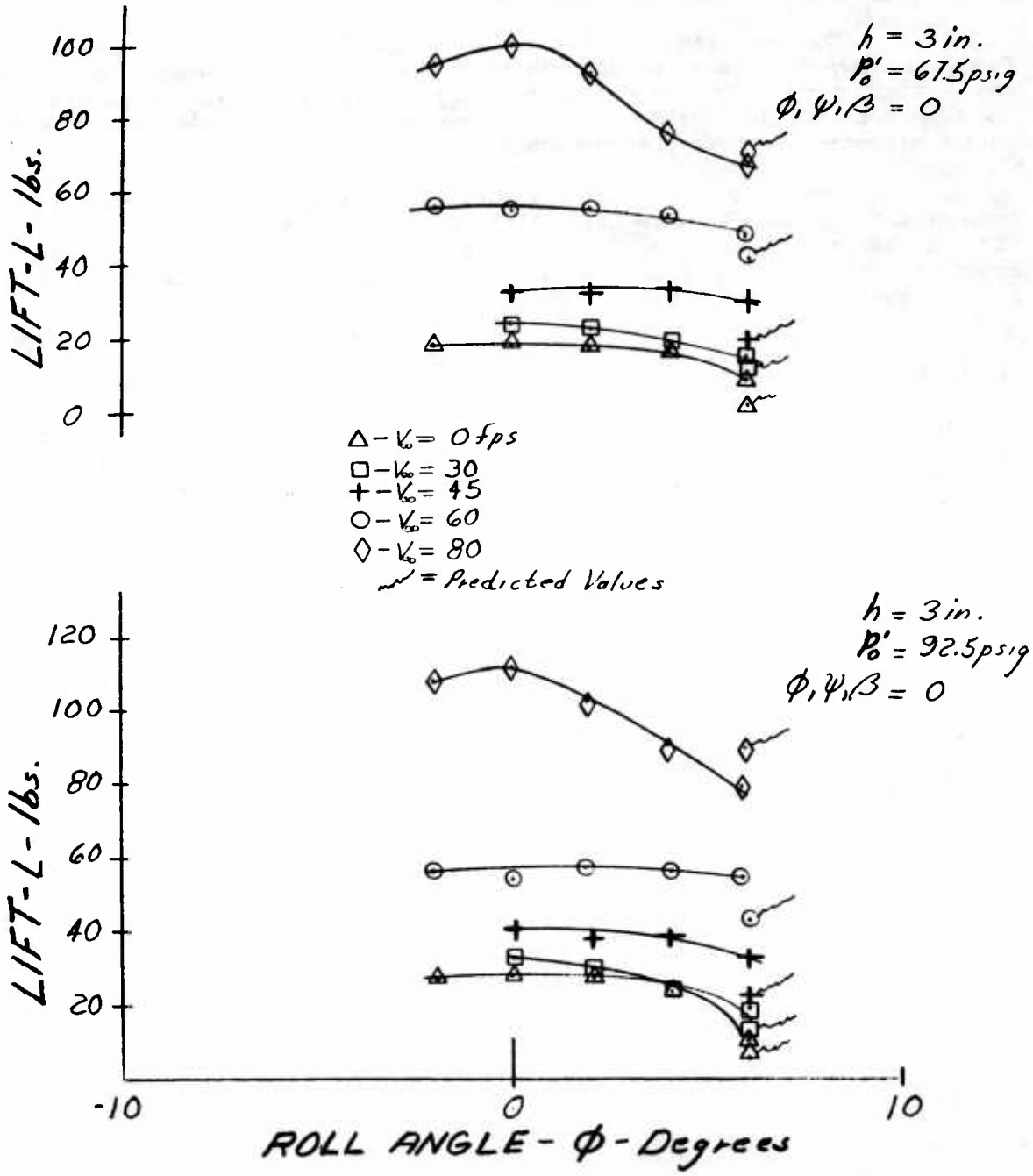

Figure 29. Effect of Roll on Lift.

4. Effect of Yaw on Lift

The test data on the effect of yaw on lift at a height of 3 inches over the velocity range is presented in Figure 30. As was expected the lift remains essentially constant. In this case the upper surface lift does not change since no additional base tilt is present and the base pressure, which is a strong function of velocity due to the attached flow condition, remains unchanged for a given velocity. This would infer that once the curtain is detached along the sides and the rear of the vehicle, due to the free stream ram effect, it remains detached under yaw conditions.

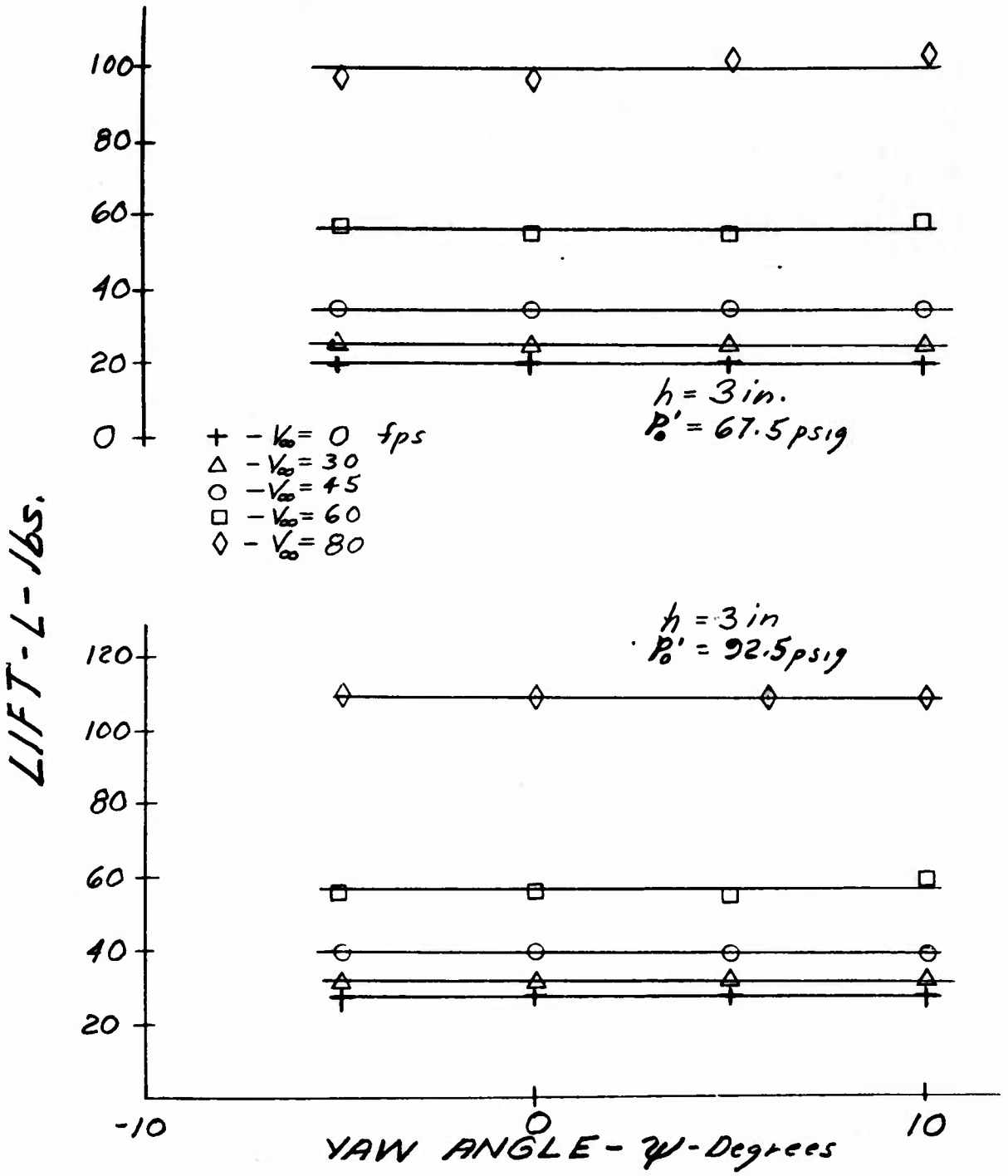

Figure 30. Effect of Yaw on Lift.

C. Experimental Drag Data

1. Effect of Height on Drag

Several tests were made over a height and speed range with the primary total pressures of 67.5 and 92.5 psig. In both cases the test data indicate a reasonably constant value of C_D at the lower heights (h = 1 and 2 inches) but a rapidly increasing one at the higher heights. The data from these runs are shown in Figures 31 and 32.

This again appears to be the effect of attached flow as was shown in the case of lift versus height for varying velocities. At the lower heights the flow in the ejector is detached, thus the frontal area presented to the free stream is essentially the same for all velocities since no air is allowed to pass under the machine. At the higher heights, when the flow is attached at the lower velocities a quantity of the free stream flow is allowed to pass under the machine thus reducing the drag coefficient. As the velocity increases and the dynamic head causes the flow of the rear and side ejectors to detach, less flow is allowed to pass under the machine thus increasing the drag coefficient. As is to be expected the value of C_D increases with increasing height since the curtain area, which is included in the frontal area presented to the free stream, increases with height.

Drag data at zero angle of attack, Roll and Yaw are summarized in Figures 33 and 34. Figure 33 shows the variation of total drag coefficient with the ratio of free stream dynamic pressure to average curtain total pressure for the various heights tested. It is immediately apparent that both height and speed have a very strong influence on total drag. From Figure 16 it is observed that the profile drag coefficient is in the range of 0.07 to 0.08 for the heights tested while the total drag coefficient shown in Figure 33 with the presence of an air cushion is as much as three times the profile drag coefficient at certain height and speed combinations. At the 5 inch height the peak drag coefficient occurs at a ratio of free stream dynamic pressure to curtain total pressure of 0.35. Thus for a base pressure of 30 psfg and a corresponding curtain total pressure of 70 psfg (from the Stanton-Jones relation with $t/h = 0.15$ & $\theta_1 = 30°$) the peak drag coefficient would occur at a flight velocity of 182 fps (124 mph). This is probably above the upper range of GEM velocities of immediate interest. The probable range of interest in GEM operation is therefore to the left of the dotted line through the drag coefficient peaks. Furthermore since base pressures in excess of 30 psfg appear to be required from size considerations, the correspondingly higher curtain total pressures will shift the peak drag coefficient to even higher flight speeds. However, it is apparent that drag coefficients appreciably greater than the profile drag coefficient may be encountered in normal GEM operation.

From observation of the center of pressure location, M/Lb - Figures 53 and 54, and the breaks in the slope of the lift curves, Figure 22, it is apparent that the peak drag coefficients are associated with the breakdown of the curtain and the onset of through-flow under the model base.

The deduction, reached earlier, that the rapid increase in drag with flight velocity (at low speeds) is associated with ejector flow detachment indicates that even higher low speed drags would be encountered for completely detached flow. This is borne out by the data of Figure 35. At the design height of 3 inches the basic model configuration with spoiler was tested over the velocity and primary pressure ranges. The high speed cushion drag ($C_D - C_{D_f}$) is seen to be unaffected by the spoiler while the low speed cushion drag was increased due to the spoiler presence and resultant flow detachment. At the peak drag coefficient, the flow is certainly detached. At higher speeds the curtain tends to collapse and results would not be expected to be affected by the spoiler. However, at lower speeds detached flow would completely block flow underneath the vehicle and appreciably raise the drag coefficient relative to the observed values with attached flow.

It is noteworthy that the total drag coefficient approaches a limiting value equal to that associated with the equivalent momentum drag of the recirculating flow. It should be remembered that intake momentum drag was not present during these tests as an external air supply was used and the momentum drag referred to here is associated with the recirculating flow. The momentum drag term is developed as follows:

Equating the cushion drag, $D-D_f$, to the momentum of the recirculating flow results in the expression,

$$D - D_f = K \cdot \rho \cdot S_j \cdot V_j \; V_\infty$$

converting to coefficient form,

$$C_D - C_{D_f} = K \frac{\rho S_j V_j V_\infty}{S_r q_\infty}$$

or

$$C_D - C_{D_f} = 2K \frac{S_j/S_r}{\sqrt{q_\infty/q_j}} = K C_{D_m}$$

Thus the cushion drag ($C_D - C_{D_f}$) varies between 0 and 100 percent of the computed momentum drag of the recirculating flow depending upon height and forward speed.

The drag data are replotted in Figure 34 against the ratio of free stream dynamic pressure to a critical free stream dynamic pressure where the critical free stream dynamic pressure

corresponds to the second critical velocity defined by N. K. Walker (Reference 2). Good correlation of the data is obtained as the introduction of the critical velocity concept removes h as a variable in the subcritical regime. The cushion drag is a linear function of the recirculation momentum drag in the subcritical regime and rises to a maximum value depending upon vehicle height. It should be observed that only h was varied in these series of tests and it can not be deduced whether (t/h) or (h/D) is the important variable in determining cushion drag.

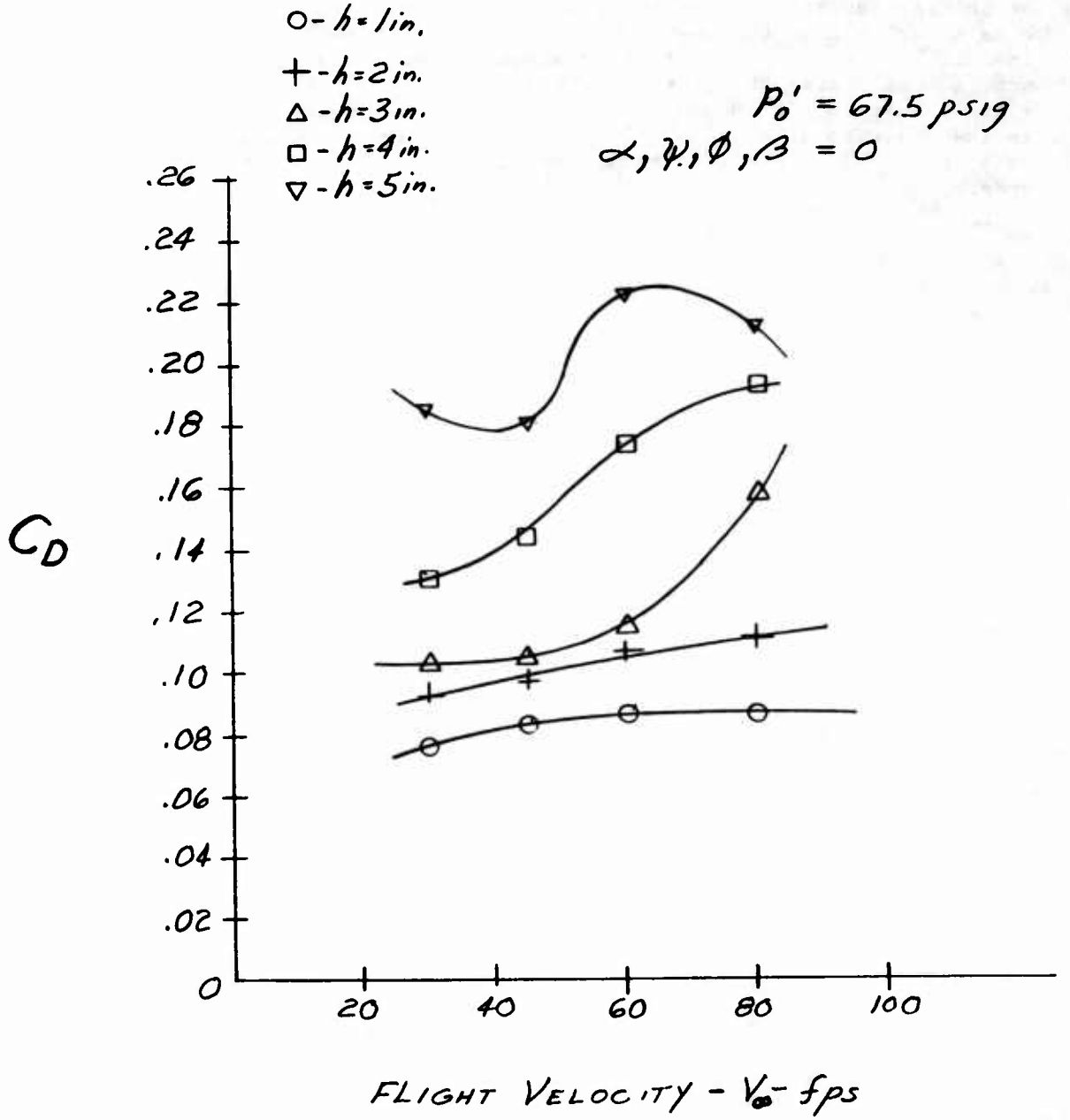

Figure 31. Effect of Speed and Height on Drag Coefficient.

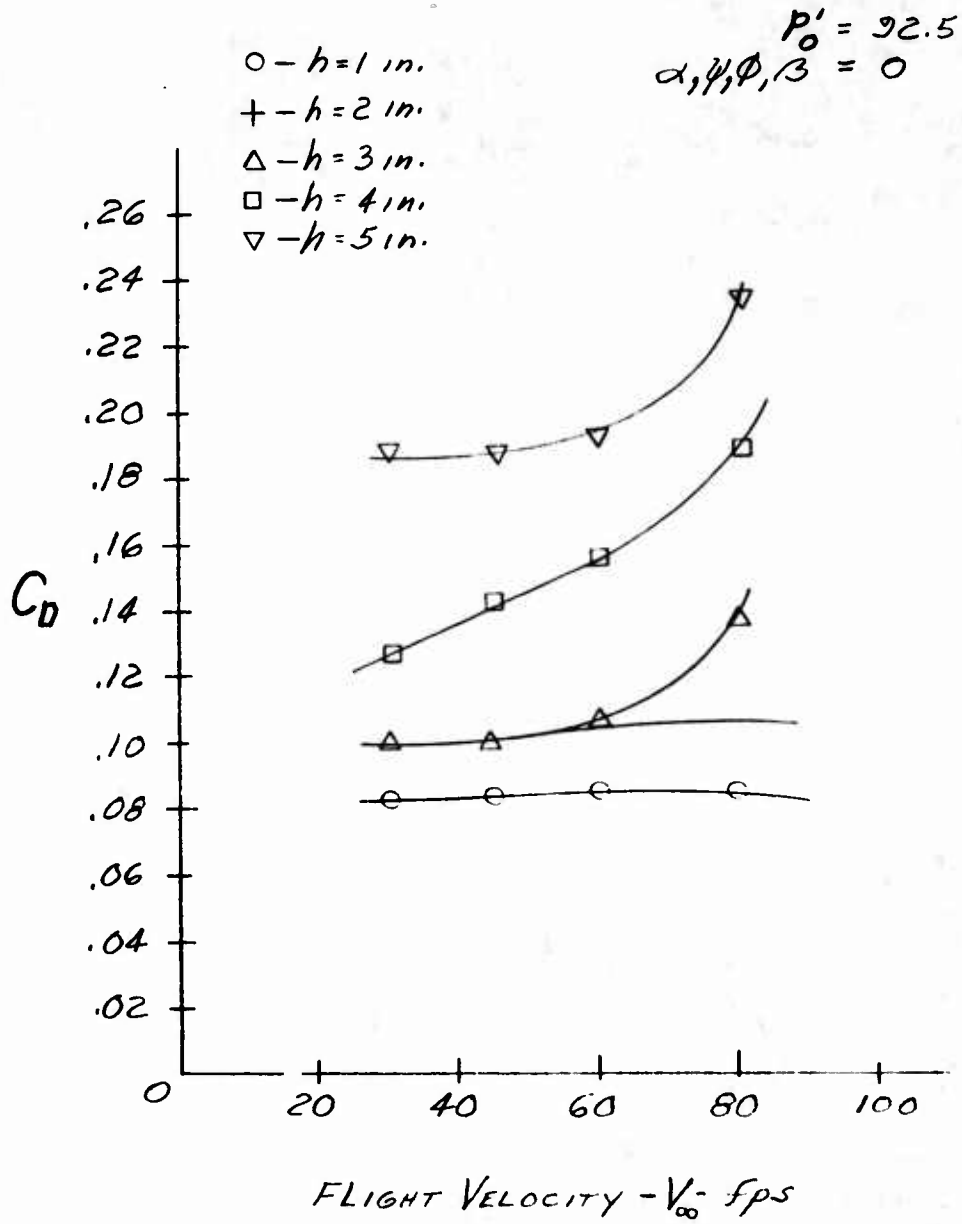

Figure 32. Effect of Speed and Height on Drag.

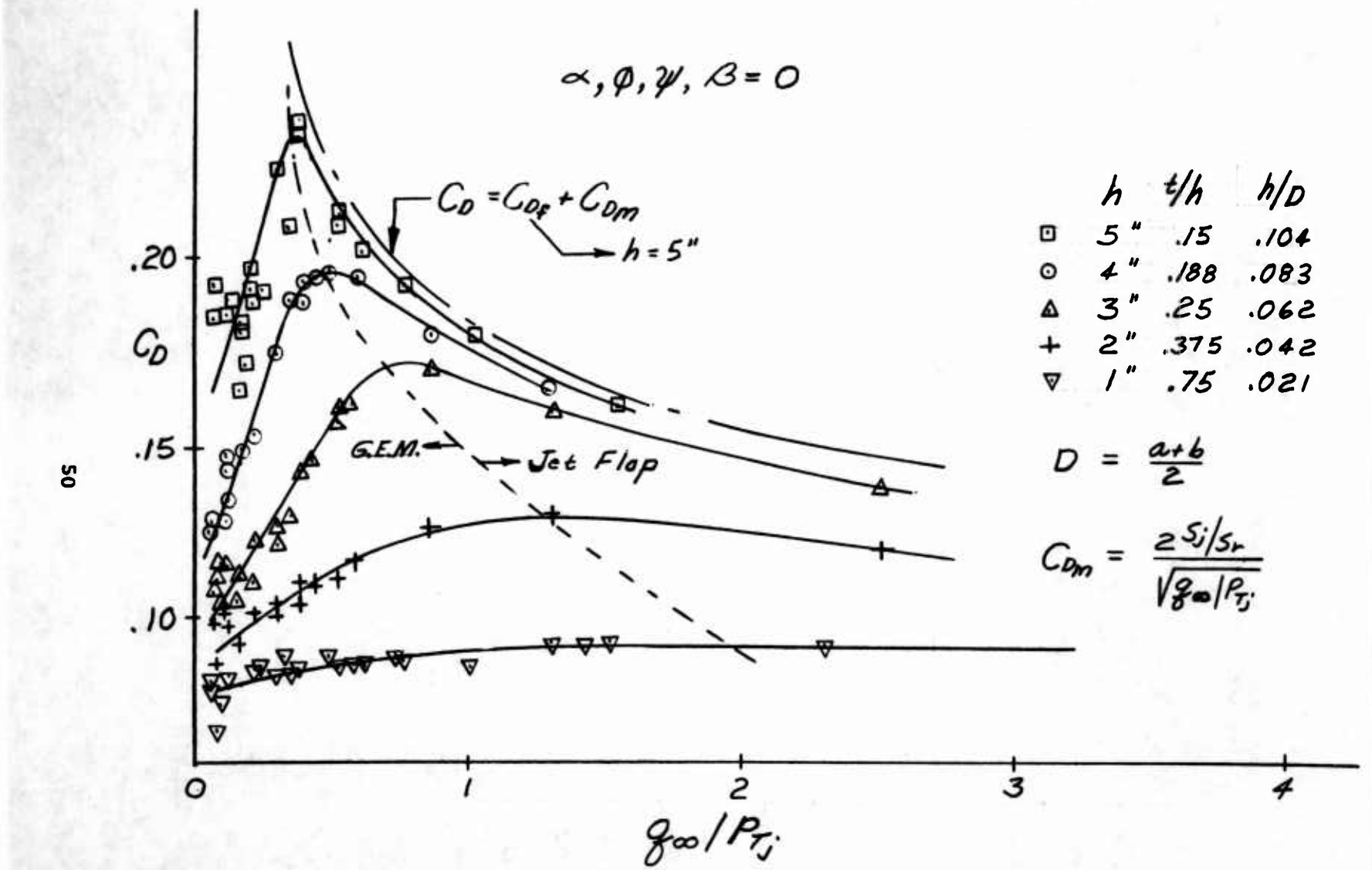

Figure 33. Effect of Speed on Drag Coefficient.

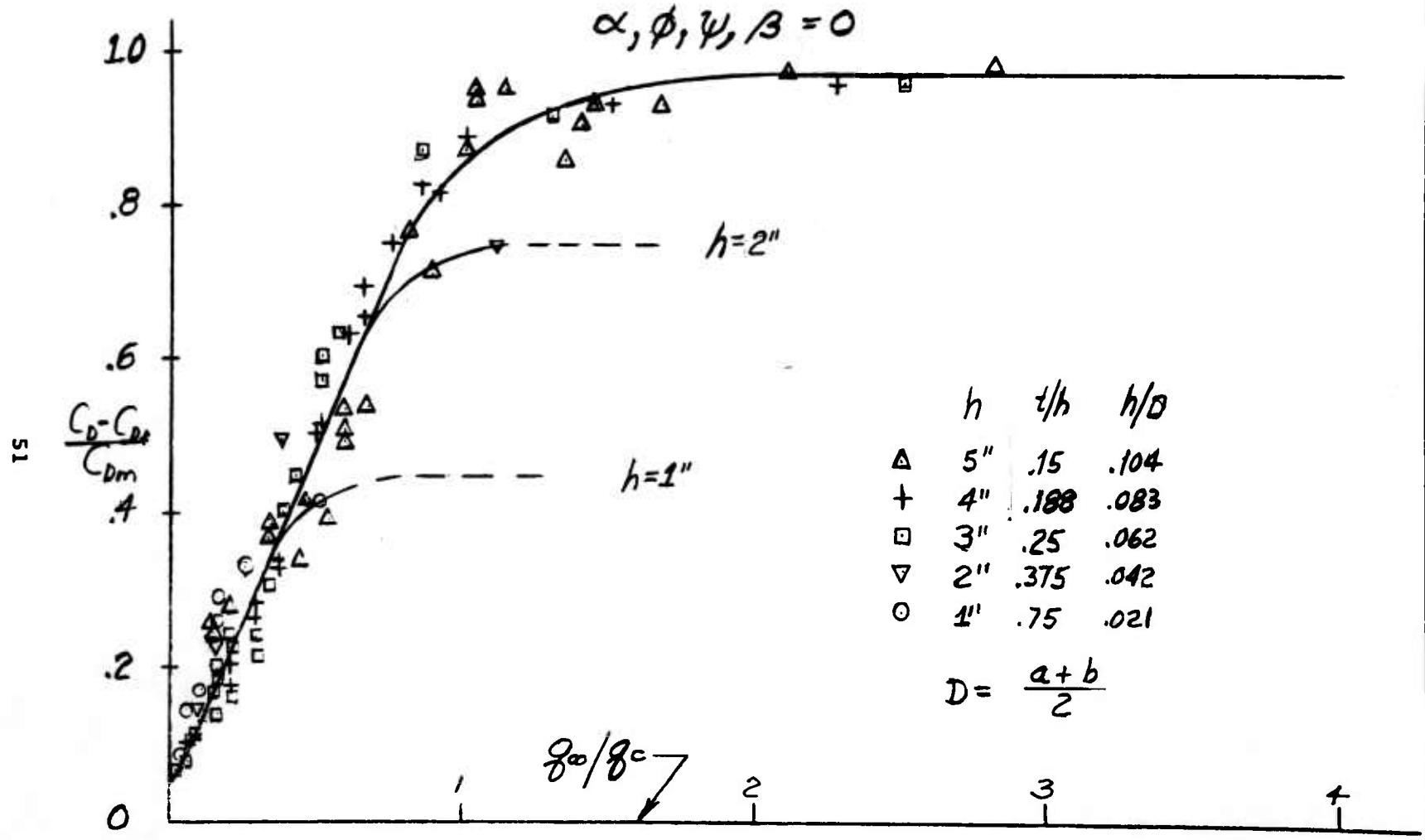

Figure 34. Effect of Speed on Cushion Drag.

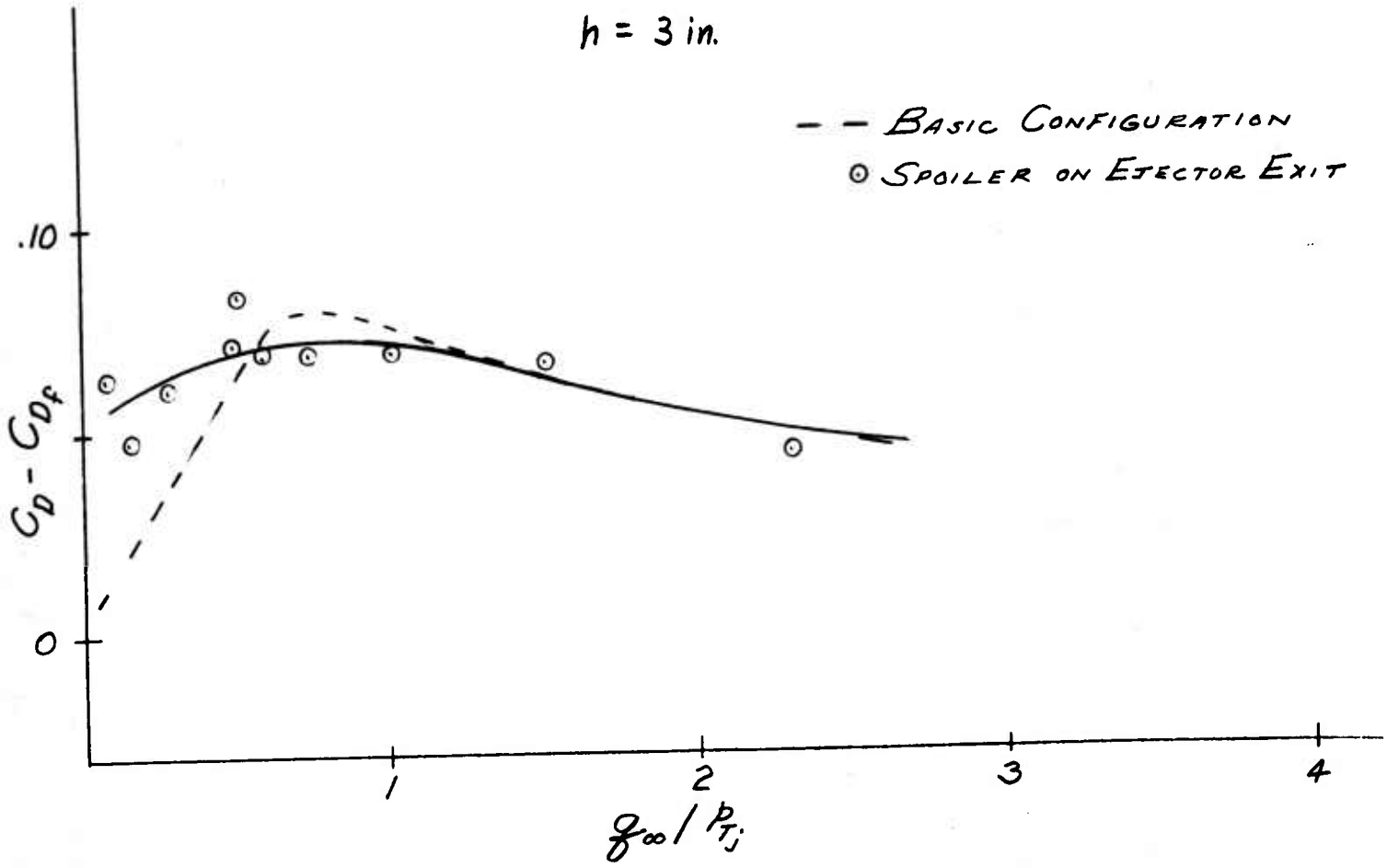

Figure 35. Effect of Ejector Spoiler on Drag Coefficient.

2. Effect of Pitch on Drag

The test data showing the effect of pitch on drag are presented in Figures 36 through 40. In this case there are several factors affecting the drag variation with pitch angle. These are:

1. Change in upper surface lift due to the varying α.
2. Effect of ram pressure on the base pressure generated.
3. Tilt of the total lift vector due to α .

In the negative α range the tilted total lift vector causes a reduction in drag since the horizontal component is forward which opposes the additional drag due to the increased frontal area encountered in pitch. Conversely in the positive α range all the drag increments are additive. The pitched up nose presents a greater frontal area, at the higher heights the ram pressure of the free-stream allows the base pressure to be regulated by the lower jets thus increasing the total lift force, and causing more of the flow to pass around the machine. The higher base pressure causes a higher drag due to its blockage effect. In addition to this the tilted total lift vector has a rearward horizontal component. This compounded effect is especially apparent at the high heights and high velocities where the slope of the curve increases rapidly over the positive α range.

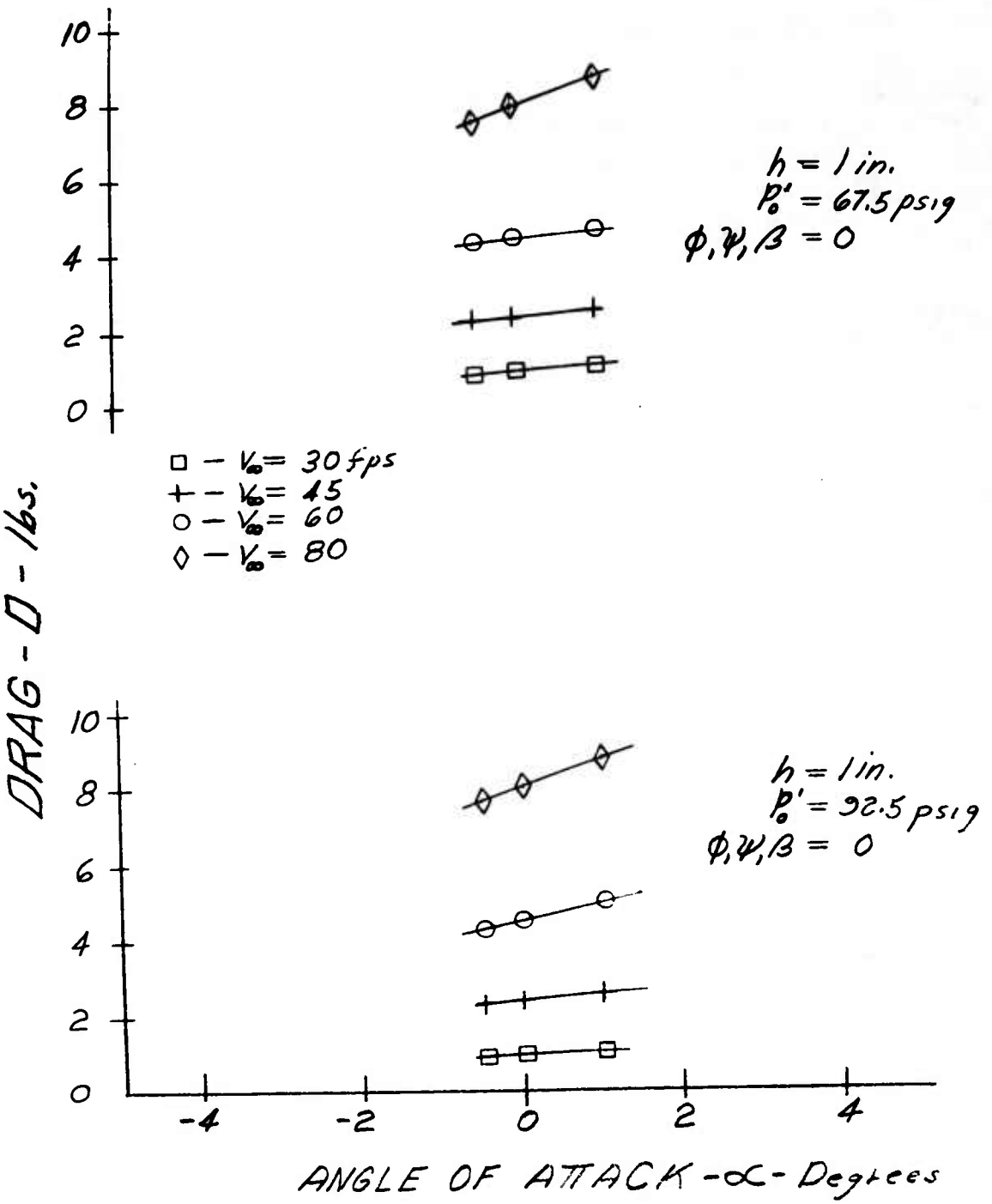

Figure 36. Effect of Pitch on Drag.

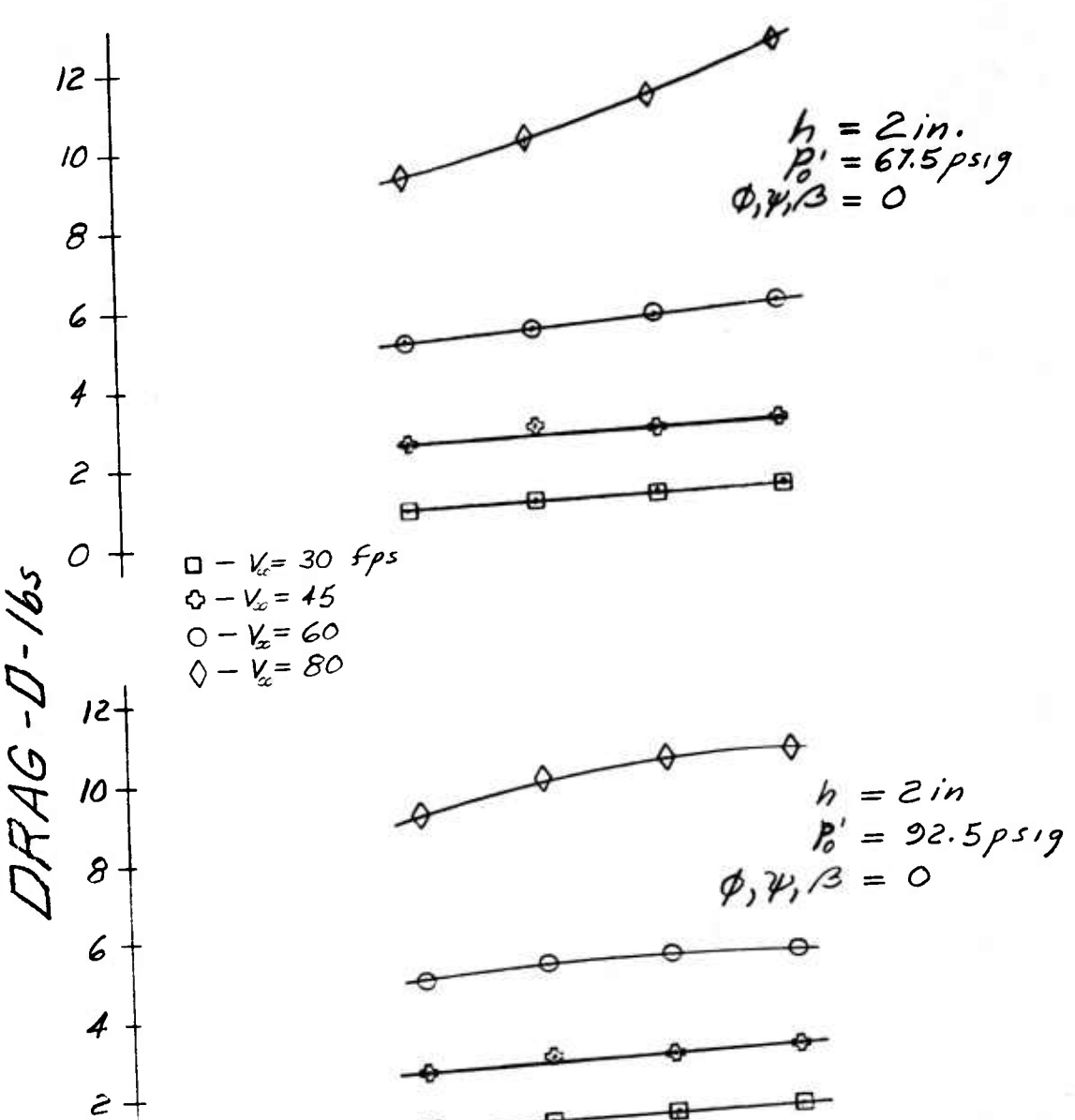

Figure 37. Effect of Pitch on Drag.

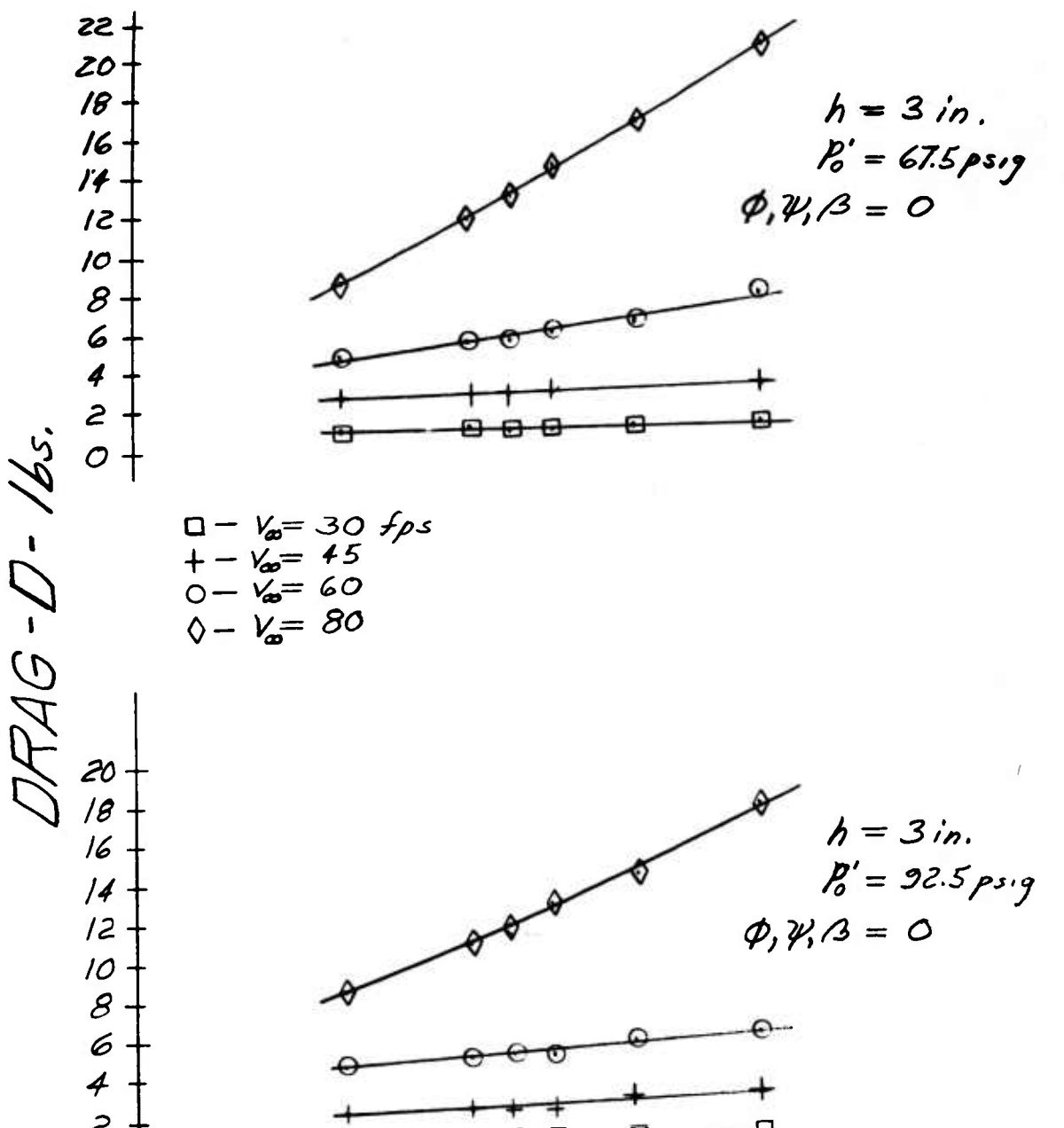

Figure 38. Effect of Pitch on Drag.

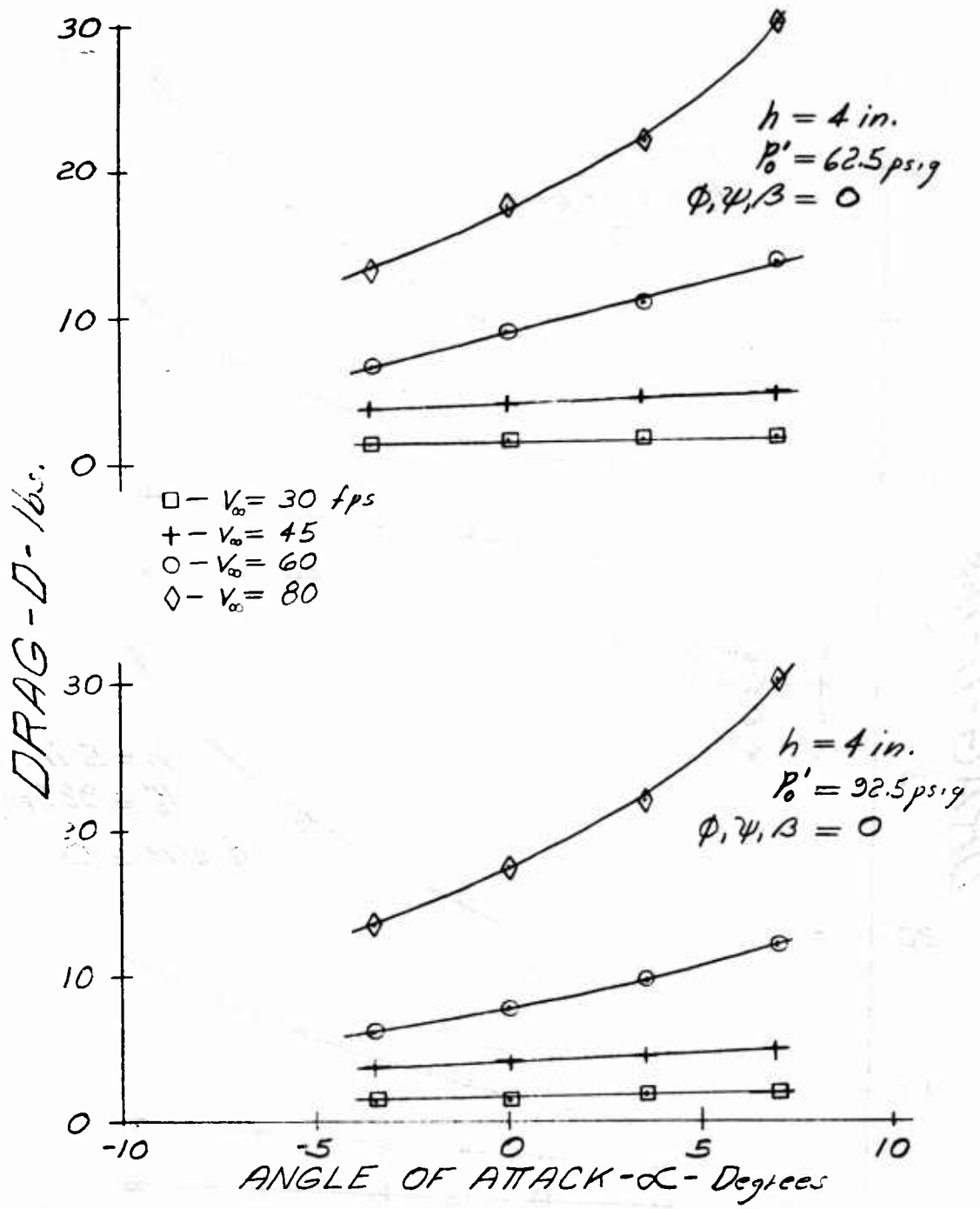

Figure 39. Effect of Pitch on Drag.

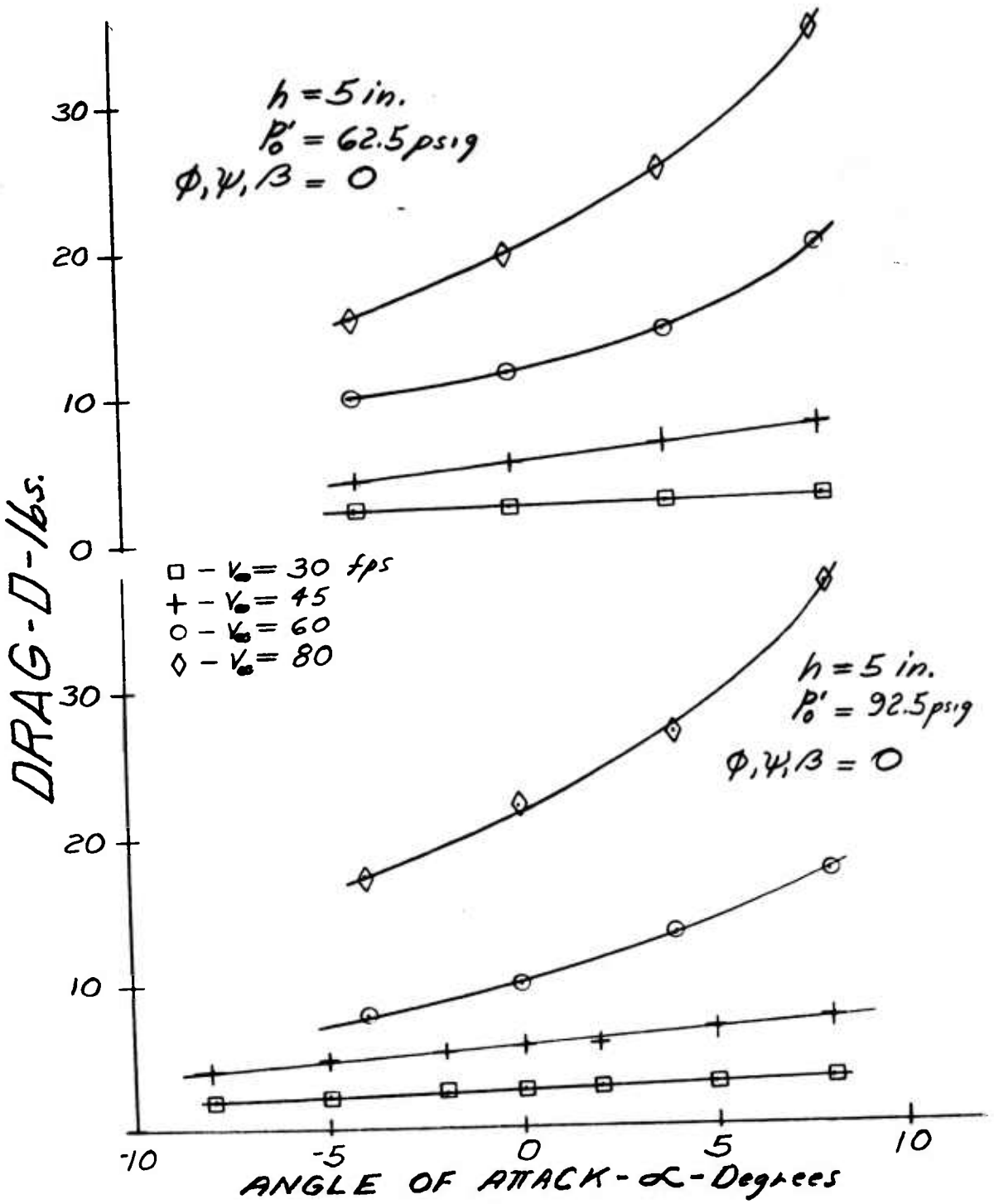

Figure 40. Effect of Pitch on Drag.

3. Effect of Roll on Drag

The drag data for this section is given in Figure 41. Since this is again a symmetric function of the roll angle, ϕ, the runs were made mainly in the positive range.

The trends of these curves can be explained by referring to the curves of drag coefficient, C_D, in Figures 31 and 32. These curves show C_D to be a nonlinear function of height for the velocities measured. The trend of the curve at V = 80 fps and p_o' = 67.5 will be given here as an example. Since the drag curve as a function of roll angle is given for a three inch height the C_D for the comparable conditions from Figure 31 is 0.157. If the machine is then rolled so that one side drops to 1 inch while the other raises to 5 inches, the low side is in a regime where the C_D is 0.086 while that of the high side is 0.211. The low side experiences a decrease of 0.071 while the high side increased 0.054. This would then indicate a trend of an overall decrease in C_D as was measured in the test. If the other velocities are also examined, the general trends can again be predicted. At 60 fps the C_D for the high side is greater in magnitude than that of the low side so this would indicate an increasing trend as again is shown. This also applies to the 30 and 45 fps velocity data. A similar analysis could also be made for the p_o' = 92.5 runs.

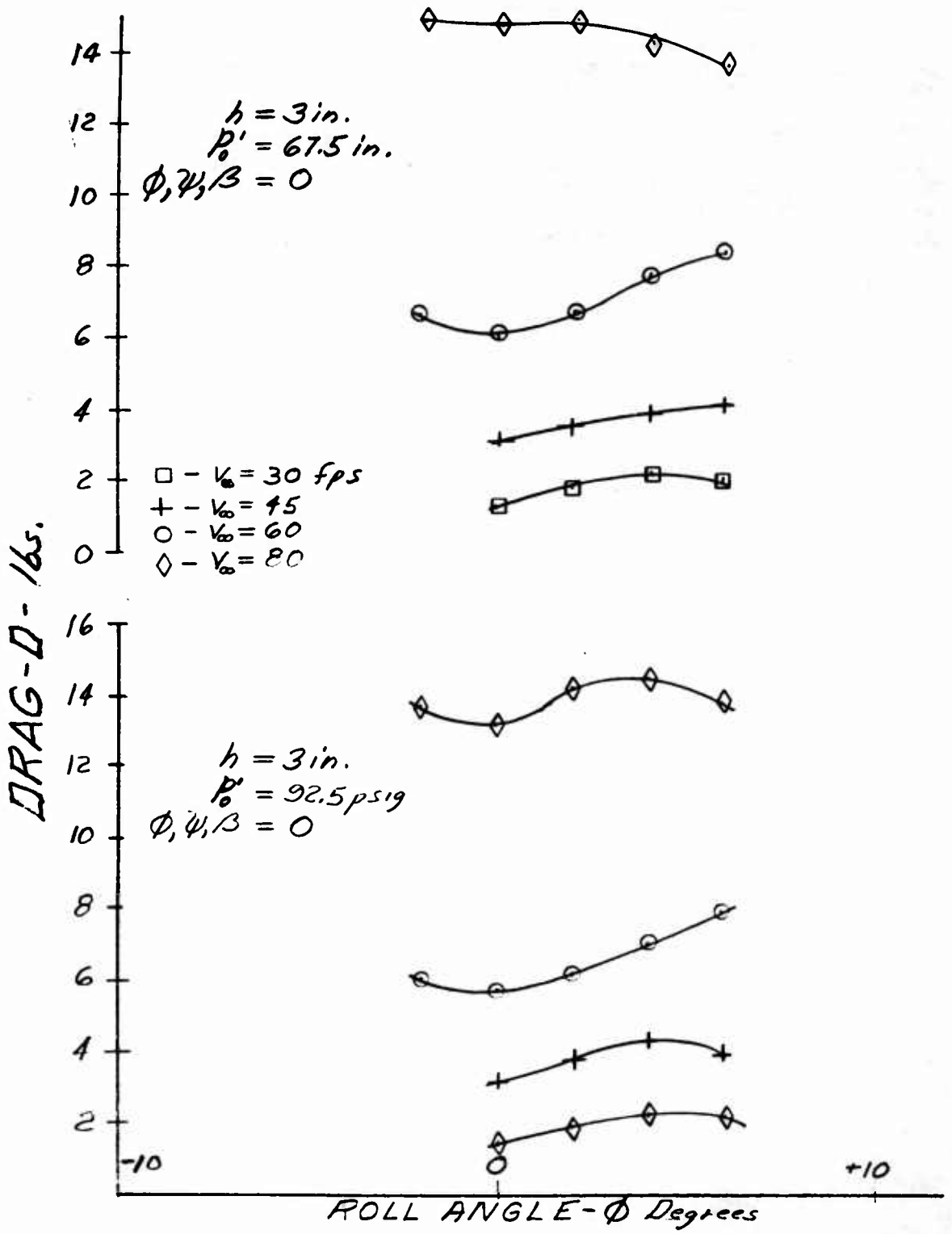

Figure 41. Effect of Roll on Drag.

4. Effect of Yaw on Drag

The data for the drag variation in yaw is given in Figure 42 for both primary pressures used at the 3 inch height. The data shows only small variations with yaw angle, as would be expected, since the only variable changing in this instance is the frontal area. Comparisons are given in Figure 42 between the measured drag and that predicted by assuming that the total drag is proportional to the frontal area presented to the free stream. With a width of 3.5 feet and a length of 4.5 feet, as measured on the model, the frontal width is

$$\text{Width} = 3.5 \cos|\psi| + 4.5 \sin|\psi|$$

The total predicted drag is then:

$$\text{Total Drag} = \left\{\text{Drag}_{@\,\psi=0}\right\}\left[\frac{3.5\cos|\psi| + 4.5\sin|\psi|}{3.5}\right]$$

The predicted values are given as dashed lines in Figure 42 and good agreement with the measured data is shown.

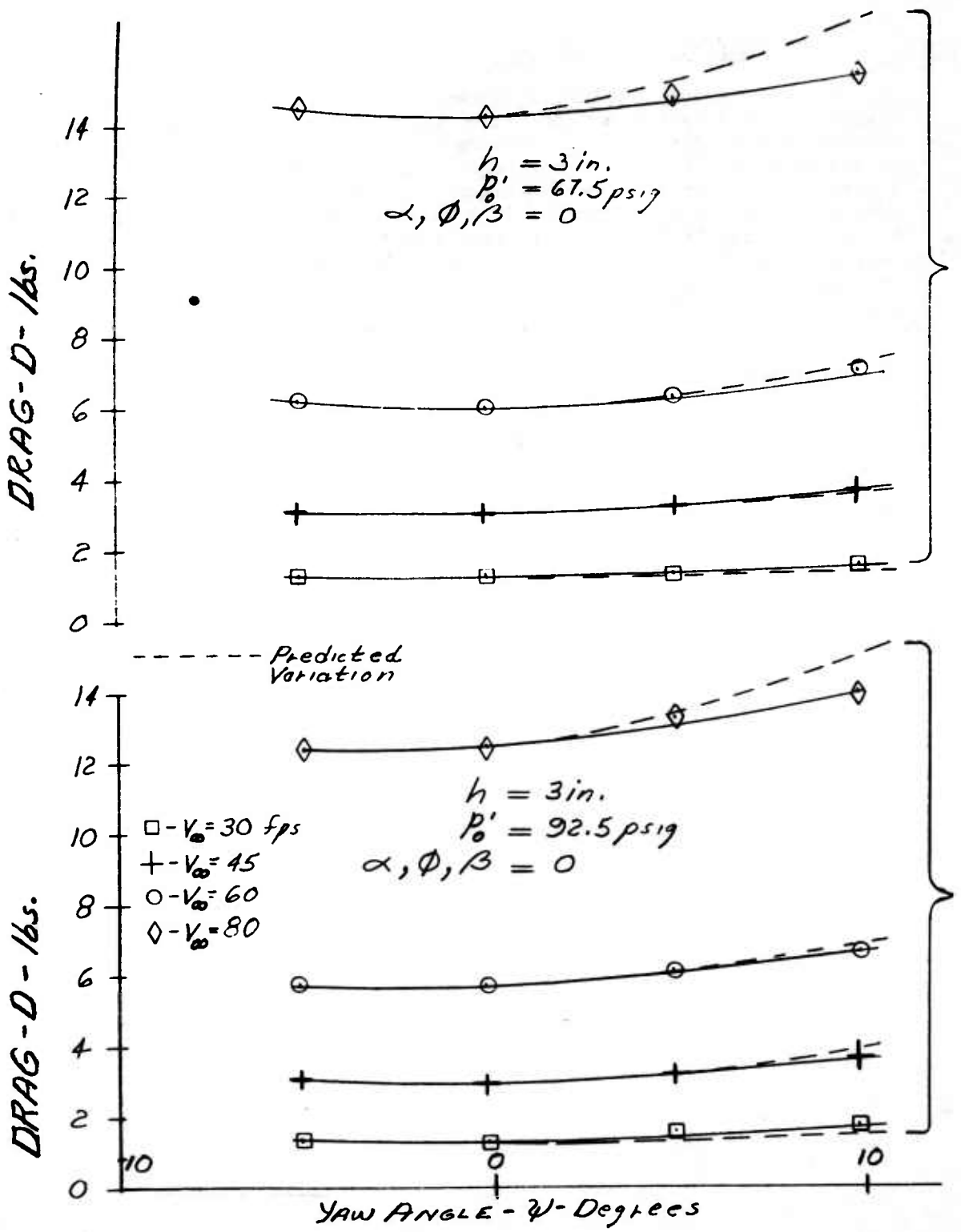

Figure 42. Effect of Yaw on Drag.

III. STATIC STABILITY

A. Hover Stability

1. Heave Stability

The static stability of the model in heave is given by the slope of the lift versus height curves shown in Figures 17 and 18. A comparison of these curves shows that the general trends are the same regardless of the total head of the primary flow, P_{∞}'.

The slope of the lift versus height curve for $P_9' = 92.5$ psig is plotted in Figure 43 as a function of height. This curve indicates that the model is stable $\left(\frac{\partial L}{\partial h} < 0\right)$ at heights over 1.5 inches for the hovering case (V = 0). The heave stability increases to a maximum at a height of approximately 2.5 inches. This peak in stability may, in part, be attributed to the planform configuration. Apparently the air curtain at the corners of the planform does not form a good seal particularly as height increases, producing a sudden drop in base pressure, indicated by the rapid loss in total lift. Ejector flow attachment, observed at the higher heights also contributes to the loss in lift.

At heights over 4 inches most of the ground effect is lost, the curtain becomes weaker and the lift does not change much with height, reducing the heave stability to a minimum.

Below a height of 1.5 inches the lift curve slope is positive $\left(\frac{\partial L}{\partial h} > 0\right)$ making the model unstable in heave. This phenomenon can be explained in terms of the basic principle of recirculation: pressure recovery. Pressure recovery is defined as the ratio of total pressure of the air curtain at the inlet of the recirculating ejector to the total pressure of the flow at the exit of the ejector. As the model is operated at lower heights the passage of the recirculating air from the exit to the inlet of the ejector becomes more restricted producing pressure drops in the flow of the air curtain which are reflected in pressure recovery and base pressure.

The effect of pitch on heave stability is depicted in Figure 44. It may be observed that as the pitch angle increases the lift is reduced particularly at the lower heights. At the higher heights the lift is low and is not affected by pitch angle. Consequently, the slope of the lift curve changes, actually reducing the heave stability.

In summary, the model exhibited heave stability over the operating height between 1.5 to approximately 5 inches.

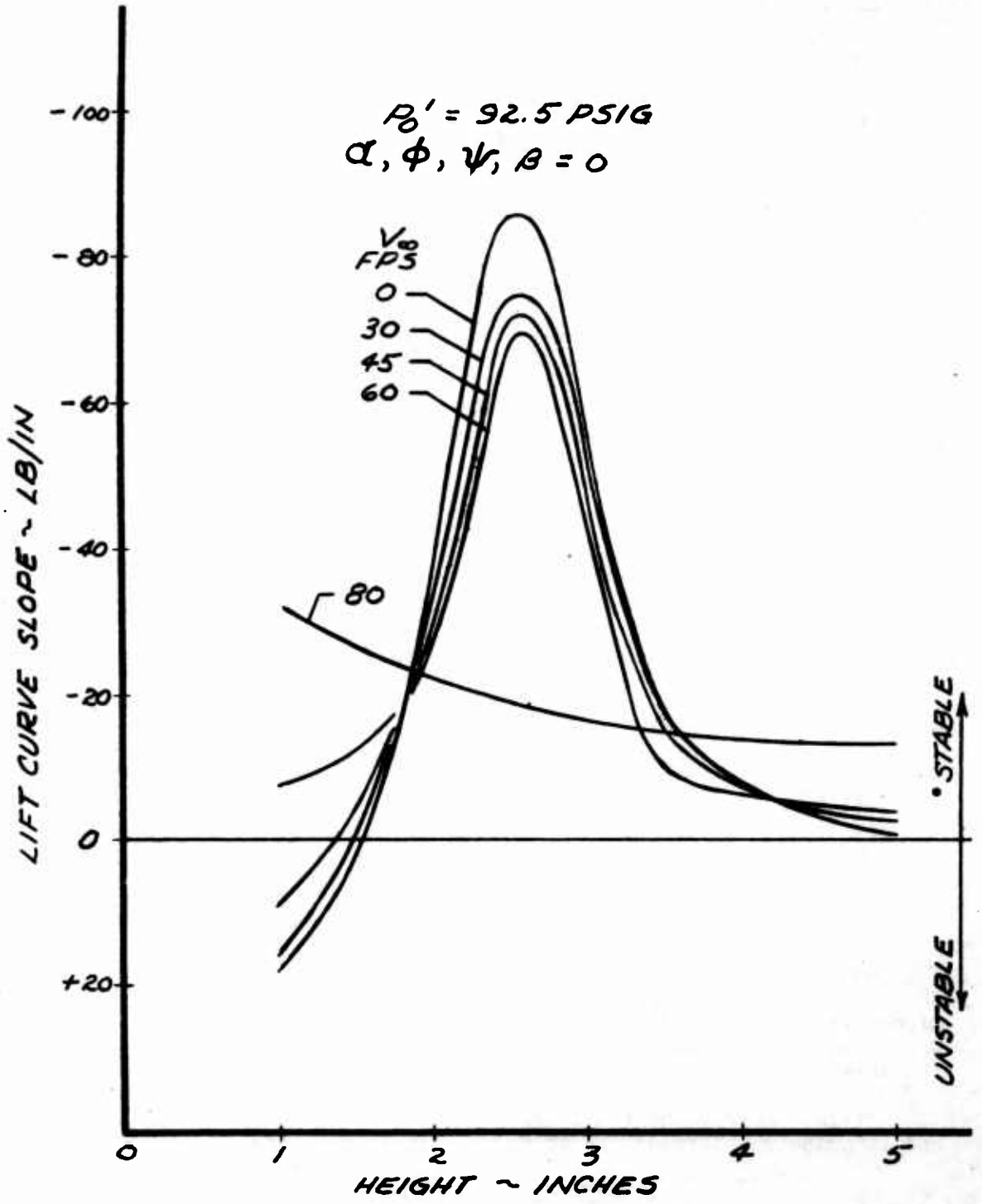

Figure 43. Effect of Height and Velocity on Heave Stability.

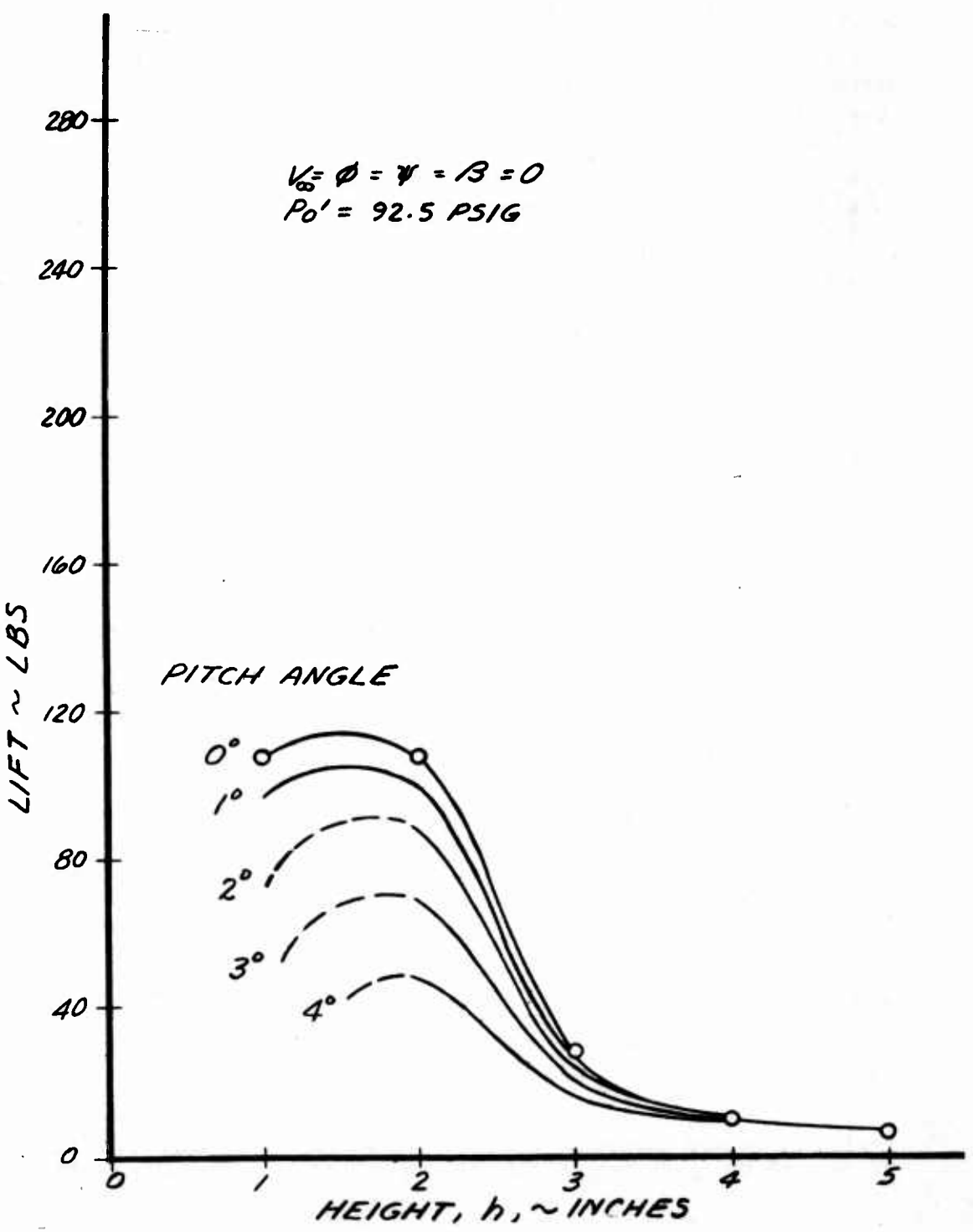

Figure 44. Effect of Pitch on Lift.

2. Pitch Stability

Curves of pitching moment versus pitch angle are presented in Figure 45, for primary flow total heads of 67.5 and 92.5 psig.

The effect of primary pressure is reflected in the magnitude of the moment, but the general trends are the same in both cases. The effect of height and pitch angle are more important. At heights of 1, 3 and 4 inches the model exhibits stability near zero alpha, while at heights of 2 and 5 inches the model is unstable and neutrally stable respectively.

The instability at h=2 inches can be explained on the basis of unpublished theoretical analysis of the cavity pressure under the ejector. The results of this analysis indicate the cavity pressure to be stabilizing above a certain height which is a function of ejector mass augmentation and exit angle. Below this height the cavity pressure is destabilizing. However, the analysis referred to is based on two-dimensional thin jet momentum theory, and neglects the effect of cross flow at small pitch angles. For this reason it is believed that the minimum height for stability of the model may be over 2 inches.

The region of stability at a height of 1 inch could not be explained on the basis of thin jet theory. At this height the jet thickness to height ratio approaches unity, and the ejecti-jet begins to function like the annular jet GEM which is known to have pitch static stability only at very low height-to-thickness ratios. At the 5 inch height the recirculating flow has apparently attached, the corner leakage is very large, and little or neutral stability is observed even at the higher primary flow pressure.

An important feature of the pitching moment curve is its reversal in direction or change in sign $\partial M/\partial \alpha$, at pitch angles near 2.5 degrees. Since the factors affecting pitch stability are several, and cannot be separated in the model, it is difficult to determine to what the reversal in pitching moment can be attributed. However, the reversal of the moment derivative does not make the moment change sign until pitch angles of 4.5 and 6 degrees are reached, at h=3 and h=4 inches respectively. Therefore, after a disturbance, the model will return to its neutral position provided these angles are not exceeded, meaning that the model may be considered to be statically stable in pitch up to these angles.

In summary, the model has pitch stability at the low angles of attack except at height of approximately 2 inches. At heights above operating heights the model becomes neutrally stable.

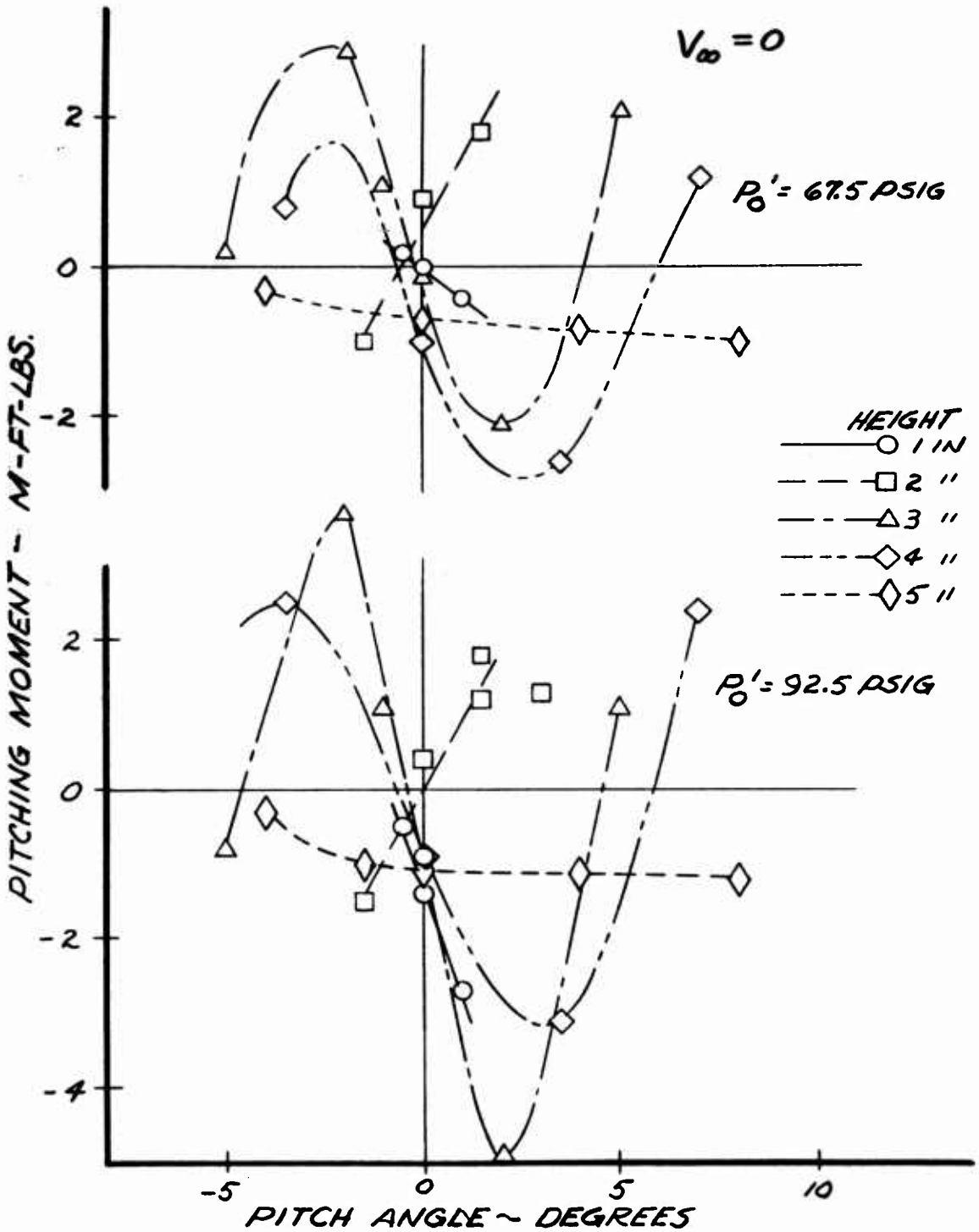

Figure 45. Hovering Pitching Moment.

3. Roll Stability

Figures 46 and 47 show the effect of roll angle on rolling moment, at primary total heads of 67.5 psig and 92.5 psig respectively. Again, as in the pitch case, the effect of primary pressure is reflected only in the magnitude of the moment, but the general trends are the same at both pressures.

At one inch height the model is stable, and the stabilizing moment increases very rapidly with roll angle. This is also evident from the plot of lateral location of the center of pressure shown in Figure 48. At the height of two inches the model is unstable as in the pitch case. Stability is regained at h=3 inches, for roll angles between -4 and 4 degrees, at which points apparently the destabilizing effect of the crossflow overcomes the stabilizing effect of cavity pressure. As the height is increased, the jet curtain becomes weaker and the magnitude of the stabilizing moment is reduced, but the location of the center of pressure indicates that the model is stable at 4 inch height.

In general, it may be concluded, the roll stability characteristics of the model are the same as the pitch characteristics, except for the magnitude of the moments.

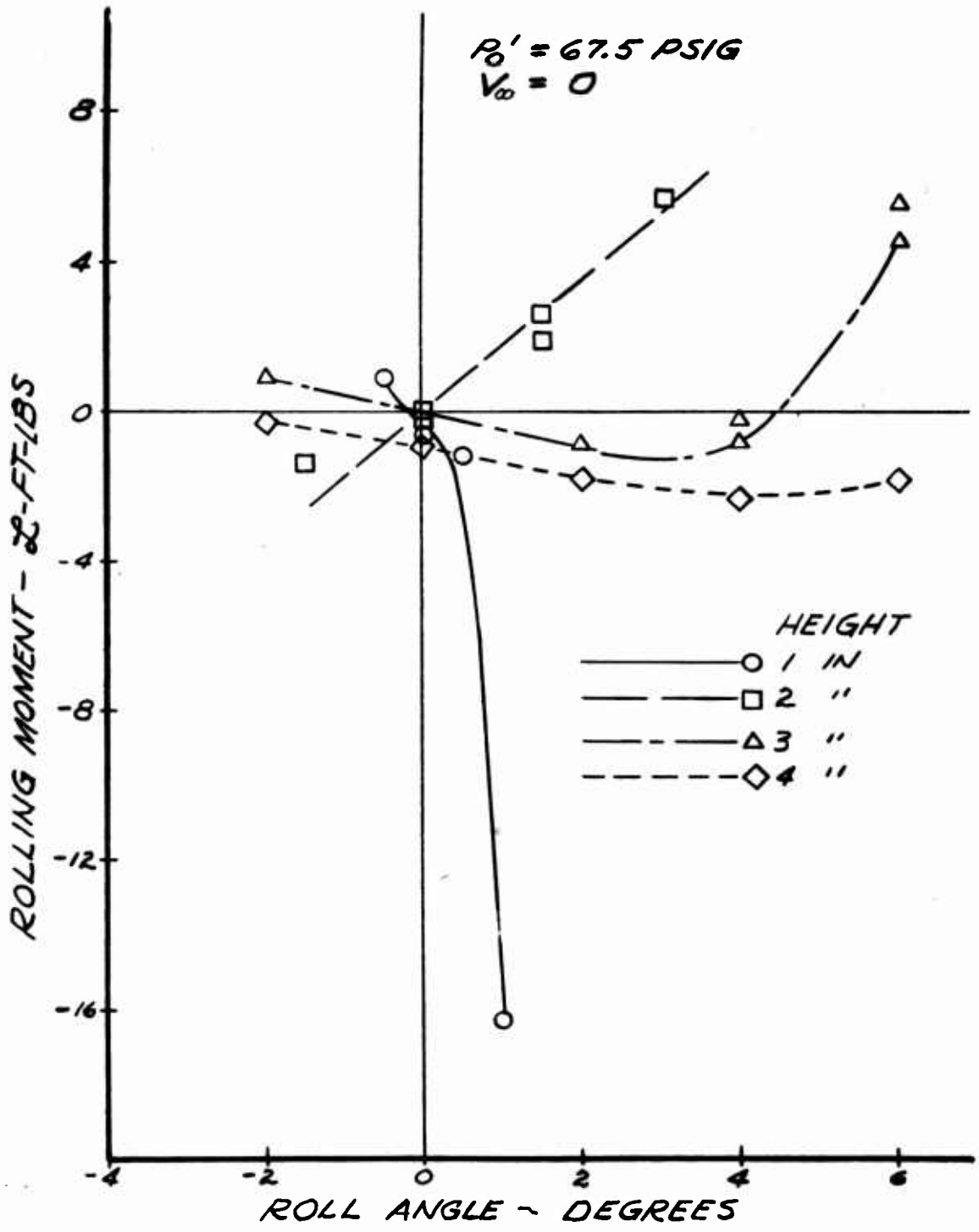

Figure 46. Rolling Moment in Hover.

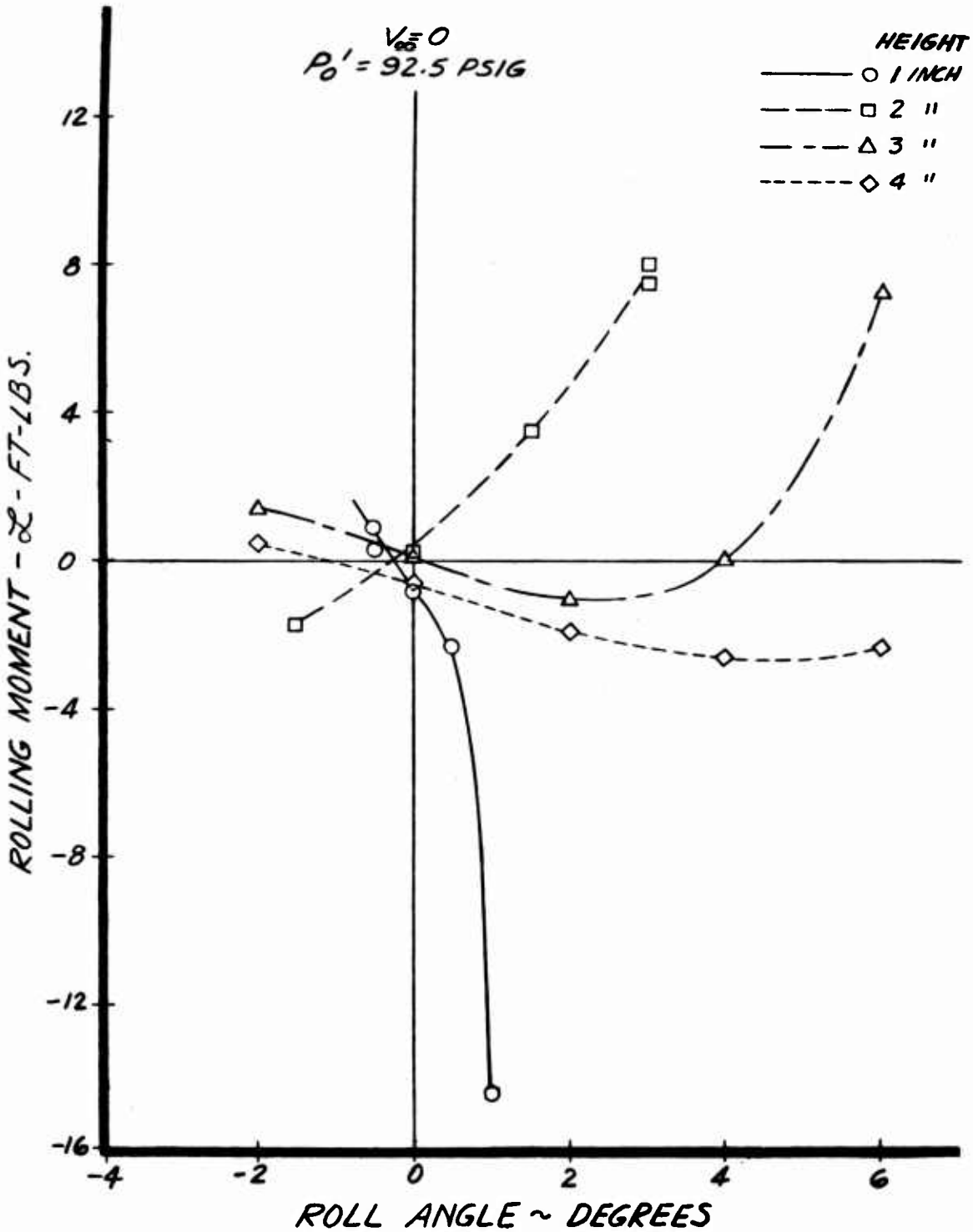

Figure 47. Rolling Moment in Hover.

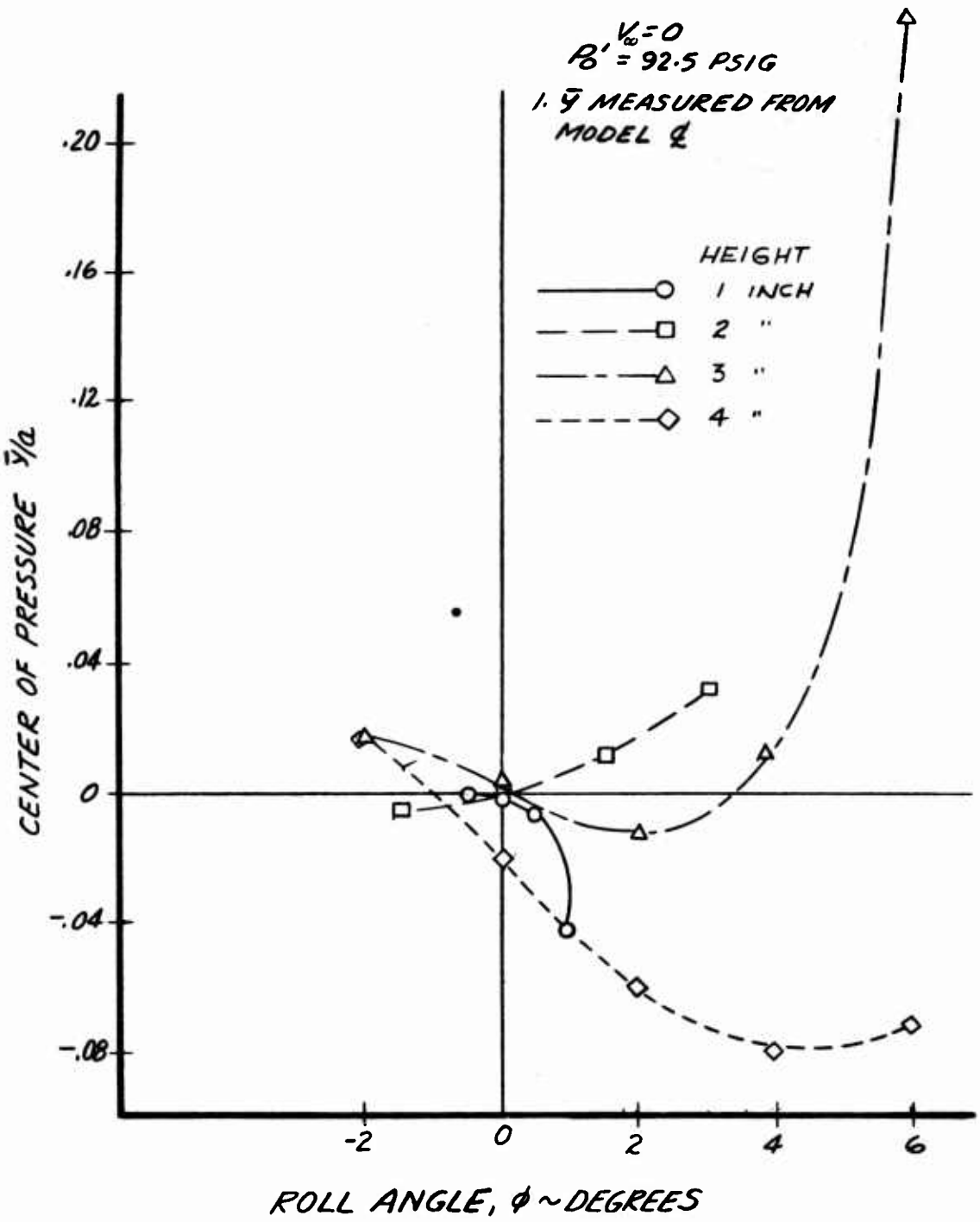

Figure 48. Lateral Location of Center of Pressure in Roll.

B. Forward Flight Stability

1. Heave Stability

The heave static stability characteristics of the model in forward flight are very similar to those in hovering flight. Figure 43 indicates that the model is stable at heights over 1.5 inches for low forward velocities. At speeds of 50 fps and over the model exhibits heave stability at all heights tested. Again, as in the hovering case, the stability reaches a maximum at h = 2.5 inches approximately at all speeds except at 80 feet per second where stability increases with decreasing height.

At this speed, the free stream dynamic pressure is sufficiently high to ram air under the vehicle and overcome the corner leakage. The net result is that the model lift does not decrease so rapidly with increasing height, and the heave stability characteristics of the model are improved as expected.

The effect of pitch on heave in forward flight is very interesting. It may be observed in Figures 25 through 28 that as in the hovering case that pitch angle deteriorates lift and heave stability but with an added forward velocity, lift develops with angle of attack. The net result is that at negative alphas the aerodynamic lift opposes the loss due to pitch. This accounts for the fact that the lift curves in hovering are symmetrical about zero alpha, while in forward flight they seem to be rotated about the axis. This effect is more pronounced as height and speed are increased, and as the curtain strength is reduced.

2. Pitch Stability

In the analysis of pitch stability in forward flight we first distinguish the effect of velocity on pitching moment at zero angle of attack. This is the pitching moment that has to be trimmed out by the pilot using the controls.

The longitudinal location of the center of pressure is presented in Figure 49. A positive value of $\bar{x}$ indicates the center of pressure is forward of the c.g., producing positive (nose up) pitching moment since the lift on the model is always positive. It may be observed that at zero angle of attack forward velocities in general produce nose up pitching moments. This is due to the external aerodynamic configuration of the model, namely the top surface.

This effect increases with speed, provided that none of the free stream flow passes under the vehicle.

As soon as the underflow starts, the cushion lift is rapidly augmented with aerodynamic lift. The vehicle profile represents an effective cambered airfoil in the free stream which tends to pitch nose down just as such a profile does at zero angle of attack.

It is evident from Figure 49 that the underflow is influenced by height and curtain strength, as well as free stream q. At h=4 and 5 inches the center of pressure begins to move rearwards at velocities of 55 fps and 45 fps respectively, while at h = 1 and 2 inches the c.p. is still moving forward at the highest speed tested of 80 fps. The reasons for this behavior of the model at zero angle of attack are the increase in curtain frontal area and the reduction of its strength with height. Both factors make it easier for the curtain to be blown in at lower speeds as h increases, and allow the passage of large under flow.

The influence of curtain strength is obvious from Figure 49. At h = 3 inches and p_o' = 97.5 psig the underflow starts at V = 75 fps, while at p_o' = 67.5 psig it starts at approximately 60 fps.

The same phenomena is depicted in Figure 50. In this figure the pitching moment is plotted as a function of primary pressure, which represents the strength of the air curtain and cushion of air under the vehicle. To simulate a very strong curtain, a dummy curtain was used under the vehicle as the limiting case.

At 60 fps forward velocity the air curtain is blown off at low p_o' and the moment is negative for the reasons mentioned above. As the curtain strength increases, the underflow is reduced, the pitching moment is then mostly due to the upper surface of the model and becomes positive, finally approaching the value obtained with the dummy cushion as p_o' increases. With the forward speed of 30 fps the free stream dynamic pressure is very low, and the aerodynamic moment small. The test results indicate an almost constant pitching moment on the order of that obtained with the dummy cushion. Possibly the region where the pitching moment reversal takes place lies between the test points, and is indicated by a dashed line.

Figure 51 summarizes this phenomenon in a plot of center of pressure versus q_∞/p_{tj} for all heights tested. Again it may be observed how, as the curtain gets stronger relative to free stream q_∞, the center of pressure moves forward.

Dummy cushion pitching moment coefficient data and center of pressure location data are summarized in Figure 52 for all heights tested. The positive pitching moments with the dummy cushion in place are contrasted to the generally negative pitching moments observed for the model alone.

Once the pitching moment at zero alpha has been trimmed the pitch stability depends only on the slope of the moment versus alpha curve. Since the pitching moment is taken about the c.g. of the model, and the lift is always positive, the location of center of pressure with respect to c.g. indicates the stability of the model.

Figures 53 and 54 summarize the center of pressure data at zero pitch angle. These slopes were obtained graphically from plots of center of pressure location versus pitch angle.

In general, at all heights it may be observed that the effect of velocity is destabilizing. This is due to the contribution of the upper profile of the model, which at angle of attack will have the aerodynamic center located near the 25 percent chord from the leading edge. The irregularities in some of the curves in Figures 53 and 54 can be attributed to the accuracy of the data, and the graphical method used for reading the slopes of the curves.

The stability of the model in forward flight changes with angle of attack and, as in the hovering case, at some heights the model is stable within an angle of attack range of approximately $\pm$ 4°. However, an additional effect is present in forward flight. Since the instability of the model is due to cross flow in pitch, at negative angles of attack the under flow is in the same direction

as the cross flow, and at positive angles of attack the under flow opposes the cross flow. The net result is that the stability region is not symmetrical about zero alpha. At the heights where the model has marginal or no pitch stability this effect is not pronounced.

The pitch stability in forward flight can then be summarized as follows. First, a zero alpha pitching moment is produced at forward velocities. This moment, which has to be trimmed out, changes in magnitude with velocity, and changes sign when the dynamic pressure is high enough to blow the front air curtain in. Second, the aerodynamic profile is an important factor in the static stability of the vehicle and at high speeds may cause instability on a vehicle that may be stable in hovering flight.

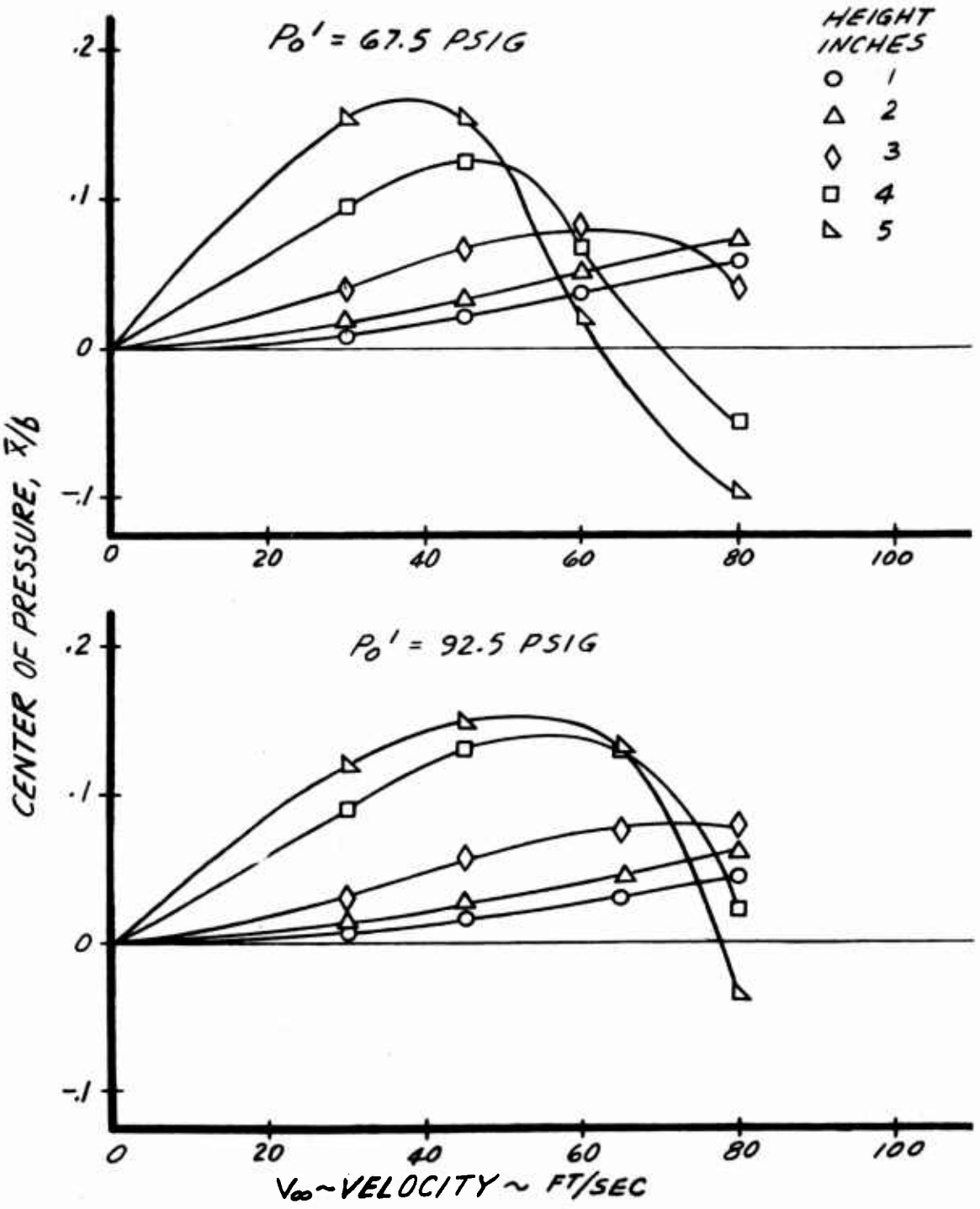

Figure 49. Effect of Velocity on Longitudinal Location of Center of Pressure at Zero Angle of Attack.

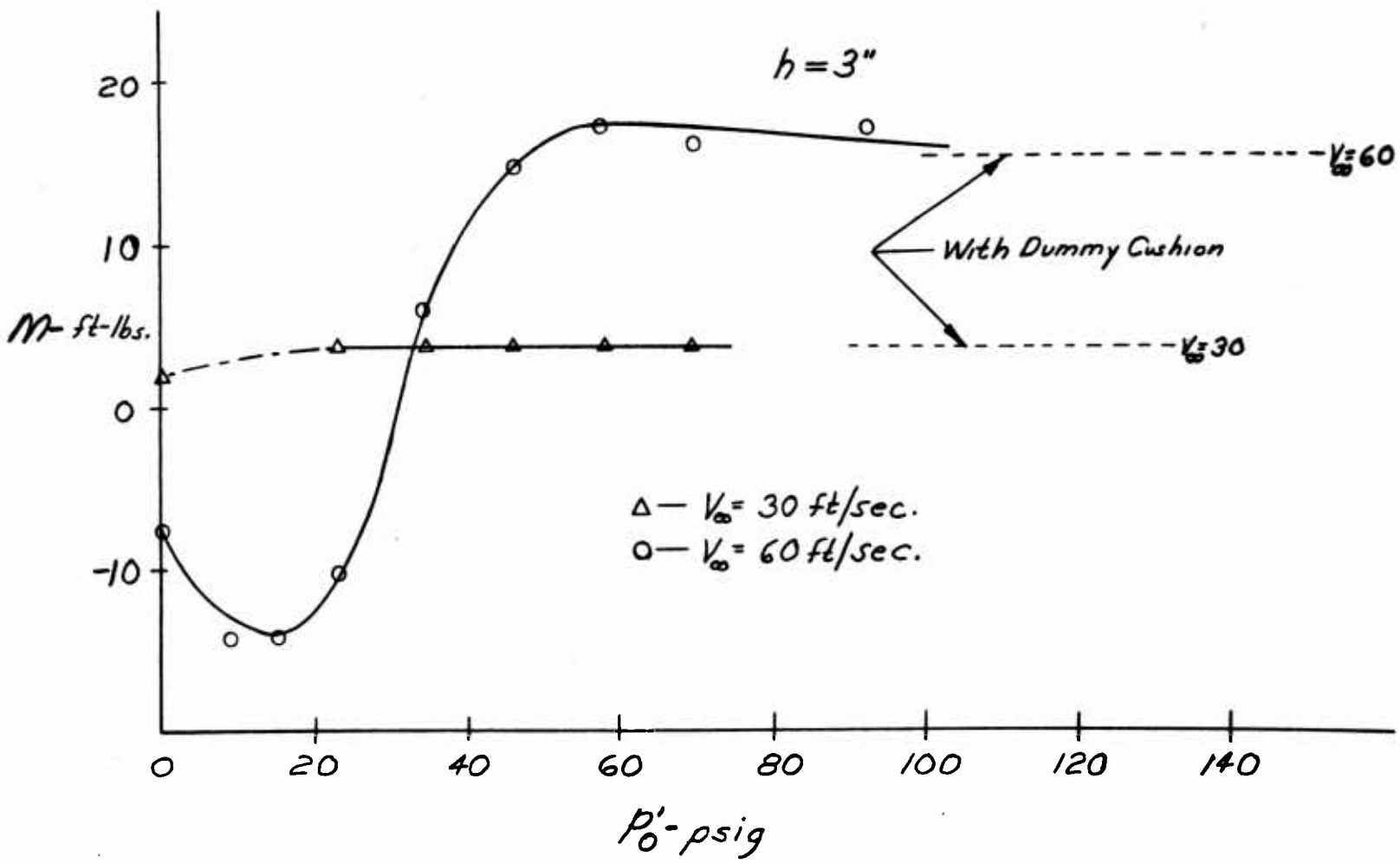

Figure 50. Effect of Primary Pressure on Pitching Moment.

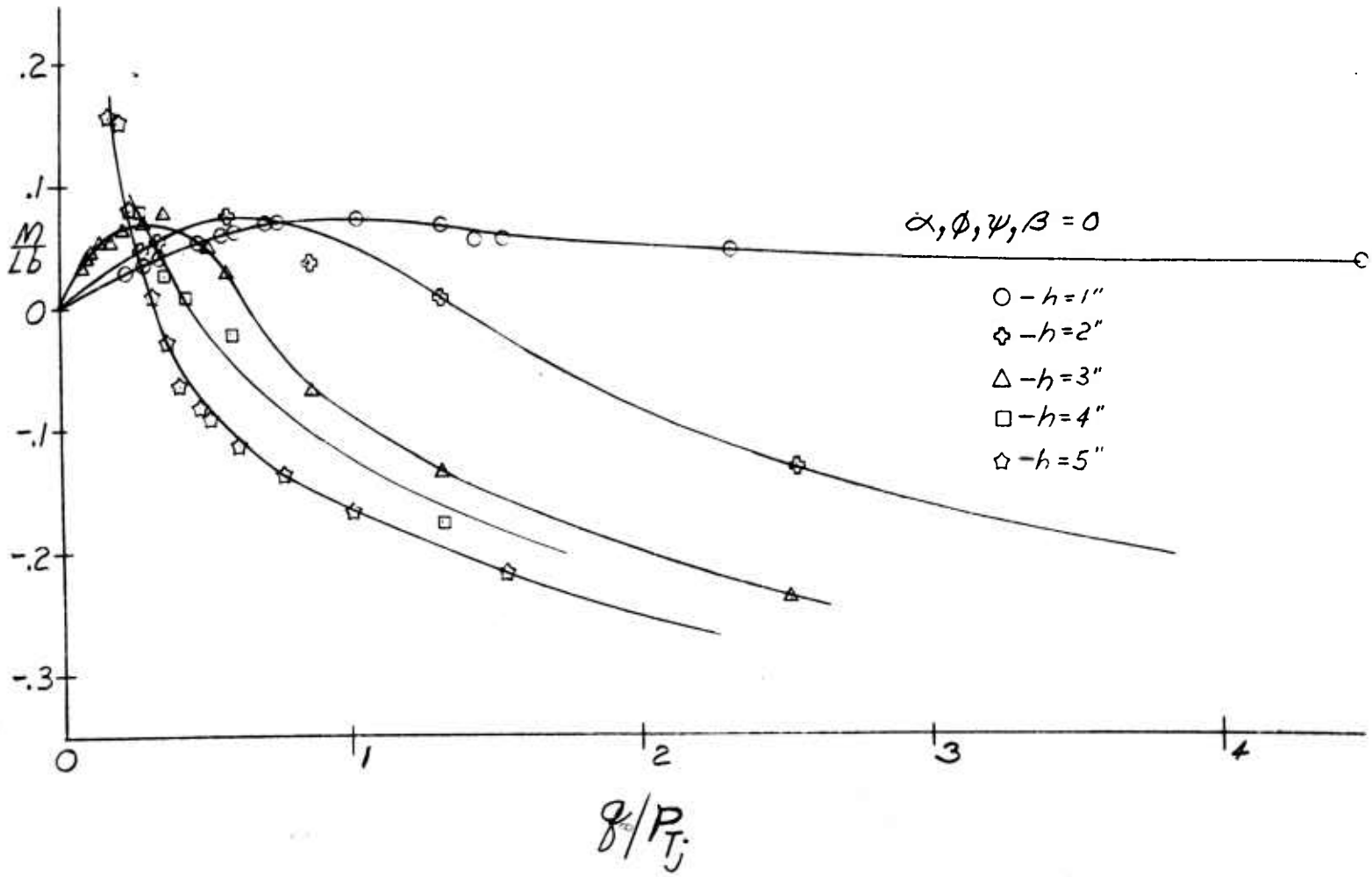

Figure 51. Effect of Forward Flight on Location of Center of Pressure.

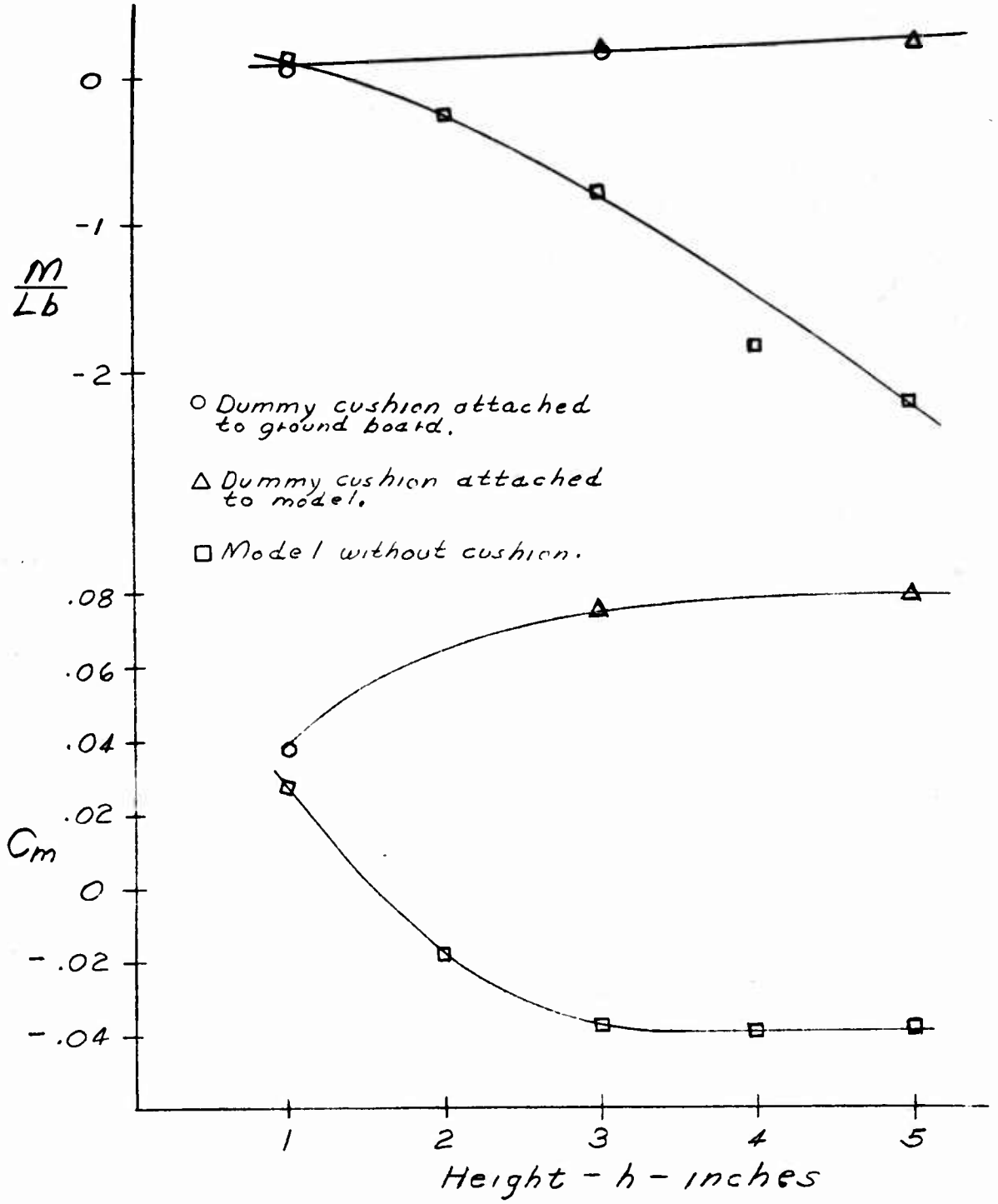

Figure 52. Pitching Moment Coefficient and C. P. Location Due to External Flow.

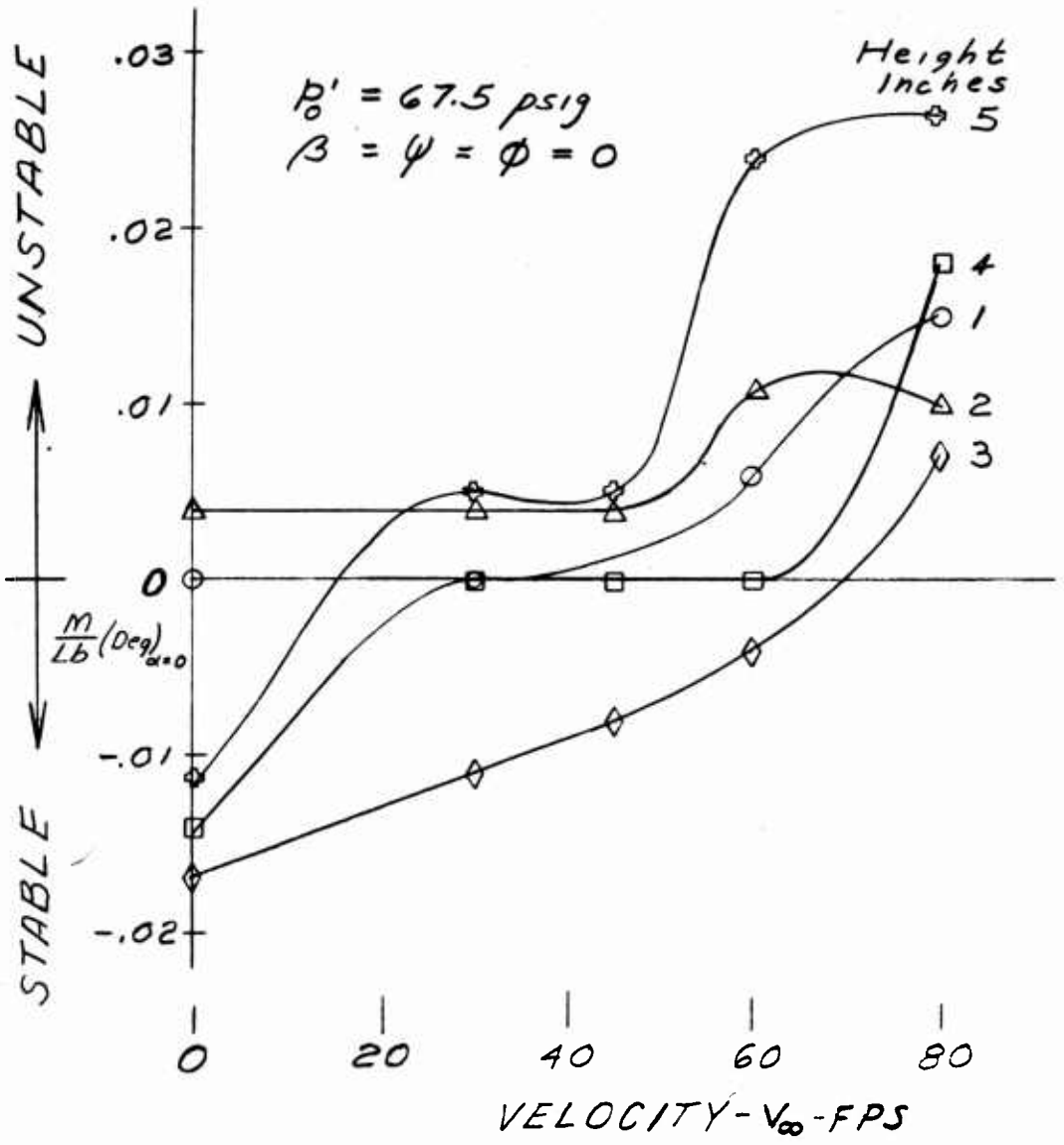

Figure 53. Range of Stability in Pitch.

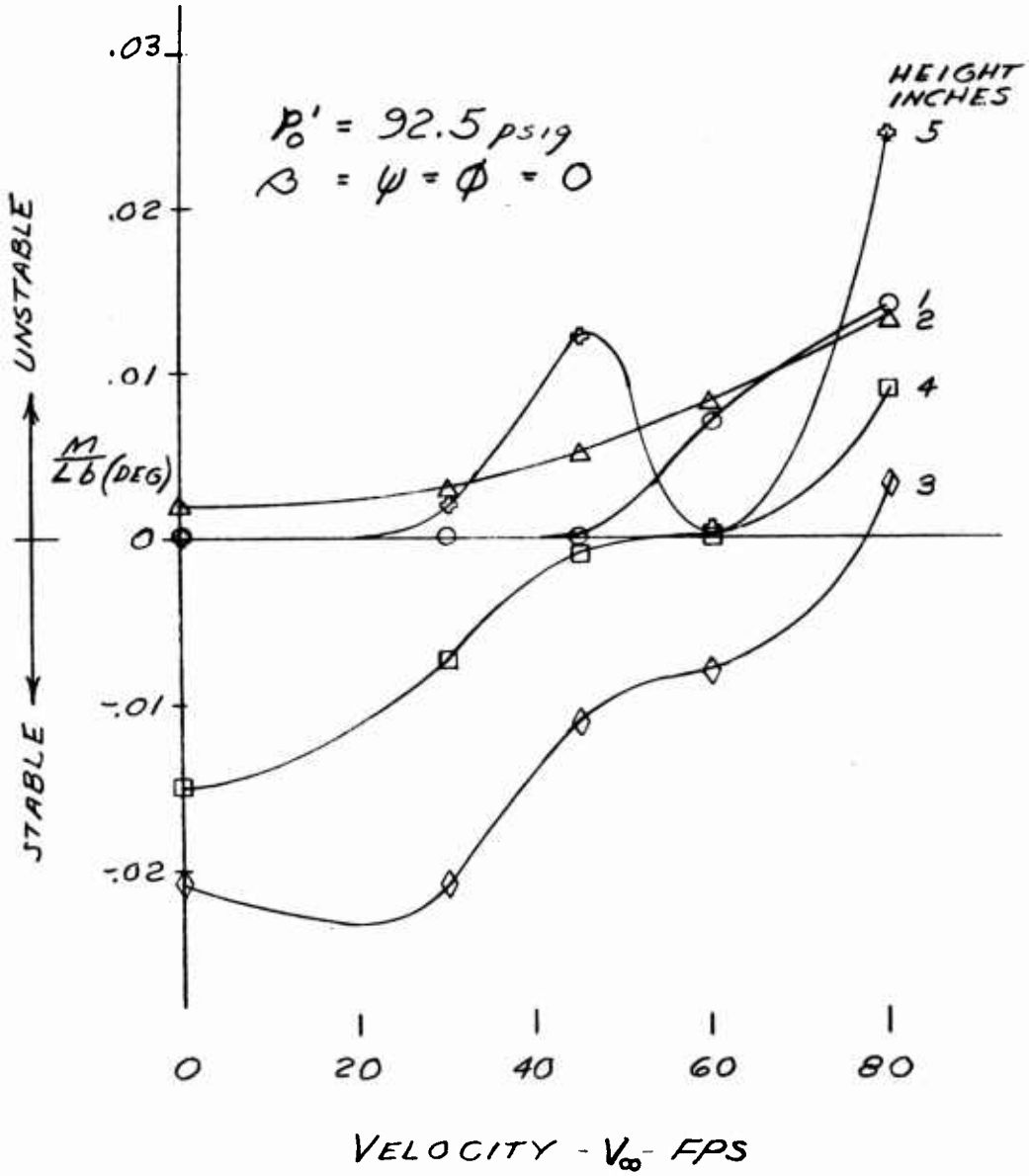

Figure 54. Range of Stability in Pitch.

3. Roll Stability

The effect of forward flight on the roll stability of the model is apparent in Figures 55 thru 58. In these figures the lateral location of center of pressure is plotted versus roll angle, ϕ, at constant heights and for the velocities tested, including $V_\infty = 0$, the hovering case.

The test results at low heights, h = 1 inch and 2 inches indicate that forward speed does not change the roll characteristics of the model to any extent, except perhaps at the higher roll angles tested. At the heights of 3 inches and 4 inches it may be observed that as speed increases the negative slope (stabilizing) of the curves near zero roll angle deteriorates, reducing the stability and finally making the model unstable. The influence of primary pressure p_o' can be noticed at the higher heights. The detrimental effect of forward velocity is not as strong at $p_o' = 92.5$ psig as it is at 67.5 psig primary pressure. While the actual phenomenon that decreases the roll stability is difficult to determine, the above results indicate that this is caused by some deterioration of the side curtains which, in turn, control the stabilizing cavity pressure on the side ejectors.

In summary, the roll stability in forward flight is much the same as in hovering flight, but the stability is reduced as forward velocity increases, this effect being less pronounced with stronger air curtains.

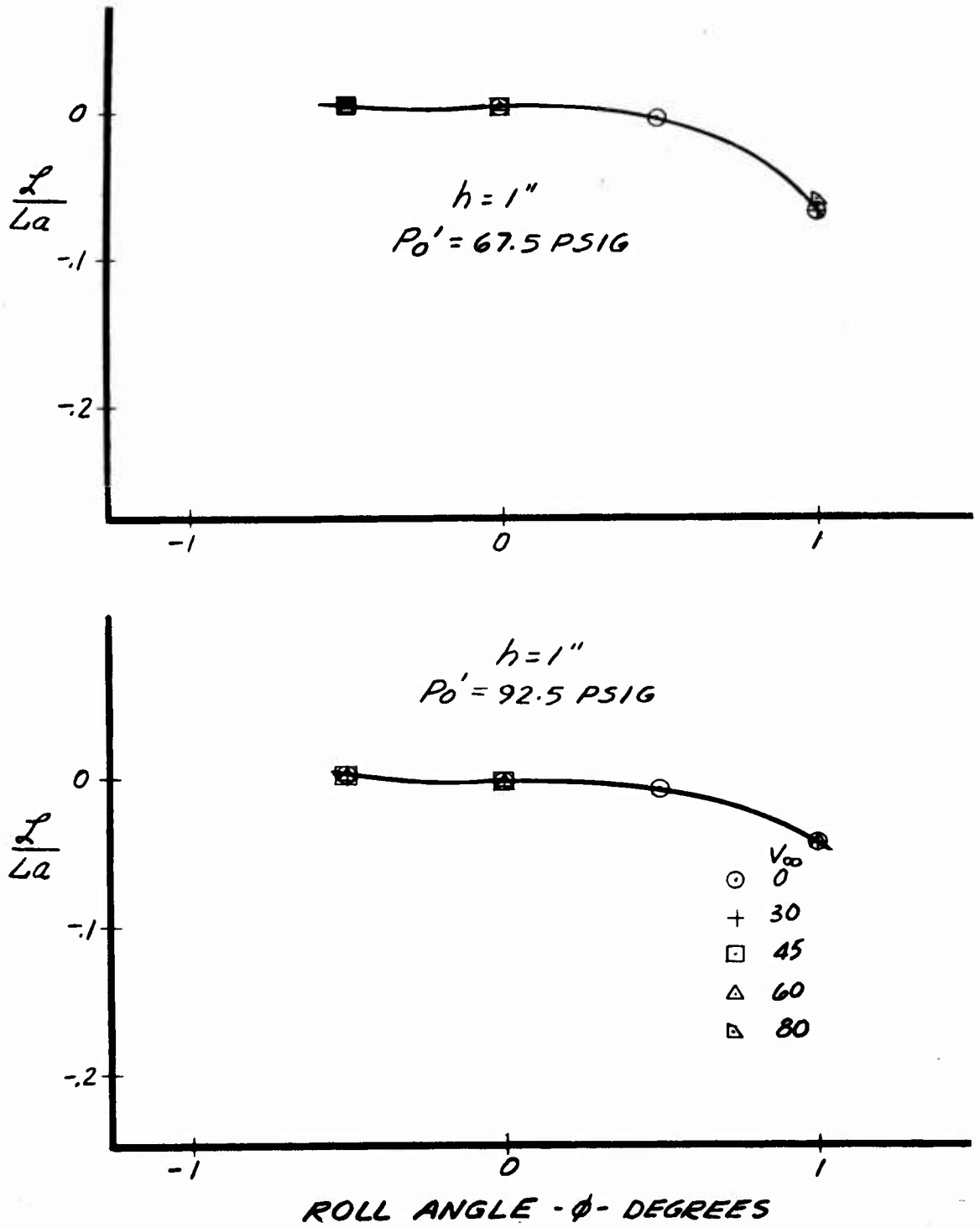

Figure 55. Rolling Moment Arm.

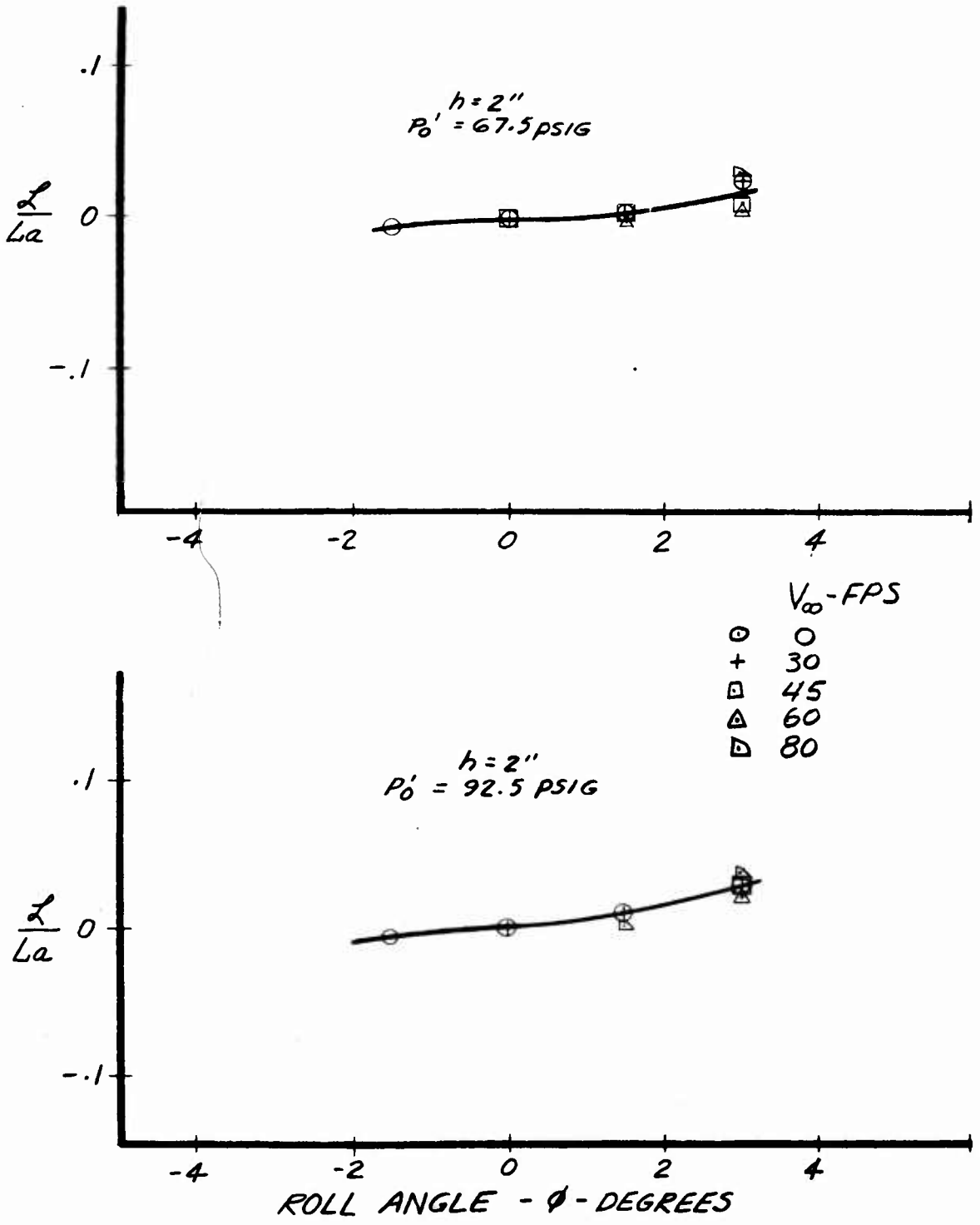

Figure 56. Rolling Moment Arm.

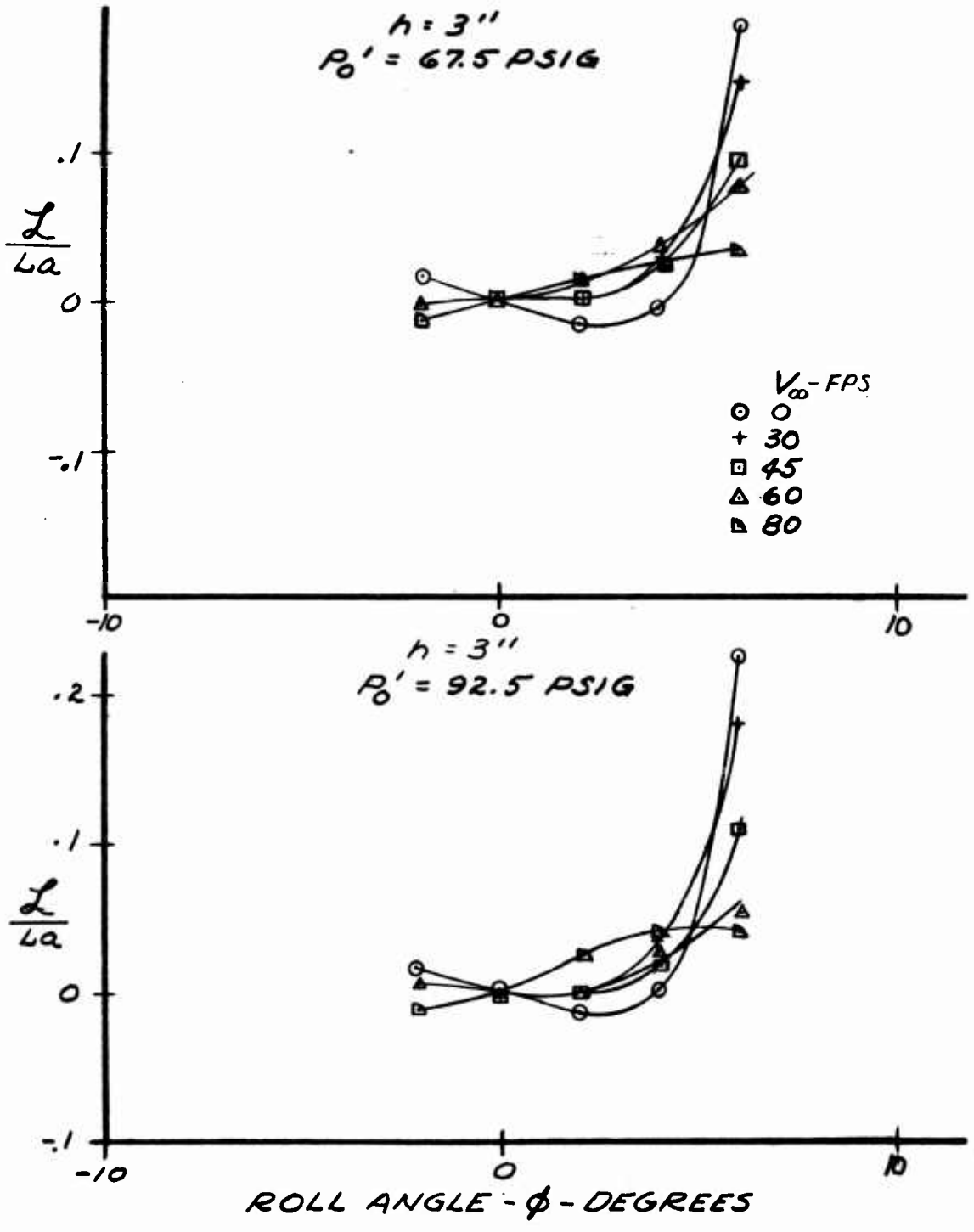

Figure 57. Rolling Moment Arm.

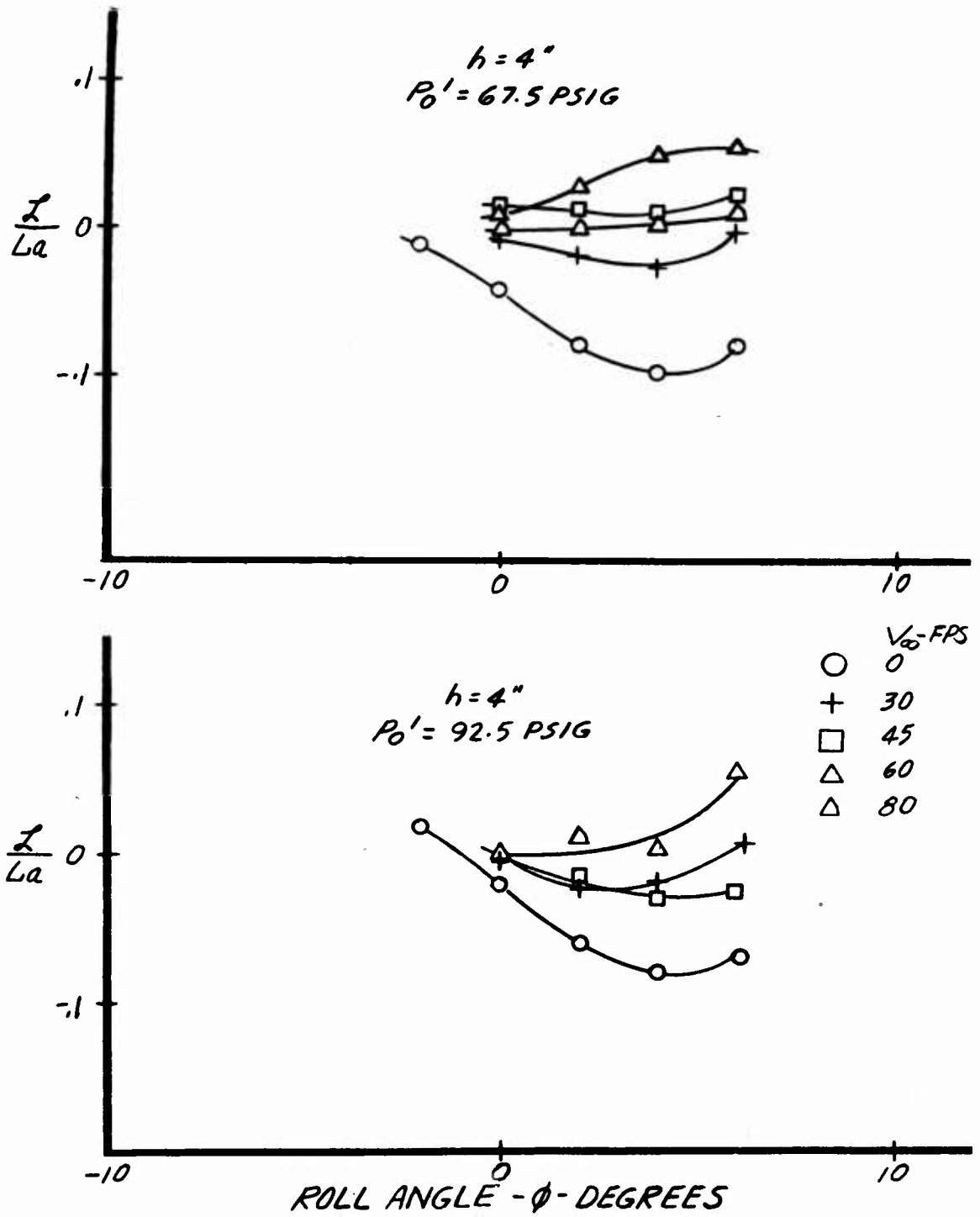

Figure 58. Rolling Moment Arm.

4. Yaw Stability

Figure 59 presents the yawing moment coefficient variation with yaw angle at speeds of 30 to 80 fps. The slope of these curves indicates that the model is unstable in yaw at all speeds. This is as expected from the configuration of the model.

Since the yawing forces depend only on the pressure distributions on the external side surfaces of the model, and no forces are transmitted from the air curtain to the model, no effects should be expected in yaw as a result of the changes in the air curtain strength. However, curtains of different strength will deflect differently in a yaw condition. This causes a different flow pattern around the model which in turn is reflected in the magnitude of the yawing forces and moments. It may be seen from Figure 59 that curtain strength have very little effect on the yawing moment of the model.

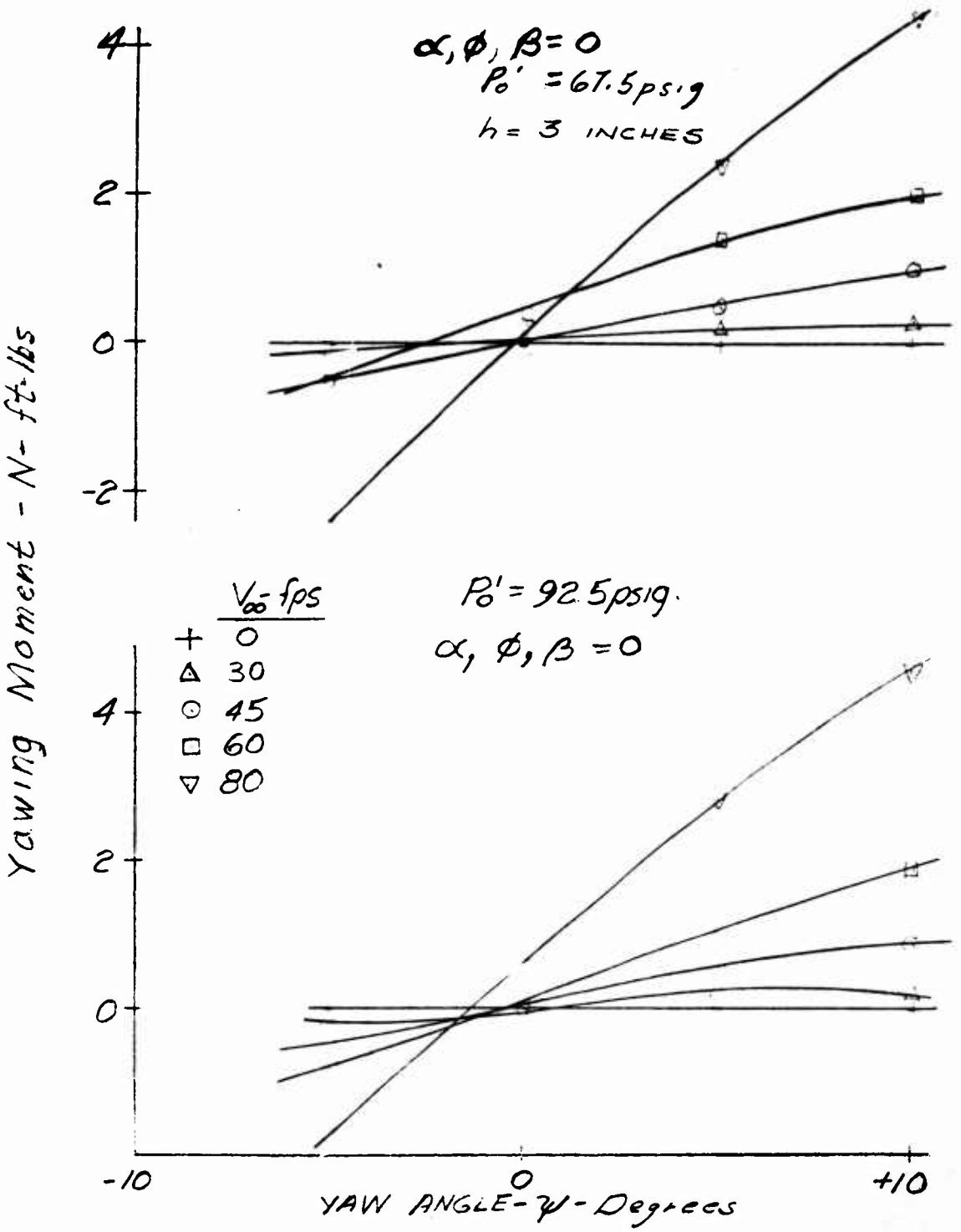

Figure 59. Effect of Speed on Yawing Moment.

BIBLIOGRAPHY

1. Martin Co., OR 2505, Recirculation Principle for Ground Effect Machines - Three Dimensional Wind Tunnel Tests - Basic Data, May 1962.

2. Normal K. Walker, Report No. 61/10, Progress Report No. 4, Contract Nonr-3412(00), 31 December 1961.

3. Martin Co., OR 2073, Recirculation Principle for Ground Effect Machines - Two Dimensional Tests, May 1962.

DISTRIBUTION

USAWC	1
USATMC(FTZAT), ATO	1
USAPRDC	1
DCSLOG	1
Rsch Anal Corp	1
ARO, Durham	2
OCRD, DA	2
Ofc of Maint Engr, ODDR&E, OSD	1
NATC	1
ARO, OCRD	1
DCSOPS	1
USAERDL	2
USAOTAC, Center Line	3
OrdBd	1
QMRECOMD	1
CofT	3
USATCDG	1
USATMC	19
USATSCH	4
USATRECOM	77
TCLO, USAERDL	1
TCLO, USAABELCTBD	1
USATRECOM LO, USARDG (EUR)	3
CNO	1
CNR	3
BUWEPS, DN (R-38)	1
BUWEPS, DN (RA-4)	1
ACRD(OW), DN	1
USNSRDF	1
USNPGSCH	1
BUSHP, DN	1
USNOTS	1
Dav Tay Mod Bas	1
MCLFDC	1
MCEC	1
USASGCA	1
Canadian LO, USATSCH	3
BRAS, DAQMG(Mov & Tn)	4
USASG, UK	1
Langley Rsch Cen, NASA	2

NASA, Wash., D. C.	6
Ames Rsch Cen, NASA	2
Lewis Rsch Cen, NASA	1
USGPO	1
ASTIA	10
USAMRDC	1
HUMRRO	2
DDRE	1
Maritime Administration	1
USSTRICOM	1

Martin Company, Orlando Division, Orlando, Fla., RECIRCULATION PRINCIPLE FOR GROUND EFFECT MACHINES, THREE-DIMENSIONAL WIND TUNNEL TESTS P. Vinson, G.Martin, and C.Casteleiro, Report No. OR-2497, TCREC Technical Rept 62-74, July 1962, 92 pp. (Contract DA 44-177-TC-710) Task 9R99-01-005-04.

Unclassified Report

The report presents the results of an experimental investigation of forward flight characteristics of a three-dimensional rectangular model of a

(over)

1. Fluid Dynamics
2. Aerodynamics

Martin Company, Orlando Division, Orlando, Fla., RECIRCULATION PRINCIPLE FOR GROUND EFFECT MACHINES, THREE-DIMENSIONAL WIND TUNNEL TESTS P.Vinson, G. Martin, and C.Casteleiro, Report No. OR-2497, TCREC Technical Rept 62-74, July 1962, 92 pp. (Contract DA 44-177-TC-710) Task 9R99-01-005-04.

Unclassified Report

The report presents the results of an experimental investigation of forward flight characteristics of a three-dimensional rectangular model of a

(over)

1. Fluid Dynamics
2. Aerodynamics

Martin Company, Orlando Division, Orlando, Fla., RECIRCULATION PRINCIPLE FOR GROUND EFFECT MACHINES, THREE-DIMENSIONAL WIND TUNNEL TESTS P. Vinson, G.Martin, and C.Casteleiro, Report No. OR-2497, TCREC Technical Rept 62-74, July 1962, 92 pp. (Contract DA 44-177-TC-710) Task 9R99-01-005-04.

Unclassified Report

The report presents the results of an experimental investigation of forward flight characteristics of a three-dimensional rectangular model of a

(over)

1. Fluid Dynamics
2. Aerodynamics

Martin Company, Orlando Division, Orlando, Fla., RECIRCULATION PRINCIPLE FOR GROUND EFFECT MACHINES, THREE-DIMENSIONAL WIND TUNNEL TESTS P.Vinson, G.Martin, and C.Casteleiro, Report No. OR-2497, TCREC Technical Rept 62-74, July 1962, 92 pp. (Contract DA 44-177-TC-710) Task 9R99-01-005-04.

Unclassified Report

The report presents the results of an experimental investigation of forward flight characteristics of a three-dimensional rectangular model of a

(over)

1. Fluid Dynamics
2. Aerodynamics

recirculation configuration GEM. The model was powered through an external high-pressure air source, using ejectors to induce the recirculating flow. Tests were conducted in the David Taylor Model Basin 8- X 12-foot subsonic tunnel, and data were obtained from a six-component balance and from pressure taps distributed over the model. The results indicate the performance and static stability characteristics to be expected of a GEM using the recirculation principle.

A basic data report, No. OR-2505, dated May 1962, is available on loan from the Library, USATRECOM, Fort Eustis, Virginia.

recirculation configuration GEM. The model was powered through an external high-pressure air source, using ejectors to induce the recirculating flow. Tests were conducted in the David Taylor Model Basin 8- X 12-foot subsonic tunnel, and data were obtained for a six-component balance and from pressure taps distributed over the model. The results indicate the performance and static stability characteristics to be expected of a GEM using the recirculation principle.

A basic data report, No. OR-2505, dated May 1962, is available on loan from the Library, USATRECOM, Fort Eustis, Virginia.

recirculation configuration GEM. The model was powered through an external high-pressure air source, using ejectors to induce the recirculating flow. Tests were conducted in the David Taylor Model Basin 8- X 12-foot subsonic tunnel, and data were obtained from a six-component balance and from pressure taps distributed over the model. The results indicate the performance and static stability characteristics to be expected of a GEM using the recirculation principle.

A basic data report, No. OR-2505, dated May 1962, is available on loan from the Library, USATRECOM, Fort Eustis, Virginia.

recirculation configuration GEM. The model was powered through an external high-pressure air source, using ejectors to induce the recirculating flow. Tests were conducted in the David Taylor Model Basin 8- X 12-foot subsonic tunnel, and data were obtained from a six-component balance and from pressure taps distributed over the model. The results indicate the performance and static stability characteristics to be expected of a GEM using the recirculation principle.

A basic data report, No. OR-2505, dated May 1962, is available on loan from the Library, USATRECOM, Fort Eustis, Virginia.

Martin Company, Orlando Division, Orlando, Fla., RECIRCULATION PRINCIPLE FOR GROUND EFFECT MACHINES, THREE-DIMENSIONAL WIND TUNNEL TESTS P. Vinson, G.Martin, and C.Casteleiro, Report No. OR-2497, TCREC Technical Rept 62-74, July 1962, 92 pp. (Contract DA 44-177-TC-710) Task 9R99-01-005-04.

Unclassified Report

The report presents the results of an experimental investigation of forward flight characteristics of a three-dimensional rectangular model of a

(over)

1. Fluid Dynamics
2. Aerodynamics

Martin Company, Orlando Division, Orlando, Fla., RECIRCULATION PRINCIPLE FOR GROUND EFFECT MACHINES, THREE-DIMENSIONAL WIND TUNNEL TESTS P.Vinson, G. Martin, and C.Casteleiro, Report No. OR-2497, TCREC Technical Rept 62-74, July 1962, 92 pp. (Contract DA 44-177-TC-710) Task 9R99-01-005-04.

Unclassified Report

The report presents the results of an experimental investigation of forward flight characteristics of a three-dimensional rectangular model of a

(over)

1. Fluid Dynamics
2. Aerodynamics

Martin Company, Orlando Division, Orlando, Fla., RECIRCULATION PRINCIPLE FOR GROUND EFFECT MACHINES, THREE-DIMENSIONAL WIND TUNNEL TESTS P. Vinson, G.Martin, and C.Casteleiro, Report No. OR-2497, TCREC Technical Rept 62-74, July 1962, 92 pp. (Contract DA 44-177-TC-710) Task 9R99-01-005-04.

Unclassified Report

The report presents the results of an experimental investigation of forward flight characteristics of a three-dimensional rectangular model of a

(over)

1. Fluid Dynamics
2. Aerodynamics

Martin Company, Orlando Division, Orlando, Fla., RECIRCULATION PRINCIPLE FOR GROUND EFFECT MACHINES, THREE-DIMENSIONAL WIND TUNNEL TESTS P.Vinson, G.Martin, and C.Casteleiro, Report No. OR-2497, TCREC Technical Rept 62-74, July 1962, 92 pp. (Contract DA 44-177-TC-710) Task 9R99-01-005-04.

Unclassified Report

The report presents the results of an experimental investigation of forward flight characteristics of a three-dimensional rectangular model of a

(over)

1. Fluid Dynamics
2. Aerodynamics

recirculation configuration GEM. The model was powered through an external high-pressure air source, using ejectors to induce the recirculating flow. Tests were conducted in the David Taylor Model Basin 8- X 12-foot subsonic tunnel, and data were obtained from a six-component balance and from pressure taps distributed over the model. The results indicate the performance and static stability characteristics to be expected of a GEM using the recirculation principle.

A basic data report, No. OR-2505, dated May 1962, is available on loan from the Library, USATRECOM, Fort Eustis, Virginia.

recirculation configuration GEM. The model was powered through an external high-pressure air source, using ejectors to induce the recirculating flow. Tests were conducted in the David Taylor Model Basin 8- X 12-foot subsonic tunnel, and data were obtained for a six-component balance and from pressure taps distributed over the model. The results indicate the performance and static stability characteristics to be expected of a GEM using the recirculation principle.

A basic data report, No. OR-2505, dated May 1962, is available on loan from the Library, USATRECOM, Fort Eustis, Virginia.

recirculation configuration GEM. The model was powered through an external high-pressure air source, using ejectors to induce the recirculating flow. Tests were conducted in the David Taylor Model Basin 8- X 12-foot subsonic tunnel, and data were obtained from a six-component balance and from pressure taps distributed over the model. The results indicate the performance and static stability characteristics to be expected of a GEM using the recirculation principle.

A basic data report, No. OR-2505, dated May 1962, is available on loan from the Library, USATRECOM, Fort Eustis, Virginia.

recirculation configuration GEM. The model was powered through an external high-pressure air source, using ejectors to induce the recirculating flow. Tests were conducted in the David Taylor Model Basin 8- X 12-foot subsonic tunnel, and data were obtained from a six-component balance and from pressure taps distributed over the model. The results indicate the performance and static stability characteristics to be expected of a GEM using the recirculation principle.

A basic data report, No. OR-2505, dated May 1962, is available on loan from the Library, USATRECOM, Fort Eustis, Virginia.